Kinematic GNSS
Precise Point Positioning

Application to marine platforms

João Paulo Ramalho Marreiros

Ph.D. Thesis in Surveying Engineering

Faculty of Sciences

University of Porto

December 2012

A thesis submitted in partial *fulfilment of the requirements for the degree of Ph.D.*

The University of Porto, 2012.

Abstract

Positioning with Global Navigation Satellite Systems (GNSS) can be performed by either one of two ways: point positioning or relative positioning. Point positioning, also known as the standalone or autonomous positioning, involves only one GNSS receiver. Relative positioning employs two or more GNSS receivers tracking the same satellites. Standard point positioning with GNSS provides worldwide 10 m accuracy level. This accuracy level is far beyond the requirement of many applications such as geodetic control, hydrographic surveying and sea level measurement, which require centimetre level accuracy or better.

Most of precise GNSS positioning, capable of providing centimetre accuracy for a moving platform, is based on relative positioning methods. Such methods need to work on the vicinity of one or more reference stations, within a few tens of kilometres, and require simultaneous observations at reference and rover stations. Precise Point Positioning (PPP) is a new method that started in the 1990's and involves the use of measurements from a single GNSS receiver to obtain accurate position without the use of measurements from reference stations. Such improvement is accomplished through the use of state space representation of the corrections to the observations, such as precise satellite ephemerides and satellite clock corrections produced from a network of worldwide monitoring stations.

In the scope of this study, a PPP methodology was developed, for the purpose of positioning static stations and marine platforms used in hydrographic surveying and oceanographic works. This methodology is implemented using the GPSTK (abbreviation for GPS Tool Kit) open source C++ library. New routines were created to solve specific problems related with the models used for modelling the error sources, the adjustment algorithm, the stochastic modelling of the observations and use of dedicated satellite clock corrections files. Results show uncertainty (standard deviation) at centimetre level accuracy for static and decimetre for kinematic positioning. The time required for the solution to converge, in kinematic mode, was 300 s.

Sea Surface Heights derived from PPP processing of data collected onboard one survey ship were compared with satellite altimetry SSH. The differences between the two data sets are within the accuracy level of satellite altimetry. This approach is a simple and flexible data collection system of SSH with respect to an absolute reference frame that can be implemented at low costs using vessels of opportunity and used for coastal altimetry calibration or sea level monitoring.

Sumário

O posicionamento com Global Navigation Satellite Systems (GNSS) pode ser realizado de dois modos: posicionamento absoluto ou posicionamento relativo. O Posicionamento absoluto, também conhecido como posicionamento autónomo, apenas utiliza um receptor GNSS. O Posicionamento relativo utiliza dois ou mais receptores GNSS e a posição é determinada a partir de uma estação de referência. O posicionamento absoluto padrão com GNSS tem cobertura mundial com uma exactidão de alguns metros. Este nível de exactidão não é suficiente para muitas aplicações, tais como a que exigem um controle geodésico, levantamentos hidrográficos e a medição do nível do mar.

Os métodos normalmente utilizados para posicionamento de precisão com GNSS, com capacidade para posicionar um objecto em movimento, são baseados em técnicas de posicionamento relativo. Tais métodos exigem a disponibilidade de uma ou mais estações de referência nas proximidades da estação móvel, dentro de algumas dezenas de km, e requerem que se efectuem observações simultâneas em todas as estações. Precise Point Positioning (PPP) é uma metodologia que começou a se desenvolvida nos finais dos anos 90 e que permite utilizar observações de um receptor GNSS para se obter a posição com exactidão centimétrica, sem necessidade de utilizar estações de referência. O PPP baseia-se na correcção ou minimização de erros através da utilização de efemérides de satélite precisas e de correcções aos relógios dos satélites determinadas a partir de uma rede global de estações de monitorização.

Este trabalho teve por objectivo desenvolver uma metodologia PPP para posicionamento estático e cinemático, com aplicação em levantamentos hidrográficos e em trabalhos oceanográficos. Esta metodologia foi implementada com recurso à biblioteca de classes C++ do GPSTk (abreviatura de GPS Toolkit). Foram criadas novas classes para resolver problemas específicos relacionados com os modelos funcionais utilizados para modelar as fontes de erro, com o melhoramento do algoritmo de ajustamento, com o modelo estocástico das observações e também com a utilização de ficheiros dedicados introdução das correções dos relógios dos satélites. Os resultados demonstram que o erro estimado (desvio padrão) do posicionamento estático é da ordem centimétrica e para o posicionamento cinemático é da ordem decimétrica. O tempo necessário para a solução convergir, em modo cinemático, foi avaliado em 300 s.

Foi efectuada a comparação da altura da superfície do mar, a partir de posicionamento PPP com receptores GNSS instalados num navio, com altimetria por satélite. As diferenças entre

os dois conjuntos de dados são da mesma grandeza que a exactidão das medições da altimetria por satélite. Este resultado indica que a metodologia adoptada com o GNSS-PPP constitui um sistema simples, flexível e de baixo custo para efectuar medições da SSH num referencial absoluto, que pode ser utilizada para a validação de dados altimétricos ou na medição do nível do mar.

.

Acknowledgements

I would like to express my special thanks in my native language, Portuguese:

Table of Contents

List of Figures

List of Tables

Acronyms and abbreviations

ANTEX – Antenna Exchange Format.

API – Application Programming Interface.

BPSK – Binary Shift Phase Keying.

C/A – Coarse Acquisition.

CDMA – Code Division Multiple Access.

CLS – Collect Localization Satellites.

COASTALT – Project on Development of Radar Altimetry Data Processing in the Coastal Zone by the ESA, http://www.coastalt.eu/.

DGNSS – Differential GNSS.

DORIS - Doppler Orbitography and Radiopositioning Integrated by Satellite.

ECEF – Earth Centered Earth Fixed.

ECMWF – European Centre for Medium-range Weather Forecast.

ESA – European Space Agency.

FOC – Full Operational Capability.

GDR – Geophysical Data Record.

GEO – Geostationary Earth Orbit.

GGOS – Global Geodetic Observing System. http://www.ggos.org/.

GIM – Global Ionosphere Maps.

GLONASS - GLObal NAvigation Satellite System.

GMF – Global Mapping Function, http://ggosatm.hg.tuwien.ac.at/DELAY/.

GPD – GNSS-derived Path Delay.

GPT – Global Pressure and Temperature, http://ggosatm.hg.tuwien.ac.at/DELAY/.

GNSS – Global Navigation Satellite System.

GPS – Global Positioning System.

GPSTk – GPS Toolkit, http://www.gpstk.org/bin/view/Documentation/WebHome.

IAG – International Association of Geodesy. http://www.iag-aig.org/.

ICS – Inter-signal correction.

IERS – International Earth Rotation Service.

IGS – International GNSS Service.

IMU – Inertial Measurement Unit.

INS – Inertial Navigation System.

ITRS – International Terrestrial Reference System.

JPL – Jet Propulsion Laboratory.

LEO – Low Earth Orbit.

LMS – Least Mean Squares.

MEO – Medium Earth Orbit.

NASA - National Aeronautics and Space Administration.

NGS – National Geodetic Survey.

NOAA – National Oceanic and Atmospheric Administration.

OOP – Object Oriented Programming.

OSR – Observation Space Representation.

PCV – Phase Centre Variation.

POD – Precise Orbit Determination.

PO.DAAC – Physical Oceanography Distributed Active Archive Center, http://podaac.jpl.nasa.gov/.

PPP – Precise Point Positioning.

PRN – Pseudo Random Noise.

RADS – Radar Altimetry Database Systems.

RMS – Root Mean Square, $x_{rms} = \sqrt{\frac{1}{n} \cdot (x_1^2 + \cdots + x_n^2)}$.

RTCA – Radio Technical Commission for Aeronautics

RTCM – The Radio Technical Commission for Maritime Services

SAPPos – Satellite Based Absolute Precise Positioning

SLR – Satellite Laser Ranging.

SNR – Signal-to-Noise Ratio.

SA – Selective Availability.

Sat Nav – Satellite Navigation System.

SBAS – Satellite Based Augmentation System.

SDev – Standard deviation.

TEC – Total Electron Content.

TGD – Total Group Delay.

UTC – Universal Time Coordinated.

WITM – Western Iberia Tide Model.

ECMWF- European Center for Medium Weather Forecast.

NCEP - National Centres for Weather Prediction.

This page was intentionally left blank

Chapter 1. Introduction

With the launch on October 4th 1957 of the first artificial satellite, the Sputnik I, the humanity stepped into the space era, an era that changed our lives, since an entire new world of opportunities was brought to the development of new technologies. New space-based positioning techniques using radio signals from satellites were developed, with increasing performance.

A satellite navigation system with global coverage is termed as Global Navigation Satellite System (GNSS). As of July 2012, only the United States Global Positioning System (GPS) and the Russian GLObal NAvigation Satellite System. (GLONASS) were fully globally operational GNSS. Other countries are in the process of creating their own GNSS such as the China Beidou and the European Union GALILEO.

Positioning with GNSS can be performed by either one of two ways: point positioning or relative positioning. Point positioning, also known as the absolute, standalone or autonomous positioning, involves only one GNSS receiver for the direct determination of absolute positions. Relative positioning employs two or more GNSS receivers and determines baseline vectors, not absolute positions.

Most currently used GNSS positioning methods that are capable of providing centimetre accuracy for a moving platform are based in relative positioning. Such methods need to work on the vicinity of one or more reference stations, within a limited range, and require simultaneous observations of the same satellites at the reference and rover stations.

Precise Point Positioning (PPP) involves the use of measurements from a single GNSS receiver, in a similar way as provided by standard GNSS services, but with the improvement resulting from the application of corrections to the observation errors sources previously determined or estimated as additional unknowns. Such improvement was first accomplished in static positioning through the use of precise satellite ephemeris and clock corrections produced from a network of worldwide monitoring stations [Zumberg *et al.*, 1997]. Subsequent developments in PPP demonstrated that it may also be used for kinematic positioning [Kouba and Héroux, 2001].

In traditional GNSS relative positioning, observations from a single or a network of reference stations are used to minimize or eliminate spatially dependent errors. This method of providing corrections is termed as observation space representation. In contrast to this, PPP uses corrections that are associated with individual observation error components, such as the satellite position, the clock errors, ionosphere, troposphere and phase-bias. This method of providing the corrections to the observations is termed as in the state-space representation, requires the determination of the complete state vector and does not require reference stations.

GNSS state-space corrections can be downloaded from a service provider for post-processing or may be transmitted directly to the rover for real time applications using data transmission protocols such as the RTCM (Radio Technical Commission for Marine Services) standards. In this way PPP, while still under development, is becoming a technique that has the potential to replace existing range limited GNSS relative positioning methods.

For the marine positioning, the use of GNSS relative positioning is limited to coastal areas where reference stations can be installed. As an advantageous alternative, PPP allows worldwide coverage for offshore applications, extending the GNSS precise positioning capability to remote areas and has the potential to reduce costs and logistical requirements in marine surveying. A wide range of oceanographic applications and studies may arise if centimetre level accuracy can be extended to oceanic areas. Examples of such applications are the direct georeferencing of shipborne or buoy sensors, sea level and wave height determination, ship dynamics determination, motion compensation and atmosphere sensing.

1.1. Motivation

The ocean is one of Earth's most valuable natural resources. It provides food in the form of fish and shellfish, about 200 billion pounds are caught each year. It is used for transportation, both travel and shipping. It provides a treasured source of recreation for humans. It is mined for minerals (salt, sand, gravel, and some manganese, copper, nickel, iron, and cobalt can be found in the deep sea) and drilled for crude oil.

The ocean is one part of the Earth system. It mediates atmosphere processes, in the transfers of mass, momentum and energy through the sea surface. The human demand for the knowledge of the oceanic currents, waves and tides goes back thousands of years. Since then oceanographers and mariners use instruments to navigate and measure ocean parameters. The

era of satellites allowed a global survey of oceanic processes from space and new positioning methods of marine platforms. Almost all observations of the ocean now come from satellites, drifters and autonomous instruments [Stewart, 2008].

Marine geodesy is the part of geodesy which deals with the ocean and has the same practical aims as land geodesy: determination of the size and shape of the Earth and its gravity field, enable reliable mapping of the seafloor and development of precise measurement technology and computation methods needed to satisfy these aims. Marine geodesy does have a unique problem: apart the use of remote observations from land, satellites or aircrafts, most work must be conducted on a dynamic and complex environment using a floating platform, such as a ship or a buoy. Early, at the advent of the space era, it was already recognized that accurate ship positioning was a requirement for marine geodesy and will play a major role in the exploration of the ocean and its resources [Mourad *et al.*, 1969].

The concept of relative kinematic positioning using GPS carrier phase observations was described by Remondi (1985). After that, several methods were developed to implement pseudo-kinematic [Remondi, 1988] and semi-kinematic [Cannon, 1989] GPS surveying, all based on static initializations. Purely kinematic GPS method, require the computation of the position of an object in permanent motion, without static initialization. This requires the determination of the carrier phase ambiguities while the object is in motion, called as ambiguity resolution on-the-fly (OTF). For an insight of basic OTF techniques see Hatch (1994). With the technological advances in hardware and software, several accurate kinematic GNSS precise relative positioning solutions started to be provided by private or governmental agencies. Kinematic GNSS positioning with centimetre accuracy is now a standard product available for a wide range of applications. However, all these solutions are confined to a limited range from a reference station or from a network of stations.

New applications, that use precise positioning at sea, were developed. These applications are related with accurate positioning requirements for anchoring or maneuvering floating platforms, control of maritime works, sea level measurement and hydrographic surveying. The use of GPS buoys and ships for sea level measurement is a technique used for validation/calibration of satellite radar altimetry [IOC, 2006]. The technology of using kinematic GNSS precise relative positioning for vertical control in hydrographic surveys is now a commonplace after being in a research-to-operations mode for several years [IHO, 2005]. Other applications use GNSS sea surface measurements for tsunami detection [Kato *et*

al., 2005; Schöne *et al.*, 2011]. However, all these applications are restricted to coastal areas, in the vicinity of one or a network of reference stations.

Either seen as a competition or complementary to relative positioning techniques, PPP is going to become an efficient alternative to relative kinematic positioning at sea. The success of this method will significantly improve the operational flexibility of precise positioning using GNSS and at the same time reduce the field operational costs. Such method will increase the number of applications using GNSS technology, and will play a major role in marine geodesy, offshore surveys and physical oceanography allowing precise positioning in extensive ocean areas where it was not possible before.

The potential for application of GNSS to precise positioning in the oceans remains to be exploited and many attractive possibilities can be developed. In marine surveying, new methods for tide reduction may be implemented without the requirement of a land based tide gauge. Accurate positioning of ships and buoys will provide valuable information of the Sea Surface Height (SSH) to complement with satellite altimetry data or as an additional sensor for tsunami early warning systems.

1.2. Objectives

The objective of this thesis was to study, develop and implement algorithms for GNSS positioning at sea, and access its performance. Within the framework of this general goal, the following specific objectives are set:

- Develop, implement and test precise point positioning algorithms that can be used for kinematic positioning;
- Adopt a software programming strategy as standard and portable between platforms as possible, through the use of an existing open source and tested GNSS software repository, the GPSTk;
- Implement the necessary modifications, program new algorithms as required for kinematic PPP;
- Assess the performance of the developed PPP algorithms in terms of their accuracy, integrity and required initialization time;
- Evaluate the use of PPP on a marine platform to get precise estimates of Sea Surface Height;

- Create a new software suite that can be used for static and kinematic positioning in the domain of hydrography and oceanography, reducing the dependency from commercial software and open for improvement in the future with new GNSS data processing methodologies.

1.3. Methodology

This study started with the literature review of the origins and evolution of PPP methodologies. This included an investigation of the methods used for error mitigation and data adjustment algorithms applied for positioning with GNSS. International GNSS Service (IGS) products were used as a source for satellite precise ephemeris and clock parameters.

The software used in this study is based on already developed and tested source code in order to avoid redundant work. The GPS Toolkit (GPSTk) C++ class library was used. Some routines were modified and others were created to implement an innovative and efficient method for kinematic PPP at sea.

Data collected at marine platforms (ships and buoys) were used to evaluate the performance of PPP by comparing it with carrier phase relative positioning. The results of PPP at sea were used for Sea Surface Height determination and compared to satellite altimetry data.

1.4. Structure

This thesis has eight chapters. After this general introduction chapter 2 deals with the measurement of the sea level, gives an overview of satellite altimetry and describes how GNSS can be used for this purpose on board ships and buoys.

Chapter 3 gives a detailed description of the GNSS observables and its error sources. This is a crucial topic for the definition of adequate observation models, the implementation of efficient algorithms and mitigation of all potential error sources that may affect the system.

Chapter 4 introduces the concept of PPP and provides a sequential overview of existing methods developed by other authors. It is presented the traditional model based on the ionosphere free combination and the adjustment procedure either by a sequential least squares or Kalman filter. This chapter also provides a brief description of existing GNSS products and PPP software.

Chapter 5 and 6 contain the main contribution of this thesis to advances in PPP applied to marine platforms. In Chapter 5 the developed PPP methodology is presented. Aspects related with data pre-processing, weighting of satellites observations and data combinations as an improvement to the traditional model are discussed. The implementation of the adjustment procedure using a Kalman filter and feasibility of carrier phase ambiguity resolution are analysed in the context of PPP.

In Chapter 6 the implemented software is described, concerning with the computational flow and software components, most of them based on using the GPSTk C++ library. The new modules created to allow the exploitation of GPSTk for kinematic applications are described with more detail.

Chapter 7 is devoted to the description of the experiments and presentation of results. The experiments were based on data collected on board ships and buoys. Positioning results were compared to relative positioning and satellite altimetry data.

Chapter 8 summarizes the major results obtained in the previous chapters, presents the final conclusions and suggests recommendations for future work.

Chapter 2. Sea level measurement using GNSS

Knowledge about the sea level and its spatial and temporal variability is essential to understand the Earth system and has a direct impact in human life and all ecosystems evolution. Sea level variations must be continuously measured, monitored and predicted in harbours to provide tidal information to mariners and many others near shore activities depending on that information. The observation of the sea surface height in the deep sea is needed for geodetic and ocean dynamic studies with a direct application in Tsunami early warning systems.

The measurement of sea level has many different facets. The data must be carefully calibrated, checked and evaluated. The sea surface is in constant motion caused by various components, from different physical sources that are usually distinguished by their period These components range from surface gravity waves with periods of 0.5 to 20 s; seiches and tsunamis with periods of over 1 hour; tides with periods centred around ½ and 1 day; meteorological effects, that may range from a few days to one year; inter-annual and decadal variability and long term-term trends caused by biological and climatic effects [IOC, 2006].

The magnitude of these sea level variation components vary enormously. Surface waves can have amplitudes up to 30 m. Tsunamis tend to be less than 1 m in the deep ocean but may be several metres near the coast. Tides are relatively small in the deep ocean, but may be several metres near the coast. Storm surges may be of the order of a few metres in shallow seas. All these components mixed together cause the ocean surface to have high temporal and spatial variations [IOC, 2006].

In general, the measurement of sea level variations is not concerned with the small period variations due to surface gravity waves, which must be filtered out of the system. For systems moored at the seabed, which are based on subsurface pressure observations to derive the sea level measurements from the hydrostatic relation, the properties of sea water (salinity, temperature and hence density) must also be considered.

2.1. Sea level measurement at coastal stations

The traditional instruments used to measure the coastal sea level are based on tide gauges installed on land fixed stations near the coast. Common to all tide measuring devices is that

its station must be connected to a reference network and have an accurate geodetic positioning.

There are fundamentally four types of measuring technology in common use [IOC, 2006]:

- A stilling well and float, in which the filtering of the waves is done through the mechanical design of the well;
- Pressure systems, in which the sub-surface bottom pressure is monitored and converted to height based on knowledge of the water density and local acceleration due to gravity. These systems may be deployed off the coast, but are not used in the deep ocean;
- Acoustic systems, in which the transit time of a sonic pulse used to compute distance to the sea surface;
- Above water fixed radar systems, similar to acoustic systems, but using electromagnetic waves at radar frequencies.

The sea level measurements made by a tide gauge provide the relative movement of the sea with respect to land. The station benchmark is not constant over long periods of time, as the Earth's surface moves due to a range of natural processes, such as seismic and plate tectonics activity, or human related activity. Sea level measurements must be decoupled from height variations due to land movements.

Tide gauge benchmarks are usually defined in terms of a National Levelling Network, (NLN). The altimetric datum used in the NLN is usually defined in terms of a tidal datum. For a tidal derived datum, a period of more than 19 years of consecutive observations should be used, because of long-term variations tidal in lunar constituents [IHO, 2005]. In Portugal, the national altimetric datum is given as the equipotential gravity surface defined by the mean sea level measured at Cascais tide gauge between 1882 and 1938 [Casaca *et al.*, 2000].

Ideally, for any studies involved with sea level, all tide gauges should be equipped with a dual frequency GNSS receiver to continuously monitor any land movement. The GNSS antenna position should be accurately determined in three dimensional geodetic coordinates and linked to the tide gauge bench mark by regular levelling, at least annual [IOC, 2006].

2.2. Buoy based systems

The development of the GNSS buoy technique was driven largely based on the demanding of accurate positioning on the ocean surface for the verification of highly accurate altimeters used on satellites for oceanographic missions, such as the ERS-1 and the TOPEX/Poseidon. Early researches were primarily proof of concept studies, utilising a range of different design configurations [Rocken *et al.*, 1990; Hein *et al.*, 1992; Kelecy *et al.*, 1994].

Satellite altimetry has proven to be a powerful tool for the study of the oceans, at present reaching centimetric accuracy in the open ocean and being widely used in sea-level and various oceanographic related researches. Owing to unknown post-launch biases and the aging of the satellite electronic components, a consistent off-shore height reference is needed.

In the coastal regions, the altimeter data are degraded due to the following main reasons: the altimeter waveforms fail to conform to the Brown model and need to be retracked; the wet tropospheric correction computed from the on board microwave radiometer (MWR) measurements becomes invalid due to land contamination in the signal coming from the large radiometer footprint; and the global ocean tide models do not properly account for local tidal effects [Fernandes *et al.*, 2010]. In the recent years much progress has been achieved in the development of techniques for processing altimeter data in the coastal zone [Vignudelli *et al.*, 2011]. These developments allow the computation of improved satellite altimetry in the coastal regions and create the need for appropriate methods for validating the new data sets.

Some altimetric satellites have their orbits passing over static tide gauges and GNSS stations installed on offshore oil rigs or on platforms near the coastline and harbors. However these locations are rare and limited to a single position. With the increasing accuracy of kinematic GPS for offshore applications, research groups have developed GPS-equipped buoys for the determination of instantaneous Sea-Surface Heights (iSSH). These buoys were deployed on the positions under the orbits of altimetric satellites and used for calibration/validation. Between 1999 and 2003, GPS water level measurement was coordinated by a special group of the International Association of Geodesy, the SSG 2.194. In its final report, the SSG 2.194 provides a summary of the main developments on using GPS buoys for water level measurements until 2003 [IAG SSG 2.194, 2003].

Each buoy design has its pros and cons in addition to suitability for specific applications. All these buoys should form a robust and stable floating platform, and follow the vertical motion

of the sea with minimum or no dumping. Regardless of buoy design, the capability for measuring the antenna height, the buoy inclination and the heave motion remains a critical issue for high accuracy applications.

Watson (2005) summarizes the development of the GPS buoy technique used for sea level measurement. According to its design these buoys can be divided into three types:

- Non-autonomous light weight wave rider or spar design, with antenna only, tethered and operated from a boat where the receiver is installed (see table 2.1);
- Light weight autonomous wave rider design capable of short periods of operation (see table 2.2).
- Ruggedized oceanic buoys capable of autonomous operation for extended periods in any sea conditions (see table 2.3).

Table 2.1 – Advantages, disadvantages and applications of the non-autonomous light weight design GNSS buoy. Table layout from Watson (2005) and Marshall and Dennys (2008).
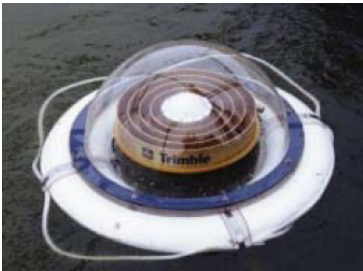
Description: - Light weight buoy usually a life preserver as the floating source; - The buoy can be operated from a boat and only houses the GNSS antenna; - The antenna offset from the sea surface is small, typically positioned 50-250 mm above it. - Wave motion compensation is not applied.	**Non-autonomous light weight buoys** from Cheng (2005)	Application examples: - Altimeter calibration; - Tidal datum transfer; - River and lake water level monitoring; - Sea surface mapping;
Advantages: - Economical and simple to construct, with low cost materials, that are readily available; - Easily portable with their small size; - No need to monitor and correct the tilt due to wave motion; - Low centre of mass.	Disadvantages: - Logistical support is required throughout the entire deployment (personal and boats); - Lack of versatility with the tether required; - Deployment restricted in rough sea state; - Short duration deployments.	

Table 2.2 – Advantages, disadvantages and applications of the autonomous light weight design GNSS buoy. Based on tables from Watson (2005) and Marshall and Dennys (2008).
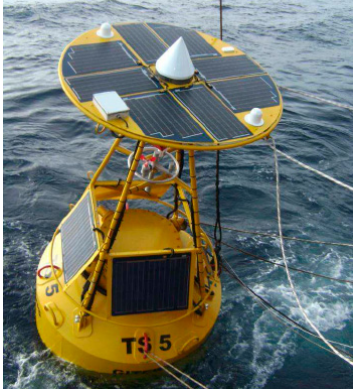
Description:	Autonomous oceanic buoys	Application examples:
- A light weight buoy that houses all the components: GNSS antenna, the receiver and the battery; - Can operate autonomously, either: anchored, drifting or tethered. - The antenna offset from the sea surface is small, typically positioned 50-250 mm above it. - Wave motion compensation is not applied.	 From Parker (2007)	- The same as for the non-autonomous light weight buoy design; - Applications requiring autonomous operations for a few days (up to one week); - Calibration of tide gauges.
Advantages: - The same as for the non-autonomous light weight buoy design; - Reduced logistics considerations with autonomous operations of up to a few days depending on the battery.	Disadvantages: - Deployment restricted in rough sea state; - Short duration deployments up to a few days, depending on the battery.	

Table 2.3 – Advantages, disadvantages and applications of the autonomous large scale design GNSS buoy. Based on tables from Watson (2005) and Marshall and Dennys (2008).

Description:	Autonomous large scale	Application examples:
- A large scale rugged buoy that houses the GNSS system and the wave motion compensation system in addition to power storage and generation and data communications; - Can operate autonomously for long periods; - The antenna reference point is typically a few metres above the sea surface.	 From Shöne *et al.* (2011)	- Tsunami monitoring; - Tidal datum determination; - Absolute altimeter calibration; - Applications at high seas requiring long period autonomous operation.
Advantages: - Can operate for a long periods and in rough sea conditions; - Additional sensors can be integrated in the buoy such as meteorological instruments.	Disadvantages: - High cost; - Not easily portable, requires a ship equipped with winches and cranes for deployment; - Requires the correction of buoy inclination and heave caused by wave motion. - Reliability issues with power generation, power storage and communications.	

To estimate the instantaneous Sea Surface Height (SSH), GNSS measurements are used to estimate epoch-by-epoch positions of the antenna. The estimated value is corrected for inclination and heave motion of the buoy. For the determination of the height component, the accuracy of the GNSS positioning should be at centimetre level, in order to allow accurate measurements of SSH.

The antenna should be carefully installed in order to avoid additional multipath and interference from the buoy components; the antenna reference point should be positioned in the buoy body frame including the vertical distance to the buoy fluctuation line. The wave rider type buoys does not requires monitoring the inclination and heaving. The effect of the tether on the buoyancy and dynamics of the buoy may affect its performance as a sea level sensor.

The first applications of GNSS buoys were constrained to the precise relative positioning over relatively short distances [Watson, 2005]. With new developments in GNSS data processing, precise kinematic absolute positioning is feasible with PPP and this will extend the use of GNSS buoys to a potential unrestricted global application [Luo *et al.*, 2010]. The output of GNSS instantaneous velocity derived from Doppler measurements can be used to obtain wave measurement data on GNSS buoys [Doong *et al.*, 2011].

2.3. Ship based systems

The principle of sea level measurement with GNSS on board ships is essentially the same as described for GNSS buoys, since the ship is a floating platform. Anchored or drifting buoys may be considered as approximately static stations at the sea, while the vessel moves and is capable of measuring the instantaneous SSH along a planned navigation trajectory. In addition it is usually easy to install permanent or temporary GNSS receiver stations on board ships, without additional costs, and less vulnerable to damage when compared to buoys. On board data acquisition may be periodically monitored for any malfunction and the communication systems of the ship may be used to download precise corrections for PPP processing. GNSS on board ships are equivalent to moving tide gauges that may complement observations at fixed positions, being a valuable source for marine geodesy and ocean dynamic studies.

The nomenclature of the ship motions floating at sea is summarized in table 2.4 with a translation to Portuguese language, from Paulo (1997).

	High frequency		Permanent or long period		Axis
	Portuguese	**English**	**Portuguese**	**English**	
Translations	avanço	surge	-	-	y
	deriva	sway	abatimento	drift	x
	arfagem	heave	imersão	sinkage	z
Rotations	cabeceio	pitch	caimento	trim/tilt	x
	balanço	roll	adornamento	heel/tilt	x
	guinada	yaw	guinada	swing	z

Table 2.4 – Ship body frame coordinate axes and ship motion nomenclature, from Paulo (1997).

For the determination of the SSH, the ship's GPS antenna geodetic heights have to be corrected for all the motions of the platform due to the following effects:

- Motion of the ship caused by wave effects (pitch, roll and heave);

- Variation of the ship's sinkage and tilt due to variations of load (such as fuel consumption);

- Hydrodynamic effects as the ship "rises" the bow wave, when moves through the water. This may cause a variation of sinkage (lifting) and trim;

- Squat effects, causing variation in the sinkage and pitch.

The ship motion caused by the wave action (roll, pitch and heave) is measured by on board systems usually based on inertial systems. The correction required to refer the measured quantities to the ellipsoid adopted in the GNSS positioning, neglecting the deflection of the vertical, is given by the following expression (see figure 2.1):

$$h_{corr} = h_{GPS} - (z_0 - z_{rot}) - heave$$

$$\begin{bmatrix} x \\ y \\ z \end{bmatrix}_{rot} = R_{pitch} \cdot R_{roll} \cdot \begin{bmatrix} x \\ y \\ z \end{bmatrix}_0 =$$

$$= \begin{bmatrix} \cos(pitch) & 0 & -\sin(pitch) \\ 0 & 1 & 0 \\ \sin(pitch) & 0 & \cos(pitch) \end{bmatrix} \cdot \begin{bmatrix} \cos(pitch) & 0 & -\sin(pitch) \\ 0 & 1 & 0 \\ \sin(pitch) & 0 & \cos(pitch) \end{bmatrix} \cdot \begin{bmatrix} x \\ y \\ z \end{bmatrix}_0$$

(2.1)

Where $\begin{bmatrix} x \\ y \\ z \end{bmatrix}_0$ is the position of the GNSS antenna in the body frame coordinate system;

$\begin{bmatrix} x \\ y \\ z \end{bmatrix}_{rot}$ is the position of the GNSS antenna after correction for pitch and roll (two

rotation matrices);

h_{corr} is the GPS antenna height after correction for pitch and roll and heave

h_{GPS} is the uncorrected GNSS antenna height, from the GNSS positioning solution;

z_0 is the GNSS antenna height in the ships body frame.

z_{rot} is the GNSS antenna height in the ships body frame after rotation of pitch and

roll, in accordance with equation 7.1.

The heave correction is a simple transformation, applied as a vertical translation of the

antenna.
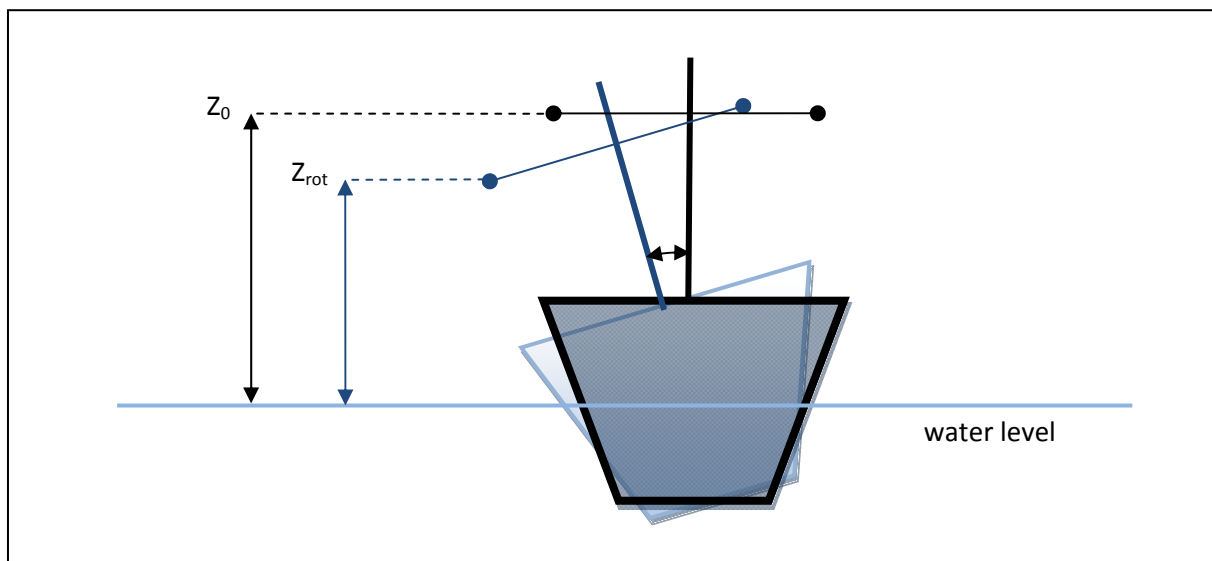
Figure 2.1 – Ships antenna height variation due rotation in roll.

As the ships moves through the water, a system of hydrodynamic forces change its trim and increases draft when compared to a neutral position. The algebraic sum of both, sinking and trimming is called squat. Recent research indicates that the squat depends on the ship speed-through-water, size and shape of the ship´s hull and the cross section of the waterway. Squat may be estimated by empirical or analytical (based on fluid dynamics computations) methods [Briggs, 2006; Jachowski, 2008]. Direct determination of squat, for each ship class, are possible from photogrammetric or levelling methods from a fixed survey station onshore. Another method for direct determination of squat is based on precise positioning with on board GNSS receivers and one GNSS receiver on board an escort vessel. The on board GNSS receivers measure the variations in trim and list, while the GNSS on the escort vessel allows the determination of unperturbed water level at the measurement position [Reiking and Härting, 2007].

The variation of the ship's load during a mission (for example due to fuel consumption) will cause a variation in the ship's draft. A change in the distribution of ship's load will cause variations in the ship´s trim and list. The value of these variations may be inferred from the ship´s stability tables.

2.4. Motion compensation of buoys and ships

Many applications at sea require the correction of the effect on the GNSS receiver antenna caused by the vessel motion (roll, pitch, yaw and heave). This is a key point when measuring the Sea Surface Height with GNSS. The most common sensors used for motion compensation of floating platforms, either buoys or ships, are based on inertial systems. Inertial systems can be found in various forms, but the core is constituted by the sensor assembly, composed by a set of three orthogonal accelerometers (linear acceleration sensors) and three gyroscopes (angular rate sensors). The sensors are placed in the same frame which sense the same motions as the vessel (strapdown system) or in a stabilized platform (gimballed system). The sensor assembly can be used separately, as a so-called Inertial Measurement Unit (IMU), or can be combined with a navigation computer to form an Inertial Navigation System (INS) [Deurloo, 2011].

The output of the IMU provides an estimation of sum of the accelerations caused by all the forces acting on the ship including the gravity vector and the external forces due to the wave and wind action on the ship. The data from the accelerometers can be low-pass filtered to

remove high frequency variations due to wave-action, quick turns and sudden velocity variations and provide a good estimate of the gravity vector; the direction from which the angular rate sensors measures the angular displacements (roll, pitch and yaw). The heave is determined by double integration of the linear acceleration sensed in the apparent vertical direction [IHO, 2005].

When the vessel undergoes a systematic acceleration, whose duration exceeds the time constant of the low pass filter applied to the accelerometers measurements, such as prolonged turns, or velocity variations, the centripetal or tangential acceleration are sensed as a horizontal acceleration causing a deflection of the apparent vertical from the true vertical with the consequent errors on the measurements. This is particularly critical in hydrographic surveying where the ship must follow planned survey lines and prolonged ship turns are made after the end of each line to align with the next. An error in the vessel tilt and heave will induce an error in the depth measurement.

The best option for ship motion determination is to use an integrated GNSS/IMU or GNSS/INS system. There are several modes of integrating these two systems [Deurloo, 2011]. The result allows the achievement of higher accuracies and is less vulnerable to vessel turns, when compared using these systems in standalone mode. If a two GNSS antenna system is used then additional ship rate of turn information can be used for the correction of the apparent vertical motion. Usual system accuracies, at 95% confidence level, are 0.05º for roll and pitch, 0.2º for yaw and 10 cm or 10% of heave height whichever is greater [IHO, 2005].

2.5. Satellite altimetry

Satellite radar altimetry is a modern technology, a result of the space era, used to map the ocean surface. The principle of radar altimetry was envisaged in the sixties. A brief historical resume is given in Benveniste, J. (2011), starting with the first observation of the Earth surface made by the SkyLab mission, launched in 1973. The radar measurement principles are described in the literature [Chelton *et al.*, 2001].

Radar altimetry measures the distance between the satellite and the surface bellow, transmitting radar pulses, the echoes of which are bounced back from the surface, whether ocean, ice cap, sea-ice, desert, lake, or river. The altimeter system is made up of a set of independent instruments and measurement processes, which combine to allow the

determination of the SSH in an absolute coordinate reference frame and other secondary quantities of interest related with the sea state.
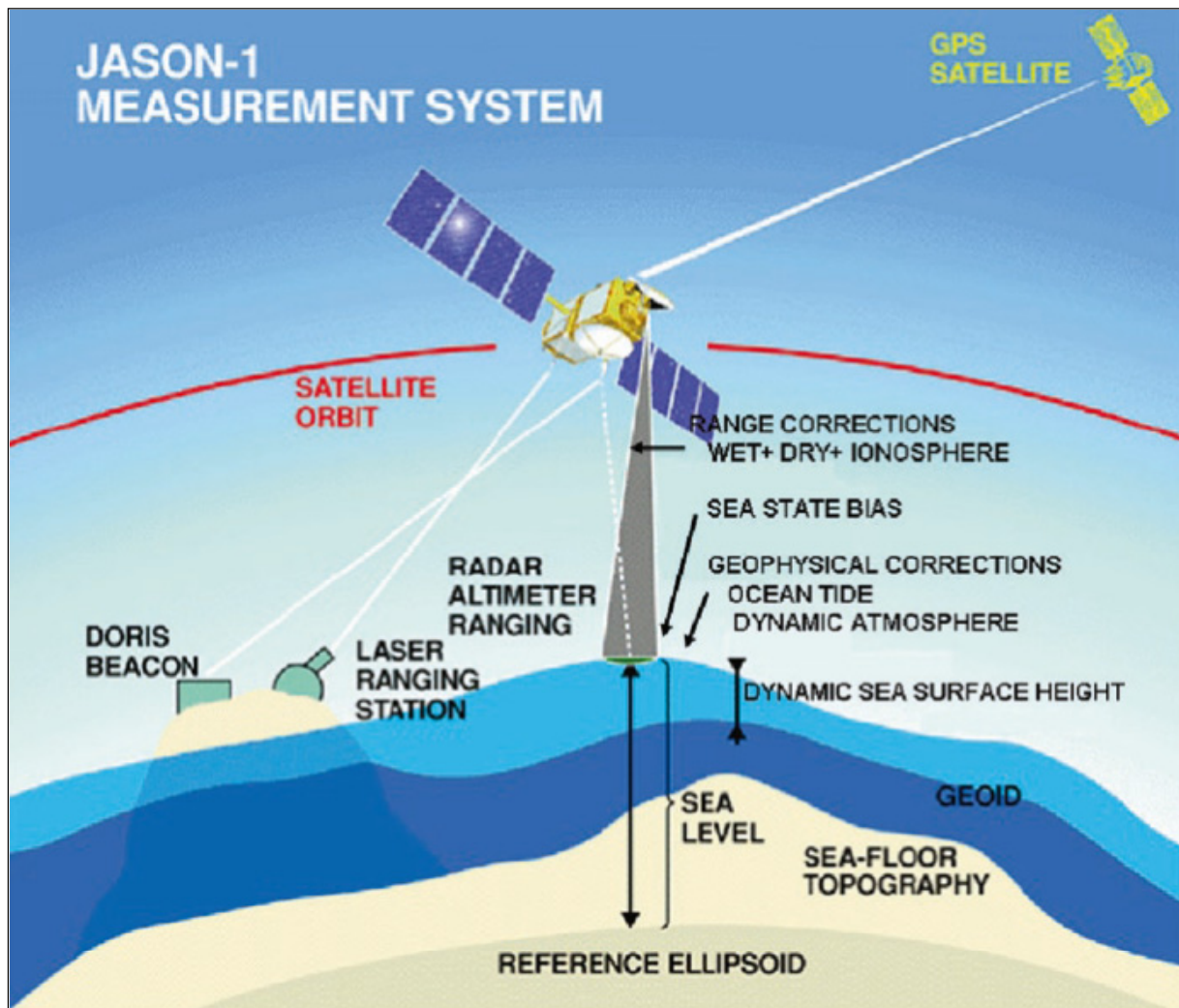
Figure 2.2 – Schematic illustration of the principle of satellite altimetry and the corrections applied to the altimeter observations of SSH (from Andersen and Scharroo, 2011).

The conceptual method for range determination is based on a signal, formed by a short pulse of micro-wave radiation, transmitted by the satellite towards the Earth. The signal interacts with the sea surface and part of it is returned to the satellite where the travel time is measured:

$$R = \frac{(t_r - t_t) \cdot c}{2}$$
(2.2)

Where R is the range;

t_t is the time of transmission of the signal by the satellite;

t_r is the time of reception of the signal by the satellite;

c is the velocity of propagation of electromagnetic waves.

In practice the range determination is significantly more complicated. Each altimetric measurement, provided in Geophysical Data Records (GDR), results from the average of thousand of returned pulses. This averaging procedure results in a SSH estimate every second, corresponding to a 6-7 km track profile for a Low Earth Orbit (LEO) satellite with an orbital altitude of about 1300 km, such as the JASON-1 and JASON-2 (1336 km). The SSH determination process can be divided into three basic components:

- Range determination from the satellite to the surface;
- Orbit determination in a Terrestrial Reference Frame and with respect to a reference ellipsoid;
- Corrections to the range due to atmospheric refraction, instrumental corrections, sea surface corrections and geophysical adjustments.

The accuracy of SSH determination from satellite altimetry measurements depends on the accuracy of the satellite orbit with respect to a Terrestrial Reference Frame and expressed relative to a reference ellipsoid. The determination of the satellite position at centimetre level accuracy requires a satellite tracking system that may incorporate different technologies, in a method designated as Precise Orbit Determination (POD). Most altimetry satellites support tracking by SLR (Satellite Laser Ranging), GPS and DORIS (Doppler Orbitography and Radiopositioning Integrated by Satellite). As illustrated in figure 2.2, the SSH is determined by:

$$SSH = h^{sat} - R \qquad (2.3)$$

Where h^{sat} is the height of satellite above the ellipsoid determined by POD.

2.5.1 Corrections to the altimeter radar range

The current accuracy of SSH determined from 1-Hz range measurements and precise orbit determination is aimed at the 2-3 cm [Dufau *et al.*, 2011]. To achieve this accuracy the satellite is assumed to be calibrated, its orbital position at the same accuracy level and the range measurement must be corrected from all possible error sources. The range and geophysical corrections fall into four groups [Andersen and Scharroo, 2011]:

- Instrumental corrections due to tracker bias, antenna gain pattern, Doppler shift, oscillator drift and pointing angle.
- Atmospheric refraction corrections due to dry gases, water vapour and ionospheric electrical charges.
- Sea-state bias caused by the difference between the distribution of the mean scattered surface and the actual sea level. This difference depends on the sea-state.
- Geophysical adjustments due to ocean tides, ocean tide loading, solid Earth tide, polar motion and atmospheric pressure loading.

To compute the corrected SSH, all the corrections are given in the GDR and must be added to the observed satellite raw range (or subtracted from the raw SSH), as represented in the following equation:

$$R = R_{obs} + corr =$$
$$= R_{obs} + \left(\Delta R_{inst} + \Delta R_{dry} + \Delta R_{wet} + \Delta R_{ion} + \Delta R_{SSB} + \Delta R_{ocean} + \Delta R_{earth} + \Delta R_{load} + \Delta R_{polar} + \Delta R_{atm} \right)$$

(2.4)

Where R_{obs} is the observed uncorrected raw range;

ΔR_{inst} is the instrumental correction;

ΔR_{dry} is the atmosphere refraction correction due to dry gases;

ΔR_{wet} is the atmosphere refraction correction due to water vapour;

ΔR_{ion} is the atmosphere refraction correction due to the ionosphere;

ΔR_{SSB} is the sea state bias correction;

ΔR_{ocean} is the ocean tide correction;

ΔR_{earth} is the solid Earth tide correction;

ΔR_{load} is the ocean tide loading correction;

ΔR_{polar} is the polar motion correction;

ΔR_{atm} is the atmospheric pressure loading correction.

2.5.2 Calibration of altimetry satellites

Calibration and validation are important performance requirements of altimeter missions to check the SSH measurement accuracy. Calibration and validation embraces a wide variety of activities, including the interpretation of information from internal calibration modes and validation of fully-corrected SSH estimates by using other independent measurement systems.

Considering the accuracy goal for SSH determination of about 2-3 cm or better, altimeter calibration represents and extremely challenging geodetic problem. The calibration and validation process starts before the satellite launch with rigorous laboratory calibration of all sensors and verification of the results from the altimeter processing system. After launch of the satellite, starts a verification phase of a few months, when engineering assessment and statistical assessment of the GDR is made with high priority. The results of the verification phase will lead to a tuning of the algorithms of the altimeter data processing system. Once the performance requirements are accomplished the GDR are released for scientific studies [Chelton *et al.*, 2001].

After the validation phase, the GDR should be systematically verified to check for integrity of the measurements and subtle bias or drift errors that may occur. This verification is based on the comparison with validated SSH from Earth's surface stations. Two main techniques have emerged in the global calibration effort of altimetric satellites: installation of absolute calibration sites (point calibration) and the utilization of tidal gauges networks (network calibration) [Chelton *et al.*, 2001; Watson, 2005]. In most basic form, the altimeter bias is defined as:

$$bias_{sat} = SSH_{sat} - SSH_{land} \tag{2.5}$$

Where SSH_{sat} is the SSH derived from the satellite;

SSH_{land} is the SSH derived from a Earth's surface station.

An absolute calibration site monitors successive passes of the altimeter satellite at a specific location. Site essential are the existence of accurate tide gauges and a means of referencing it to the same geographic reference system used for the satellite altimetry. Accurate estimates of the satellite orbit height as the satellite overflies the site are critical. Although satellite laser

ranging systems remain valuable for determining estimates of the orbit heights, over experiment sites, the DORIS and GNSS are also important tools for both satellite and tide gauge positioning in calibration experiments [Watson, 2005]. The calibration station is located along one of the satellite ground tracks, enabling the comparison of SSH for each over flight. The over flight frequency is higher if the comparison point is located at a crossover location [Watson, 2005]. The following methodologies can be used for satellite altimetry calibration:

- Dedicated calibration fixed platforms such as the Harvest oil platform off the central California [Haines *et al.*, 2010];

- Anchored buoys equipped with GNSS (see section 2.2);

- Ships equipped with GNSS and motion compensation systems (see section 2.3);

The tide gauge network technique relies on monitoring the satellite altimeter by a relative comparison with a nearby coastal tide gauge network. A time series of SSH_{sat} is compiled at a position relatively close to the tide gauge network (typically within 50 km). A tide gauge time series, SSH_{land}, is compiled for the same position using an ocean coastal dynamics model. The two time series are differenced and the resulting difference contains the drift of satellite altimeter and land motion at tide gauge. The primary difficulty is to estimate the land motion at the tide gauge network stations. In the same way as for the absolute calibration technique, space techniques such as DORIS and GNSS can be used for the determination of the vertical land motion at tide gauge stations. This calibration method, while sensitive to bias drift, is unable to detect time independent offsets. Also, issues of geographically correlated errors, from the uncertainty of ocean dynamic model are also present [Watson, 2005].

Satellite altimetry over the open ocean is a mature discipline. In contrast, the processing of altimetry data collected in the vicinity of coastal regions is still a challenge. Improved coastal altimetry GDR's have the potential to be benefit coastal ocean studies and applications and the demand is high, however the following additional problems must still be addressed:

- As the satellite approaches the coast, land effect influences the returned radar echo footprint as the leading edge of the footprint deviates from the satellite altimeter tracking gate and the waveform fails to conform to the Brown model. This effect requires a comprehensive and systematic analysis of the returned waveforms. For this analysis, the satellite transmits the waveforms to the ground where the geophysical

parameters are retrieved in post processing or retracked. Retracking is required to recover the waveforms at distances from the coast less than 5-10 km [Gommenginger *et al.*, 2011].

- In the open ocean the combination of on board satellite altimeter/radiometer is satisfactory in terms of accuracy and spatial resolution. This is not the case for coastal areas where the sea/land effect influences the radiometer performance and degrades its humidity measurements. The wet troposphere correction is complex and shows high temporal variations, with rapid variations in both space and time. Therefore also more accurate wet troposphere delay correction is required [Obligis *et al.*, 2011].

- Most range and geophysical corrections need special attention in the proximity of the coast, either because the signal is much larger or the correction is less accurate in coastal regions. In the deep ocean, recent investigations showed that ocean tide models have an accuracy of around 2-3 cm [Fok *et al.*, 2010]. However, the global ocean tide models still have errors exceeding 10-20 cm close to the coast, in comparison with coastal tide gauges [Ray, 2008]. Particularly in shallow water regions, the largest accuracy gain in altimetric SSH determination is expected to come from improvement of tidal models [Andersen and Scharroo, 2011].

Chapter 3. GNSS observations and error sources

Currently two GNSS are available for public use: the very well-known and widely used USA NAVSTAR GPS and the Russian GLONASS. Two other GNSS are being implemented: the European GALILEO and the Chinese COMPASS. These systems are briefly described in annex A.

The key point for any positioning methodology is the definition of adequate observation models, the implementation of efficient algorithms and mitigation of all potential error sources that may affect the observations. As a result of the un-differenced nature of PPP, all errors caused at the satellite, propagation, environment, and receiver need to be mitigated. The mitigation can be carried out by modelling, estimating, making single station observation combinations or using differential techniques.

3.1. GNSS observables

There are three types of GNSS observations (observables) that can be used to compute the PVT (Position, Velocity and Time) solution: pseudorange, carrier phase and Doppler or phase variation with respect to time. Pseudorange and carrier phase observations are related to the distance between the satellite and the receiver's antenna, referring to the emission and reception time. The Doppler observation is related to the topocentric range rate of the satellite.

3.1.1. Pseudorange

As a first approximation, the pseudorange is a measure of the distance between the satellite and the receiver's antenna, referring to the epochs of emission and reception of the signal. The transmission time of the signal is measured by correlating identical pseudorandom noise (PRN) codes generated by the satellite with those generated internally by the receiver.

The geometric distance, ρ_r^s, between the receiver, r, and the satellite, s, is equivalent to the time interval of propagation of a signal, τ, needed to travel from the satellite to the receiver, times the velocity of propagation, c:

$$\rho_r^s = c \cdot \tau = c \cdot (tt_r - tt^s) \tag{3.1}$$

Where tt_r is the signal reception true time;

tt^s is the signal transmission true time. By true time it is meant a time epoch measured by a uniform and perfectly synchronized clock for both satellite and receiver.

The geometric distance depends on the receiver position, $\vec{X_r}(x_r, y_r, z_r)$, at signal reception true time, tt_r, and also on the position of the satellite, $\vec{X^s}(x^s, y^s, z^s)$, at signal transmitting true time, tt^s:

$$\rho_r^s(tt_r - tt^s) = \left|\vec{X_r}(tt_r) - \vec{X^s}(tt_r - \tau)\right| - \left|\vec{X_r}(tt_r) - \vec{X^s}(tt^s)\right| =$$
$$= \sqrt{\left(x_r(tt_r) - x^s(tt^s)\right)^2 + \left(y_r(tt_r) - y^s(tt^s)\right)^2 + \left(z_r(tt_r) - z^s(tt^s)\right)^2} \quad (3.2)$$

The receiver time is maintained by one clock built in the receiver and the satellite time is maintained by another clock built in the satellite. These clocks have errors when compared to a uniform time reference and are not synchronized. A uniform time system is kept continuously by the GNSS control system, the GNSS time. The GNSS can be either GPS time, GLONASS time or any other time system since it can be used as a GNSS true time reference.

The relation between true time and observed satellite clock time, t^s, and observed receiver clock time, t_r, is represented by the following equations:

$$tt_r = t_r - \delta t_r$$
$$tt^s = t^s - \delta t^s \quad (3.3)$$

where δt_r is the receiver clock bias and δt^s is the satellite clock bias.

Taking both, the satellite and receiver clock errors, into account, the derived distance corresponds to the true geometric range plus a set of errors with different physical meanings. This new distance is designated as pseudorange, P. It means the geometric distance plus a set of error terms. Accounting only for the clock biases the pseudorange observation equation is:

$$P_r^s(t_r) = c \cdot (t_r - t^s) = c \cdot (tt_r + \delta t_r) - c \cdot (tt^s + \delta t^s)$$
$$= c \cdot (tt_r - tt^s) + c \cdot (\delta t_r - \delta t^s) \quad (3.4)$$
$$= \rho(tt_r) + c \cdot (\delta t_r - \delta t^s)$$

The navigation message allows the user to compute the satellite position in an Earth Centered Earth Fixed (ECEF) coordinate system, $\vec{X^s}(x^s, y^s, z^s)$, and the satellite clock bias, δt^s. The unknowns are the receiver coordinates, $\vec{X_r}(x_r, y_r, z_r)$,, and the receiver clock bias, δt_r.

Note that the satellite position must be calculated at transmission true time. The GNSS satellites orbits have a radius of approximately 26000 km. The propagation time of the signal from the satellite to the receiver at the Earth's surface is approximately 0.07 sec. Since the satellite moves at 3800 m/s, during the transmitting period its position changes about 260 m. If the time of the received signal is used to compute the satellite position a significant error will occur.

The signal propagation time is estimated by the receiver as the time needed to align a replica of the internal PRN code with the one received from the satellite. The transmission time is equal to the reception time minus the signal propagation time, $(tt_r - tt^s)$, and can be estimated by subtracting the interval of propagation of the signal measured by the receiver:

$$tt^s = tt_r - (tt_r - tt^s) \Leftrightarrow t^s - \delta t^s = t_r - \delta t_r - \tau(tt_r - tt^s)$$
$$\Leftrightarrow t^s = t_r - \delta t_r + \delta t^s - (tt_r - tt^s) = t_r - \frac{P(t_r)}{c} \tag{3.5}$$

Note that the pseudorange is measured by the receiver clock at time, t_r, and not at true time, tt_r. This means that the range, referred at true time, parcel in equation $P_r^s(t_r) = \rho_r^s(tt_r) + c \cdot (\delta t_r - \delta t^s)$ should be at receiver time, and this requires an additional correction. For this correction, the geometric distance at true time can be linearized around the known nominal receiver time:

$$\rho_r^s(tt_r) = \rho_r^s(t_r) + \frac{d\rho(t_r)}{dt}(tt_r - t_r) = \rho_r^s(t_r) - \frac{d\rho(t_r)}{dt}\delta t_r \tag{3.6}$$

The parcel $\frac{d\rho(t_r)}{dt}\delta t_r$ represents the variation of the geometric range due to an error δt_r in the receiver clock. The satellite radial velocity $\frac{d\rho(t_r)}{dt}$ is zero if the satellite is at the closest point of approach and may reach values up to 800 m/s for elevation angles equal to 10 degrees. This means that the error in the geometric distance induced by this parcel will be smaller than 1 mm if the receiver clock error is estimated with an accuracy of 1 μs. Because of this small contribution, the term $\frac{d\rho(t_r)}{dt}\delta t_r$ is often neglected and simply not listed in all equations explicitly [Leick, 1995].

Taking all the previous corrections into consideration observation equation for pseudorange, accounting only for the receiver and satellite clock errors, is represented as follows:

$$P_r^s(t_r) = \rho(t_r) + c \cdot (\delta t_r - \delta t^s) =$$
$$= \sqrt{\left(x_r(t_r) - x^s(t^s)\right)^2 + \left(y_r(t_r) - y^s(t^s)\right)^2 + \left(z_r(t_r) - z^s(t^s)\right)^2} + c \cdot (\delta t_r - \delta t^s) \tag{3.7}$$

The above pseudorange model is used in basic absolute positioning with GNSS with pseudorange single frequency observations, such as the Standard Positioning Service with the GPS C/A code.

3.1.2. Carrier phase

The carrier phase is a measure of the phase of the received satellite signal relative to the receiver-generated carrier phase at reception time. The measurement is made by shifting the receiver-generated phase to track the received phase. This is equivalent to integrating the carrier phase Doppler magnitude and keeping track of changes in the observed range to the satellite. Thus a phase difference is measured rather than the time difference which matches identical codes.

The phase is obtained from integrating the frequency between epochs:

$$\varphi = \int_{t_0}^{t_1} f \cdot dt \tag{3.8}$$

Assuming a constant frequency, setting the initial phase $\varphi(t_0) = \varphi_0$, and taking into account the time span which the signal needs to propagate from the transmitter to the receiver, the phase observed at the receiving site at time, t, is equal to the phase at the transmitter $t - \tau$, where τ is the propagation time:

$$\varphi_r = \varphi_0 + f(t - \tau) \tag{3.9}$$

In the case of a moving receiver or transmitter, the received frequency is shifted due to the Doppler effect. This means that the received frequency by the receiver, f^s, differs from the transmitted or nominal frequency, f, apart from relativistic effects, by a value that is proportional to the relative velocity receiver-transmitter, $\frac{d\rho}{dt}$ (see next section):

$$\Delta f = f^s - f = -\frac{1}{c} \cdot \frac{d\rho}{dt} \cdot f^s \tag{3.10}$$

The GNSS receiver measurement is equivalent to the beat phase, or the difference between the received satellite phase, $\varphi^s(t_r)$, and the phase of a reference carrier generated by the receiver, $\varphi_r(t_r)$:

$$\varphi_r^s(t_r) = \varphi^s(t_r) - \varphi_r(t_r) \tag{3.11}$$

Where:

$$\varphi^s(t_r) = f^s \left(t_r - \frac{\rho}{c}\right) - f^s \cdot \delta t^s$$
$$\varphi_r(t_r) = f_r \cdot t_r - f_r \cdot \delta t_r \tag{3.12}$$

Where f^s is the received satellite frequency, affected by the Doppler shift;

f_r is the frequency generated internally by the receiver;

δ_r is satellite clock error;

δ_r is receiver clock error.

And this leads to:

$$\varphi_r^s(t_r) = \varphi^s(t_r) - \varphi_r(t_r) = -f^s\frac{\rho}{c} - f^s \cdot \delta t^s + f_r \cdot \delta t_r + (f^s - f_r)t_r \tag{3.13}$$

During signal tracking the received carrier phase and the corresponding integer count since lock-on are continuously modeled and frequently measured. In this way, the changing oscillator frequency is accounted for. Every time the phase is measured the coefficients of the phase tracking loop model are updated [Remondi, 1984]. The term $(f^s - f_r)t_r$ can be neglected if the difference $(f^s - f_r)$ if its value is small (a difference of 10^{-3} Hz causes an error less than 1 mm), if the oscillators are instable, then their behavior should be modeled [Hofmann-Wellenhof, 1992]. This leads to a simplified equation:

$$\varphi_r^s(t_r) = \varphi^s(t_r) - \varphi_r(t_r) = -f^s\frac{\rho}{c} - f^s \cdot \delta t^s + f_r \cdot \delta t_r \tag{3.14}$$

The GNSS receiver is able to measure the fractional phase at initial lock-on and to keep track of changes in the cycles as the distance between satellite-receiver changes, until a loss of lock occurs. However, the number of cycles (full carrier phase waves) between the satellite and the receiver cannot be accounted for at the initial signal acquisition and it is an ambiguous integer number. This is called the integer carrier phase ambiguity, N, a number that remains

constant when tracking is continued without loss of lock. The observed carrier phase, $\varphi_r^s(t_r)$, is composed by two terms:

$$\varphi_r^s(t_r) = \Delta\varphi_r^s(t_r - t_0) + N \tag{3.15}$$

Where $\Delta\varphi_r^s(t_r - t_0)$ is the observed fractional phase measured at time t_r augmented by the number of integer cycles since the initial epoch at lock on, t_0;

N is the ambiguous carrier phase integer ambiguity at lock on.

The equation for carrier phase observation after substituting and changing the sign convention:

$$\Delta\varphi_r^s(t_r - t_0) = f^s \frac{\rho}{c} + f^s \cdot \delta t^s - f_r \cdot \delta t_r + N \tag{3.16}$$

This equation can be simplified to a more generic and simplified expression $(f^s = f_r = f)$ in units of cycle:

$$\begin{aligned}\varphi_r^s = \Delta\varphi_r^s(t_r - t_0) &= f\frac{\rho}{c} + f(\delta t^s - \delta t_r) + N \\ &= \frac{1}{\lambda}\rho + \frac{c}{\lambda}(\delta t^s - \delta t_r) + N\end{aligned} \tag{3.17}$$

The carrier phase observation is converted to metric units by multiplying by the wavelength:

$$\Phi_r^s = \rho + c(\delta t^s - \delta t_r) + \lambda \cdot N \tag{3.18}$$

3.1.3. Doppler

The Doppler effect is the phenomenon of frequency shift of a propagating wave due to the relative motion of the emitter and the receiver. Let $v_\rho = \frac{d\rho(t_r)}{dt}$ represent the radial velocity between receiver and satellite. The received signal as a frequency of [Xu, 2007]:

$$f_r = f\left(1 + \frac{v_\rho}{c}\right)^{-1} \approx f\left(1 - \frac{v_\rho}{c}\right) \tag{3.19}$$

where f is the transmitted frequency.

There is a close connection between phase and Doppler measurements. Doppler measurements give the instantaneous phase variation and the integrated Doppler over a period of time gives the accumulated phase variation:

$$D = f - f_r = f \frac{v_\rho}{c} = \frac{v_\rho}{\lambda} = \frac{d\rho}{\lambda dt} = \frac{d\varphi}{dt} \tag{3.20}$$

The observation equation for Doppler measurements can be obtained by differentiating the carrier phase observation equation with respect to time:

$$
\begin{aligned}
D = \frac{d\varphi}{dt} &= \frac{d\rho}{\lambda dt} - c \frac{d\delta t_r}{\lambda dt} + c \frac{d\delta t^s}{\lambda dt} - \delta_f + \varepsilon = \\
&= \frac{d\rho}{\lambda dt} + f \frac{d(\delta t^s - \delta t_r)}{dt} - \delta_f + \varepsilon
\end{aligned}
\tag{3.21}
$$

Where δ_f is the frequency correction due to the relativistic effect;

ε is the remaining error.

Effects with low frequency variations such as the ionosphere and troposphere are canceled out.

3.2. Error sources in GNSS observables

A GNSS signal is formed at satellite electronics, transmitted by an antenna, propagated trough the space, received by an antenna and processed by the receiver electronics. The GNSS range related error sources are defined as all the influences that apply directly to the geometric distance measurement, since the formation of the signal at the satellite to the processing output at the receiver. All these errors should correspond to one parcel in the observation equation for pseudorange and carrier phase measurements and are represented as follows:

δt_r: receiver clock error (in seconds);

δt^s : satellite clock error (in seconds);

δ_{rel}: relativistic effects (in metres);

δ_{trop}: slant neutral atmosphere delay effects (in metres);

$\delta_{ion,f}$: ionospheric delay (in metres);

$\delta P_{mult,f}$: pseudorange multipath error (in metres);

$\delta \Phi_{mult,f}$: carrier phase multipath error (in metres);

$\delta a_{r,f}$: combined receiver antenna offset and phase centre variation (in metres);

$\delta a^{s,f}$: combined satellite antenna offset and phase centre variation (in metres);

$bP_{r,f}$: receiver pseudorange bias (in metres);

$bP^{s,f}$: satellite pseudorange bias (in metres);

$b\Phi_{r,f}$: receiver carrier phase bias (in metres);

$b\Phi^{s,f}$: satellite carrier phase bias (in metres);

δ_{wnd}: carrier phase wind up error (in cycles);

εP_f: pseudorange observation noise and other unmodelled effects (in metres);

$\varepsilon \Phi_f$: carrier phase observation noise and other unmodelled effects (in metres);

f: to indicate if the error is frequency dependent;

r: to indicate if the error is receiver dependent.

s: to indicate if the error is satellite dependent.

These observation errors will be discussed in detail later on this chapter, can be divided into three main groups (receiver, satellite and frequency dependent, see table 3.1) and summarized as follows:

- Satellite dependent effects: antenna offset and antenna phase centre variations;
- Signal propagation effects: ionosphere propagation, neutral atmosphere propagation and multipath;
- Receiver dependent effects: clock error, antenna offset and antenna phase centre variations;
- Relativistic effects: frequency effect, path range effect and Earth's rotational effect;
- Carrier phase windup effect.

Table 3.1 – Summary of GNSS observation errors and its dependency on the receiver, satellite, frequency and observation type (pseudorange or carrier phase).

Error type		Depending on…			
		Receiver	Satellite	Frequency	Obs. type
Rec. clock error	δt_r	Yes	No	No	No
Sat. clock error	δt^s	No	Yes	No	No
Relativity	δ_{rel}	Yes	Yes	No	No
Troposphere	δ_{trop}	Yes	Yes	No	No
Ionosphere	$\delta_{ion,f}$	Yes	Yes	Yes (known relation)	Different sign
Multipath	$\delta P_{mult,f}$	Yes	Yes	Yes	Yes
	$\delta \Phi_{mult,f}$	Yes	Yes	Yes	Yes
Rec. antenna offset	$\delta a_{r,f}$	Yes	No	Yes	No
Sat. antenna offset	$\delta a^{s,f}$	No	Yes	Yes	No
Receiver bias	$bP_{r,f}$	Yes	No	Yes	Yes
	$b\Phi_{r,f}$	Yes	No	Yes	Yes
Satellite bias	$bP^{s,f}$	No	Yes	Yes	Yes
	$b\Phi^{s,f}$	No	Yes	Yes	Yes
Windup	δ_{wnd}	Yes	Yes	Yes	Carrier phase only

Other error sources that affect the accuracy of the PVT solution are related with the satellites orbits accuracy and with receiver site displacements due to Earth's deformation. The receiver site displacements include the effects caused by the solid Earth tide, rotational deformation due to polar motion and Earth's deformation due to mass loading. These satellite-receiver signal and site dependent errors will be discussed later, on the next subsections of this chapter.

3.2.1. Satellite and receiver hardware delays

The hardware delay is caused at the satellite or receiver hardware by electronic components such as the RF and signal processing stages (other than clock biases). When combining signal processing by all components together, several delays can occur, as illustrated in figure 3.1 for the legacy GPS signals (those signals transmitted by the satellite block IIR class, before modernization). A similar phenomenon can also be observed in the receiver when it generates the signal replica.

L1 ($154f_0$)
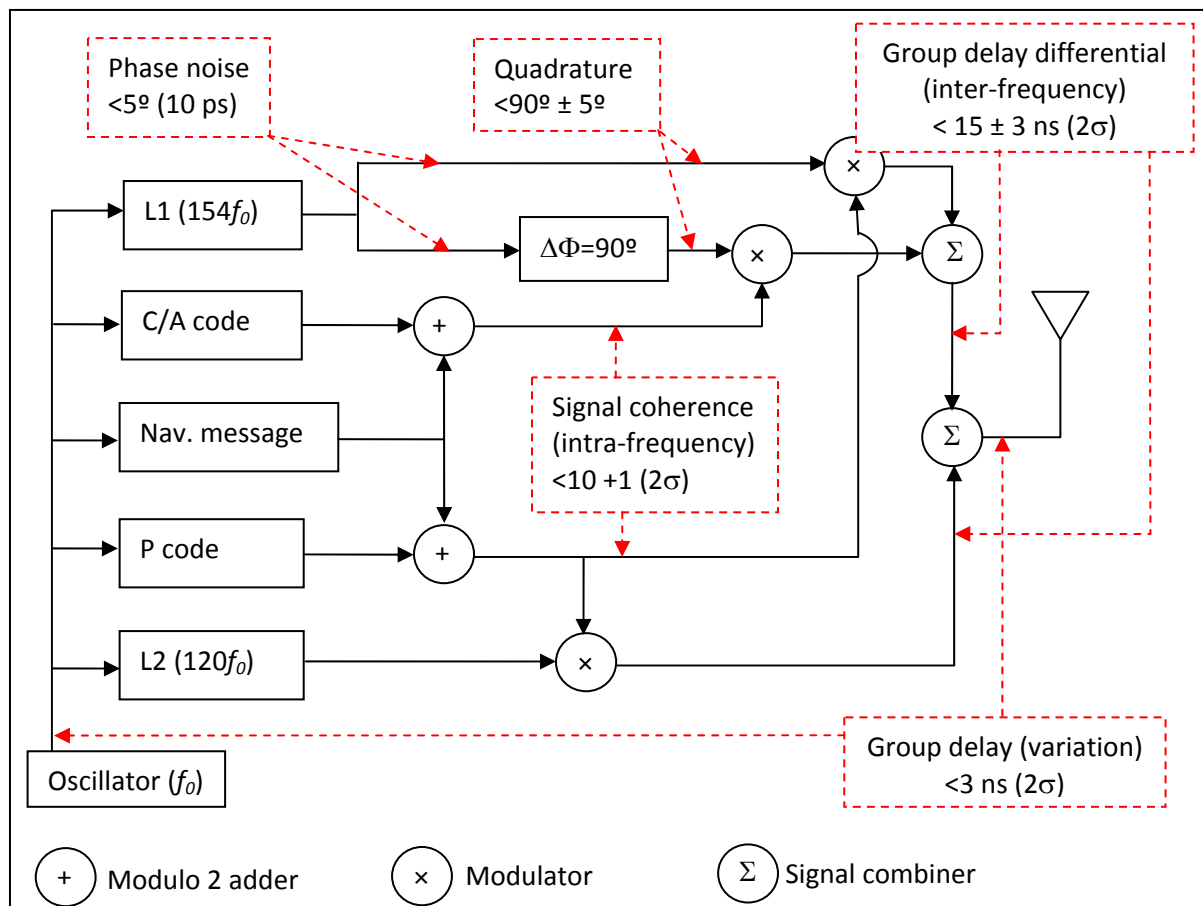
Figure 3.1 – GPS satellite hardware biases (based on Wells *et al.* [1987] and IS-GPS-200F [2011]).

From the IS-GPS-200F (2011) the hardware delay signal tolerances for the GPS signal are, with reference to the sections of the mentioned publication:

- Section 3.3.1.3, phase noise: the carrier phase should be tracked with and accuracy of 0.1 radians rms. This is equivalent to 5 degrees or 10 ps for the GPS frequencies;

- Section 3.1.1.5.1, quadratures: the two L1 components are modulated by the C/A code and the P code in phase quadrature (the C/A signal lagging the P signal by 90 degrees) within 0.1 radians.

- Section 3.3.1.7.1, group delay: "group delay is defined as the delay between the signal modulated output of a specific satellite (measured at the antenna phase centre) and the output of that satellite on-board frequency source; the delay consists of a bias term and an uncertainty. The bias term is of no concern to the user segment since it is included in the clock correction parameters". The group delay uncertainty shall not exceed 3.0 ns (2σ).

- Section 3.3.1.7.2, group delay differential (inter-frequency): "the group delay differential consists of random plus bias components...the absolute value of the mean

differential delay shall not exceed 15.0 ns…the variation about the mean shall not exceed 3.0 ns (95% probability)". Corrections for the bias components of the group delay differential are provided in the navigation message using parameters designated as Total Group Delay (TGD) and Inter-Signal Correction (ISC).

- Section 3.3.1.8, signal coherence (intra-frequency): The average difference between the chips of the signals modulated on the same carrier frequency, the L1 P – L1 C/A and L2 P – L2 C, shall not exceed 10 ns. The variable time difference shall not exceed 1 ns (95% probability).

A note on the TGD and ICS [IS-GPS-200F, 2011]:

- The TGD is only for the benefit of single frequency (L1 P or L2 P) users. It is necessary by the fact that the SV clock offset estimates transmitted by the navigation message are based on two frequency ionospheric corrections. For the case of ionospheric-free data combination, the TGD bias is zero, by definition (when using L1 P and L2 P). The user who uses only L1 P or L2 P shall apply this correction with the following equations:

$$\delta t_{L1P}^s = \delta t^s - TGD$$

$$\delta t_{L2P}^s = \delta t^s - \left(\frac{f_1^2}{f_2^2}\right) TGD$$

(3.22)

- The ISC accounts for the inter-signal biases between L1 P – L2 P, L1 P – L1 C/A and L1 P – L2 C, based on measurements made for each satellite during manufacture and may be subsequently updated on-orbit. For maximum accuracy the single frequency user must make modifications to account for this inter-frequency delay with the following equations:

$$\delta t_{L1C/A}^s = \delta t^s - TGD + ISC_{L1C/A}$$

$$\delta t_{L2C}^s = \delta t^s - TGD + ISC_{L2C}$$

(3.23)

When combining code and phase observations in point positioning, hardware biases become a major concern. These biases that cannot be eliminated tend to merge with other parameters and may alter the estimated values. Follows a summary of the way each bias affects the estimation process [Banville *et al.*, 2008]:

- Satellite code biases are mostly eliminated from the code observations by using the satellite clock corrections (from the broadcast message or the IGS) along with the appropriate TGD and ICS.

- Receiver code biases tend to propagate into code residuals and to the estimates of other parameters, such as the receiver coordinates.

- Satellite phase biases are different for each satellite on each carrier frequency and they tend to merge into the ambiguity parameters. This is not a problem when using the ionosphere-free combination because the ambiguities are no longer integers. For ambiguity resolution, this aspect becomes a major concern.

- Receiver phase biases are expected to be the same for each satellite but dependant on frequency. They will tend to merge into several parameters, such as the receiver clock, the phase ambiguities and potentially to the coordinate estimates.

3.2.2. Ionosphere effect

The ionosphere, extending from 50 to 1000 km above the Earth, is characterized by a highly dynamical plasma density, which is difficult to model and acts as dispersive medium (frequency dependent) for the propagation of electromagnetic waves. Different regions of the ionosphere are produced by different chemical components, affected by different wavelengths of the radiation of the Sun, with the harder solar radiation, the X rays, penetrating farther into the atmosphere and the less extreme UV radiation being stopped at greater heights where they produce ionization [Klobuchar, 1996].

To understand the behavior of radio signals transmitted through a medium it is necessary to know the refractive index of that medium. The refractive index is the ratio of the speed of light in vacuum, c, and the speed of light in the medium, v:

$$n = {}^c\!/_v \tag{3.24}$$

The refractive index of the ionosphere is usually associated with Eduard Appleton and is known as the Appleton-Hartree formula, or Appleton-Lassen formula, or simply as the Appleton formula [Davies, 1989]. For the L-band, this formula can be simplified to an accuracy of better than 1% given by the following expression [Klobuchar, 1996]:

$$n = 1 \pm \frac{N_e e^2}{2\epsilon_0 m \omega^2} = 1 \pm \frac{N_e e^2}{8\pi^2 \epsilon_0 m f^2} = 1 \pm \frac{e^2}{8\pi^2 \epsilon_0 m} \cdot \frac{N_e}{f^2} = 1 \pm 40.30 \cdot \frac{N_e}{f^2} \tag{3.25}$$

Where N_e is the electron density and has the units of reciprocal metres cubed;

e is the is the electron charge ($-1.602 \cdot 10^{-19}$ C);

m is the rest mass of a electron ($9.109 \cdot 10^{-31}$ kg);

ϵ_0 is the permittivity of free space ($8.854 \cdot 10^{-12}$ F/m);

$\omega = 2\pi f$ where f is the operating frequency in Hz.

The propagation in a dispersive medium such as the ionosphere causes an advance in the phase and a delay in the pseudorange. Considering the propagation along the ray path s, the ionosphere delay can be modeled by the following expressions:

For the carrier phase (advance): $\delta\Phi_{ION} = -\frac{40.3}{f^2}\int_s N_e ds = -\frac{40.3 \cdot TEC}{f^2}$ (3.26)

For the code (delay): $\delta P_{ION} = +\frac{40.3}{f^2}\int_s N_e ds = +\frac{40.3 \cdot TEC}{f^2}$ (3.27)

Where TEC is the abbreviation for Total Electron Content, which is the integrated electron density integrated along the signal path. The TEC is expressed in electrons/m^3 or in TEC units (TECU) where one TECU is defined as 10^{16} electrons/m^3. The TEC is a function of time of day, user location, satellite elevation angle, season, ionizing flux, magnetic activity, sunspot cycle and scintillation. The daily variability normally ranges between 10^{16} and 10^{19}, with the minimum intensity occurring around midnight, high latitude, high elevation and solar minimum activity, and the maximum occurring at mid-afternoon, low latitude and solar maximum activity [Kaplan and Hegarthy, 2006].

The above expressions represent the TEC along the signal propagation path, TEC_ρ. The value for TEC along the zenith direction, TEC_z, can be computed from models. To derive the TEC in the signal propagation path from the TEC in the zenith direction, a slant factor or mapping function has to be introduced, which depends on the zenith angle of the signal path [Xu, 2007]:

$$TEC_\rho = TEC_z \cdot map(z)$$ (3.28)

Due to the dispersive nature of the ionosphere, the first-order propagation error may be fully corrected by combining the signal at two different frequencies. Traditionally PPP [Zumberge, 1997; Kouba and Héroux, 2001] uses ionosphere free pseudorange and carrier phase combination (see annex C):

The pseudorange ionosphere free combination: $P_{IF} = \frac{f_1^2 P_1 - f_2^2 P_2}{f_1^2 - f_2^2}$ (3.29)

The carrier phase ionosphere free combination: $\Phi_{IF} = \frac{f_1^2 \Phi_1 - f_2^2 \Phi_2}{f_1^2 - f_2^2}$ (3.30)

All the terms in the observation equation remain the same as the raw observations except the ambiguity, biases and noise, which are frequency dependent.

The ionosphere-free combination has some disadvantages:

- The combinations are not totally ionospheric free. They cannot remove the higher order of the ionosphere effects. Although the higher order ionosphere effects usually cover less than 0.1% of the total effects, they can still be several tens of centimetres of range error during times of high TEC [Parkinson and Klobuchar, 1996];
- The noise level increases by nearly a factor of three as compared to the noise level of the corresponding original code and carrier phase observables;
- The combined ambiguity values are not integers.

3.2.3. Tropospheric effect

The neutral atmosphere is the lower part of the atmosphere over the Earth's surface. It includes the lower part of the stratosphere and the troposphere. Unlike the ionosphere, this atmospheric layer is an electrically neutral layer and behaves as non-dispersive medium at GNSS carrier frequencies [Mendes, 1999]. In the literature the neutral atmosphere is referred as troposphere. To be precise, the term "troposphere" is a misnomer because roughly 25% of the delay effect is caused by atmospheric gases above the troposphere, specifically gases in the tropopause and stratosphere [Spilker, 1996].

While the effects of the electrically charged layer, the ionosphere, behaves as a dispersive medium at radio frequencies and its delay effect can be estimated using dual-frequency techniques, the non-dispersive nature of the neutral atmosphere can be more problematic, requiring modelling or other techniques to reduce its impact on the satellite positioning.

The electromagnetic signals are affected by the neutral atoms and molecules in the troposphere by an attenuation and refraction type effect, reducing signal power and causing a delay. The troposphere produces signal attenuation that is generally bellow 0.5 dB and delay effects on the order of 2 to 25 m. These effects vary both with the elevation angle because

lower elevation angles produce a longer path length through the troposphere and with the detailed atmospheric gas density profile *versus* altitude [Spilker, 1996].

There are two major tropospheric delay effects: a hydrostatic component and a wet component:

$$\delta_{trop} = \delta_{hyd} + \delta_{wet} \tag{3.31}$$

The first and larger component, δ_{hyd}, is the hydrostatic tropospheric delay. It is caused by the atmosphere dry gases composition, primarily by N_2 and O_2. The zenith dry atmosphere delay corresponds approximately to 2.3 m and varies with local temperature and atmospheric pressure in a reasonably predictably manner and its temporal variability is slow, less than 1% in a few hours.

The second component, the wet atmosphere delay, δ_{wet}, is caused by the atmosphere water vapour component. This effect is generally smaller than the dry atmosphere delay, about 1 to 50 cm at zenith (may vary between 1/10 and 2/10 the value of the dry atmosphere delay), but its temporal and spatial variation is much more significant, 10 to 20% in a few hours, and is less predictable even with surface humidity measurements [Spilker, 1996].

The estimation process is facilitated by a simple parameterization using mapping functions that describe the elevation angle dependence of the delay for the hydrostatic and wet delay components [Niell, 1996]. The total tropospheric in the slant direction delay can be parameterized by:

$$\delta_{trop}(e) = m_{hyd}(e) \cdot \delta_{hyd,z} + m_{wet}(e) \cdot \delta_{wet,z} \tag{3.32}$$

Where $\delta_{hyd,z}$ is the hydrostatic zenith delay;

$m_{hyd}(e)$ is the mapping function for the hydrostatic delay;

$\delta_{wet,z}$ is the wet zenith delay;

$m_{wet}(e)$ is the mapping function for the wet delay;

e is theelevation angle.

3.2.3.1. Hydrostatic zenith delay

The hydrostatic zenith delay can be accurately computed based on reliable surface pressure data using the formula of Saastamoinen (1972) as given by Davis *et al*. (1985) [IERS Conventions, 2010]:

$$\delta_{hyd,z} = \frac{(0.0022768 \mp 0.0000005) \cdot P_0}{f_s(\phi, H)}$$

$$f_s(\phi, H) = 1 - 0.00266 \cdot \cos(2\phi) - 0.00000028 \cdot H$$

(3.33)

Where ϕ is the geodetic latitude, H is station orthometric height and P_0 is the total atmospheric pressure in hPa (equivalent to milibars) at the antenna reference point.

If meteorological instrumentation is not available, local pressure data, required to compute the dry zenith delay, may be estimated with the empirical global model GPT [Boehm *et al.* 2007].

3.2.3.2. Wet zenith delay

There is currently no simple method to estimate an accurate value for the wet tropospheric delay. So in most applications, when sub-decimetre accuracy is sought, the wet zenith delay is estimated as an additional variable besides the other geodetic variables, such as the station position. This wet zenith tropospheric delay unknown is a common practice in PPP and has been implemented since the first PPP processing methods that can be used for kinematic positioning [Kouba and Héroux, 2001; Gao and Shen, 2001].

3.2.3.3. Mapping functions

The hydrostatic and wet mapping functions for the troposphere depend on the vertical distribution of the hydrostatic and wet refractivity above the geodetic sites. The general form of the hydrostatic and wet mapping functions is a continuous fraction, function of the elevation angle [Herring, 1992]:

$$\delta_{hyd,s} = \frac{1 + \dfrac{a}{1 + \dfrac{b}{1 + c}}}{\sin(e) + \dfrac{a}{\sin(e) + \dfrac{b}{\sin(e) + c}}}$$

(3.34)

where e is the elevation angle and a, b and c are coefficients which are different for the hydrostatic and wet components. These coefficients should be related with sufficient accuracy to account for the characteristics of the atmosphere at the time and position of the observation.

The updated Vienna Mapping Functions (VMF1) are recommended for high accuracy global applications. VMF1 are based on numerical weather models data for the determination of the coefficients. The hydrostatic and wet coefficients "a" (see equation 3.29), are given on a global grid sampling of 2.5 degrees north to south and 2.0 degrees west to east, and for each parameter there are four files per day, at 0, 6, 12 and 18 hours Universal Time [Boehm *et al.*, 2006a]. VMF1 are currently the mapping functions providing globally the most accurate and reliable geodetic results [IERS Conventions, 2010]. The use of VMF1 requires the availability of files with the coefficients to be interpolated for the station and observation. The coefficients are provided in files that can be downloaded at http://ggosatm.hg.tuwien.ac.at/DELAY/GRID, with a latency of 34 hours.

The Global Mapping Functions (GMF) are empirical mapping functions, in the tradition of the Niell Mapping Function (NMF) [Niell, 1996], whose parameters are determined from site coordinates and day of the year. NMF were widely used mapping functions because is easy to implement and one of the best among the empirical mapping functions, prior to GMF [Mendes, 1999].

The GMF are based on an expansion of VMF1 parameters into spherical harmonics, up to degree and order 9, on a global grid. Their parameters are calculated using only station latitude, longitude (not in the NMF, which are symmetrical along the equator), height and day of the year. The results for the comparison of GMF and NMF with VMF indicate that [Boehm *et al.*, 2006b]:

- The regional height biases and annual errors of NMF are significantly reduced with GMF;

- GMF agrees much better with VMF1, however it was found a slight degradation in the short-term precision and climate anomalies phenomena such as the El Niño cannot be accounted for with such empirical mapping function.

GMF are easy to implement, were developed with the goal to be more accurate than the NMF. It can be used in replace of the VMF1, when the highest accuracy is not required

[IERS Conventions, 2010]. This makes GMF the preferable mapping function for use in PPP.

3.2.4. Relativity corrections

Einstein's special relativity is based on two postulates [Ashby and Spilker, 1996]:

- No inertial system is preferred. The equations expressing the laws of physics have the same form in all inertial systems.

- The speed of light is a universal constant independent of the state of motion of the source. Any light ray moves in the inertial system of coordinates with constant velocity, c (the speed of light in the vacuum), whether the ray is emitted by a stationary or by a moving source.

The formula of the special relativity effects caused by a constant motion of a moving inertial coordinate system viewed from a resting inertial coordinate is given by [Xu, 2007]:

$$\frac{\Delta t - \Delta t'}{\Delta t'} = \frac{\Delta s - \Delta s'}{\Delta s'} = \frac{f - f'}{f'} = \frac{1}{2}\left(\frac{v}{c}\right)^2 \qquad (3.35)$$

where: $\Delta t, \Delta s, f$ is the time interval, length and frequency measured by a system at rest;

$\Delta t', \Delta s', f'$ is the time interval, length and frequency measured by a moving system with constant speed;

v is the speed of the moving system with respect to the system at rest.

This indicates that:

- $\frac{\Delta t}{\Delta t'} > 1$, the time interval viewed at the system at rest is shorter that the time interval viewed in the system at constant speed,

- $\frac{\Delta s}{\Delta s'} > 1$, the length viewed at the system at rest is shorter that the length viewed in the system at constant speed.

- $\frac{\Delta f}{\Delta f'} < 1$, the frequency observed in the moving system increases when compared to the frequency observed at the system at rest.

Einstein's general relativity incorporates gravitation by the principle of equivalence: The laws of physics are the same in a uniformly accelerated reference frame or in a uniform gravitational field.

The mathematics of general relativity is extremely complex. However for the treatment of relativistic effects on GPS, only a simplified approach is required. Note that the right-hand side of the above equation represents the unit mass kinetic energy ($v^2/2$) scaled by the speed of light. That is, the speed relativistic effects may be interpreted as the effects caused by kinetic energy due to motion. Analogous effects may also be caused by potential energy due to the gravity field. To equation 3.35 is added one parcel due to the potential energy [Xu, 2007]:

$$\frac{\Delta t - \Delta t'}{\Delta t'} = \frac{\Delta s - \Delta s'}{\Delta s'} = \frac{f - f'}{f'} = \frac{1}{2}\left(\frac{v}{c}\right)^2 + \frac{\Delta U}{c^2} \tag{3.36}$$

where ΔU is the difference of the Earth's gravitational potential at the satellite and the potential at the receiver position due to the presence of a gravitational field U.

The concept of satellite ranging is based on the observed time difference between transmission and reception of a radio signal. Two factors affect the concept of time:

- Motion. The satellite is moving with reference to a receiver and this causes the satellite clock tends to be slower than the receiver clock;
- Gravity. The satellite is subjected to the Earth's gravity field, which is less than the forces on the receiver at the Earth's surface. This phenomenon causes the satellite clock to run faster.

3.2.4.1. The frequency effect

If the satellite transmits at frequency f' then all receivers observe frequency f , due to relativistic effects. This offset depends on the relative velocity and on the potential energy of the receiver relative to the satellite, and can be determined by equation 3.36.

This frequency offset has been implemented in the satellite and the users do not need to consider this effect, considering its orbital velocity and the gravitational potential with reference to the geode. For GPS, the offset of its fundamental frequency (10.23 MHz) is approximately 0.00457 Hz and the satellite clock frequency is set in conformity.

For the receiver at the Earth's surface, its frequency is also affected due to the velocity of rotation of the Earth. The effect can be represented analogously by equation 3.36, where $\Delta U = 0$ and v is the velocity of the receiver due to the Earth rotation.

These effects are corrected by the receiver's software, both the satellite orbital motion and receiver (Earth rotation) motion [Xu, 2007].

3.2.4.2. The path range effect

The path range effect due to the general relativity can be computed by [Holdridge, 1967]:

$$\Delta\rho_{rel} = \frac{2GM_E}{c^2} \ln \frac{\rho^j + \rho_i + \rho_i^j}{\rho^j + \rho_i - \rho_i^j} \tag{3.37}$$

where G is the Gravitational constant;

M_E is the Mass of the Earth;

ρ_i is the Geocentric distance to the receiver;

ρ^j is the Geocentric distance to the satellite;

ρ_i^j is the Distance between the receiver and satellite.

This correction has the units of length and a maximum value of 2 cm.

3.2.4.3. The orbit eccentricity effect

The orbit eccentricity effect is given by [Xu, 2007]:

$$\Delta t_e = \frac{2}{c^2}\sqrt{GM_{Earth}a}\, e \sin E + const = \frac{2}{c^2}\left(\vec{r^j} \cdot \vec{v^j}\right) + const \tag{3.38}$$

Where G is the universal gravitational constant;

M_{Earth} is the mass of the Earth;

a is the semi-major axis of the orbit;

E is the eccentric anomaly of the orbit;

e is the eccentricity of the orbit;

$\vec{r^j}$ is the satellite position vector;

$\vec{v^j}$ is the satellite velocity vector.

The second term is a constant that cannot be separated from the clock offset. This total correction has already been taken into account in the GPS orbits determination and is broadcasted in the navigation message by the parameters of the clock error polynomial [IS-GPS-200F, 2011]. Therefore, this correction only needs to be considered in the satellite orbit determination [Xu, 2007].

3.2.4.4. The Earth's rotational effect

This Sagnac-like effect is caused by the variation of the distance satellite-receiver during signal transmission due to the Earth's rotation and can reach up to 30 m for a fixed receiver rotating with the earth. This correction must also be applied for kinematic GNSS receivers that are not fixed at the Earth's surface. The receiver velocity vector with respect to an inertial reference is given by:

$$\vec{v_r} = \vec{\omega_e} \times \vec{r_i} + \vec{v_i} \tag{3.39}$$

where: $\vec{\omega_e} \times \vec{r_i}$ is the velocity vector of the receiver due to the Earth's rotation;

$\vec{\omega_e}$ is the angular velocity of the Earth;

$\vec{r_i}$ is the receiver geocentric position vector;

$\vec{v_i}$ is receiver velocity vector with reference to the Earth's surface.

The first term on the right hand side of equation 3.30 is the velocity due to the Earth's rotation and the second term is the kinematic velocity vector of the receiver related to the Earth's surface.

The correction due to the Earths rotational during to the signal propagation time can be presented as [Ashby and Spilker, 1996]:

$$\Delta\rho = \frac{(\vec{r_i} - \vec{r^s}) \cdot \vec{v_r}}{c} \tag{3.40}$$

Where $\vec{r^s}$ is the satellite geocentric position vector.

A kinematic motion of 100 km/h can cause additional Sagnac effect up to 2 m.

3.2.5. Carrier phase wind-up effect

As described in a previous section, from the incoming signal, the receiver extracts carrier phase and code measurements that provide information which allows the estimation of the range equivalent quantities between the transmitter and receiver. In particular, the observed carrier phase is actually the difference of the relative phase between the phase of the incoming electromagnetic wave and the reference phase generated receiver. GPS satellites transmit Right Hand Circularly Polarized (RHCP) electromagnetic waves. This implies that the observed carrier phase depends on the relative orientation of the satellite and receiver antennas. Therefore, a relative rotation between the transmitter and receiver antennas will influence the carrier phase measurement, and the result will be an apparent variation of the range. A relative rotation of either receiver or satellite antenna around its bore axis will change the carrier phase up to one cycle (one wavelength). This effect is designated as the "phase wind-up" effect [Wu *et al.*, 1993].

Wu *et al.* (1993) noted that antennas having different spatial orientations (which is inevitable on long baselines) will measure different relative phases at the same transmit time (*i.e.*, when sampling the same carrier wavefront) that can persist at the level of 1 cm or more after double differencing. For point positioning this effect is quite significant as it can reach up to half wavelength. They provide a model of this "phase windup" which eliminates the anomaly and modestly improves residuals and solution stability. The phase wind-up correction can be evaluated as given by the following equations (see figure 3.2):
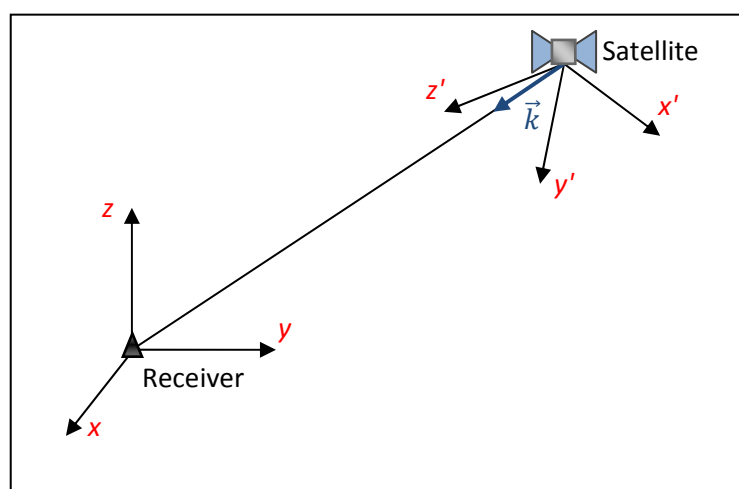
Figure 3.2 – Phase wind-up satellite-receiver geometry.

44

$$\delta_{wnd} = sign(\xi)\,acos\left(\frac{\overrightarrow{D'} \cdot \vec{D}}{|\overrightarrow{D'}||\vec{D}|}\right)$$

$$\xi = \vec{k} \cdot \left(\overrightarrow{D'} \times \vec{D}\right) \tag{3.41}$$

$$\vec{D} = \vec{x} - \vec{k}(\vec{k} \cdot \vec{x}) - \vec{k} \cdot \vec{y}$$

$$\overrightarrow{D'} = \overrightarrow{x'} - \vec{k}(\vec{k} \cdot \overrightarrow{x'}) - \vec{k} \cdot \overrightarrow{y'}$$

where: $\vec{k}$ is the satellite-to-receiver unit vector (see figure 3.2);

$\vec{D}$ and $\overrightarrow{D'}$ are the dipole vectors of the satellite and receiver;

x, y and *z* are satellite body coordinate unit vector (as in the satellite antenna offset);

x', y' and *z'* are the receiver local coordinate unit vector (north, east, up).

For the most common terrestrial applications such as static surveying, the antenna does not suffer for rotations and therefore the error caused by the wind-up is small (of the order of centimeters. Note that a full rotation introduces an error of one wavelength, which is 0.19 m for L1, 0.24 m for L2) and can be estimated. For this reason, the wind-up is usually neglected on GPS applications that do not require centimeter level accuracy.

Due to its accumulative nature, the wind-up effect can be relatively large for certain applications with spinning antennas. This is the case, for guided rockets that use spinning rotation as a means of stabilization. An antenna mounted on the tip of such a spinning rocket will generate large values of wind-up [Garcia-Fernandez *et al.*, 2005].

For static point positioning, not correcting for unexpected wind-up effect due to relative satellite rotation while in orbital motion, will result in decimetre level positioning error. Rapid phase wind up error can occur in the case of eclipses (when a straight line, starting from the Sun, intersects the satellite and then the centre of the Earth, or when the line from the Sun intersects the centre of the Earth and then the satellite), when the satellite manoeuvres to reorient their solar panels toward the Sun [Kouba and Heroux, 2001].

For kinematic positioning there is additional wind-up due to receiver motion, but apply to all satellites approximately with the same magnitude. This means that the wind up effect due to receiver motion may be ignored without significant error, since it will be mostly absorbed into the receiver clock bias estimate [Tolman *et al.*, 2010] or can be estimated in an algorithm

that incorporates accurate ionospheric corrections and integrates three carriers ambiguity fixing in an undifferenced user navigation filter [Hernandez-Pajares *et al.*, 2004].

3.2.6. Antenna phase centre variation

The geometric distance between the satellite (at signal emission time) and the GNSS receiver is referred to the electronic phase centre of the two antennas. Two distinct situations must be considered: the phase centre of the transmitting signal at the satellite antenna and the phase centre of the incoming signal at the receiver antenna.

3.2.6.1. Satellite antenna phase centre correction

The requirement for satellite antenna phase centre correction derives from the separation between the GNSS satellite ECEF coordinates computed from orbital parameters and the antenna phase centre position in where the signal starts its propagation to the receiver. The broadcast GPS ephemerides are referred to the satellite phase centre [IGS-GPS-200F, 2011], therefore no correction is required. But this is not the case for IGS precise orbits and clocks.

IGS precise orbits and clocks are estimated using dynamic force models; therefore, the resulting orbital data refers to the centre of mass of the satellite. The separation between the centre of mass and the phase centre depends mainly on the satellite model. To correct the observation for this separation the user must know the satellite phase centre offsets and monitor the orientation of the offset vector in space, as the satellite orbits the Earth. A satellite body coordinate system must be defined to describe the antenna phase centre offset (see figure 3.3).

$\vec{z}$ axis – pointing to the centre of mass of the Earth, coinciding with the antenna pointing direction.
$\vec{y}$ axis – solar panel axis, kept perpendicular to the vector pointing to the sun.
$\vec{x}$ axis – perpendicular to the other axes, to form a right handed coordinate system.
$\vec{n}_{Sun}$ – Unit vector pointing to de sun. On the *xz* plane.
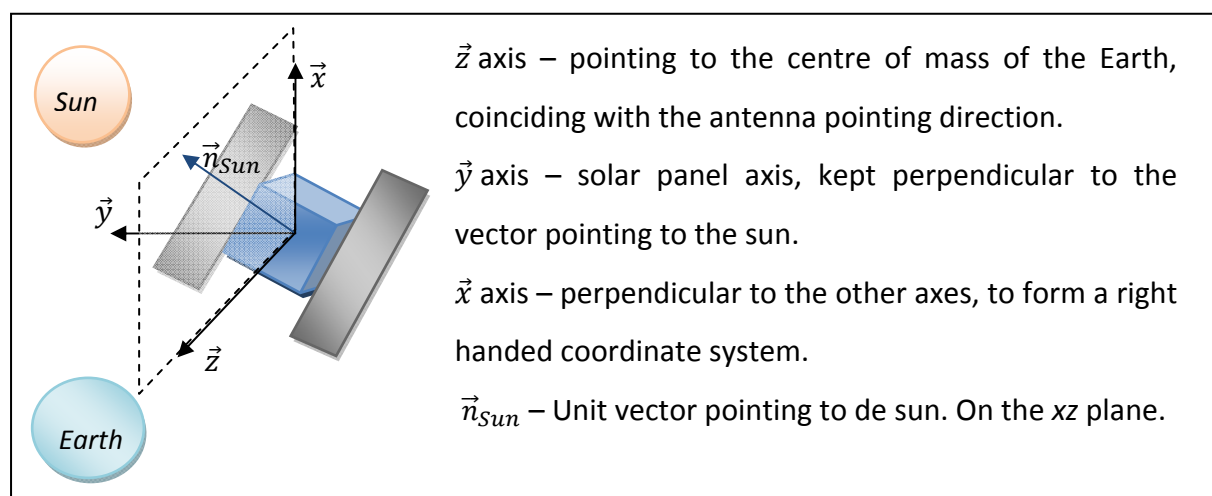
Figure 3.3 – Satellite fixed coordinate system (adapted from Kouba, 2009).

Since November 5, 2006 (GPS Week 1400), the IGS applies absolute phase centre corrections for both satellite and receiver antennas [Schmid *et al.*, 2007]. The current models for the GNSS satellites body frame antenna phase centre offset are available at from the IGS website at http://igscb.jpl.nasa.gov/igscb/station/general/general on Antenna Exchange Format (ANTEX) files.

The corrections are computed in the form of a geocentric displacement vector that is added to the satellite geocentric position vector. This requires the satellite body frame antenna offset vector to be transformed to a geocentric vector. The algorithm is described by Xu [2007].

3.2.6.2. Receiver antenna phase centre correction

The receiver antenna phase centre is not a fixed physical or geometrical mark that the user can refer to. The antenna phase centre depends on the elevation and azimuth of the incoming electromagnetic signal. This anisotropy is modeled by a phase centre offset from a physical reference point to the mean electrical phase centre pattern, with its elevation and azimuth dependent variations.

The current models for the GNSS satellites body frame antenna phase centre offset and variations are also available at the IGS website, in the same ANTEX files as for the satellite antennas.

The correction vector applies directly to the receiver antenna position vector after conversion to geocentric coordinates. If the antenna is on a moving platform, an additional correction may be required to compensate for motion tilting.

3.3. Observation equations

An observation equation expresses a measured value as a function of one or more unknowns. The GNSS observation equations used for positioning are described in this section focusing on the most important aspects only. For further information refer to the literature [Leick, 1995; Xu, 2006; Seeber, 2003].

For precise positioning all error sources should be accounted for. Taking all the effects that apply in the observations domain, as described in the last sections, the pseudorange and carrier phase observation equations, derived in 3.1., are completed with the terms, corresponding to each one of the mentioned effects:

Pseudorange
(in metres):

$$P_{r,f}^s = \rho + c \cdot (\delta t_r - \delta t^s)$$
$$+ \ \delta_{rel} + \delta_{trop} + \delta_{ion,f} + \delta P_{mult,f} + \delta a_{r,f} + \delta a^{s,f} + bP_{r,f} + bP^{s,f} + \varepsilon P \qquad (3.42)$$

Carrier phase
(in metres):

$$\Phi_{r,f}^s = \rho + c(\delta t^s - \delta t_r) + \lambda_f \cdot N_{r,f}^s$$
$$+ \ \delta_{rel} + \delta_{trop} - \delta_{ion,f} + \delta\Phi_{mult,f} + \lambda_f \cdot \delta_{wnd} + \delta a_{r,f} + \delta a^{s,f} + b\Phi_{r,f} \qquad (3.43)$$
$$+ \ b\Phi^{s,f} + \varepsilon\Phi$$

Some remarks:

- Terms that do not depend on the observation type neither the frequency, the geometric part: ρ, $c(\delta t^s - \delta t_r)$, δ_{rel}, δ_{trop} ;

- Terms that are common to pseudorange and carrier phase observations: ρ, $c(\delta t^s - \delta t_r)$, δ_{rel}, δ_{trop}, $\delta_{ion,f}$ (the ionospheric effect has the same magnitude but with different sign for pseudorange and carrier phase), $\delta a_{r,f}$, $\delta a^{s,f}$;

- Terms that are not common (may have a different value) to pseudorange and carrier phase observations: $N_{r,f}^s$, $\delta P_{mult,f}$, $\delta\Phi_{mult,f}$, δ_{wnd}, $bP_{r,f}$, $bP^{s,f}$, $b\Phi_{r,f}$, $b\Phi^{s,f}$.

3.4. Site displacement effects

This section describes the effect on reference marks on the Earth's crust displacements due to the effect of the external tide generating potential causing the solid Earth tide and displacements due to ocean tide loading.

3.4.1. Solid Earth tide

The solid Earth tide is a phenomenon of the deformation of the elastic body of the solid part of the Earth caused by the gravitational attracting force of close distance celestial bodies, the Moon and the Sun. The periodic vertical and horizontal site displacements caused by tides are represented by spherical harmonics of degree and order $n \times m$ characterized by the Love number, h_{nm}, and the Shida number, l_{nm}. The effective values of these numbers weakly depend on station latitude and tidal frequency and need to be taken into account when an accuracy of 1 mm is required for station position determination. However for 1 cm accuracy, only the second degree tides, supplemented with a height correction term are necessary [IERS, 2010]. The vector displacement of one station due to second degree tides is given by:

$$\Delta\vec{r} = \sum_{j=2}^{3} \frac{GM_j R_e^4}{GM_e R_j^3} \left\{ h_2 \vec{r} \left(\frac{3}{2} (\vec{R_j} \cdot \vec{r})^2 - \frac{1}{2} \right) + 3l_2 (\vec{R_j} \cdot \vec{r})(R_j - (\vec{R_j} \cdot \vec{r})r) \right\} \qquad (3.44)$$

Where GM_e is the gravitational parameter of the Earth;

GM_j is the gravitational parameters of the Moon (j=2) and de Sun (j=3);

R_e is the Earth's equatorial radius;

$\overrightarrow{R_j}$ is the unit vector from the geocenter to Moon or Sun and R_j is the magnitude of that vector;

$\vec{r}$ is the unit vector from the geocenter to the station and r is the magnitude of that vector;

h_2 is the nominal degree 2 Love number: 0.6078;

l_2 is the nominal degree 2 Shida number: 0.0847.

In the equation above, the terms factorized by h_2 and l_2 are the radial and transverse components of the tidal displacement. In order to account for the latitude dependence of the effective Love and Shida numbers, h_2 and l_2 shall have the form of [IERS, 2010]:

$$h_2 = 0.6078 - 0.0006 \frac{3 \sin^2(\varphi) - 1}{2}$$

$$l_2 = 0.0847 - 0.0002 \frac{3 \sin^2(\varphi) - 1}{2}$$

(3.45)

where φ is the geocentric latitude of the station.

3.4.1.1. Permanent part of tidal deformation

There is a permanent (time independent) part of the tidal deformation included in the degree 2 tidal potential. The projections of the permanent displacement into radial and the transverse components are, in metres [IERS, 2010]:

Radial component: $[-0.1206 + 0.0001 \cdot P_2(\sin\varphi)]P_2(\sin\varphi)$

(3.46)

Transverse component: $[-0.0252 + 0.0001 \cdot P_2(\sin\varphi)] \sin 2\varphi$

where $P_2(\sin\varphi) = (3\sin^2\varphi - 1)/2$

According with IERS (2010), "these are the components of the vector to be added to the conventional tide-free position to obtain the mean tide position. The radial component of this

restitution to obtain the "mean tide" values amount to about -12 cm at the poles and about +6 cm at the equator".

3.4.1.2. Tidal surfaces used in geodetic analysis

Site coordinates derived using the correction for the solid Earth tide formulation, are referred to the "conventional tide free" surface. A "truly tide free" surface (imagine the Earth alone, without the Sun, the Moon or any other attracting space body) is fundamentally unobservable, since the solid Earth tide formulation depends on nominal or conventional values for the Love numbers. To remove the permanent tide component and define a "truly tide free" surface, the fluid limit Love numbers must be used [IERS, 2010].

Restoring the permanent component of the Earth tide using the above formulation (see previous section) yields the "mean tide" (see figure 3.4). As stated by Dennis Milbert, the easiest way to imagine the "mean tide" surface (http://home.comcast.net/~dmilbert/softs/solid.htm, accessed on March 2012) "is to pretend that the Moon and Sun orbit around the Earth. Imagine them orbiting faster and faster, so that, on the average, they are "smeared" into bands around the Earth. Alternatively, you can imagine the Moon and Sun as chopped into tiny bits and spread around the Earth in a two-band system. These "average bands" will cause a permanent gravitational attraction leading to an increased equatorial bulge of the non-rigid Earth. In other words, most of the Earth's equatorial bulge is due to the Earth's rotation. But, there is a portion of the bulge that is created by the average tug of the Moon and Sun".

Resolution 16 of the 18th General Assembly of the IAG (1984) recommends the use of the "mean tide" surface for quantities associated with station displacements. However this recommendation has not been implemented in the algorithms used for tide modelling by the geodetic community in the analysis of space geodetic data [IERS, 2010].

The satellite altimetry GDR's comply with the above IAG resolution, however GNSS derived coordinates are referred to one ITRF or a "conventional tide free" surface.
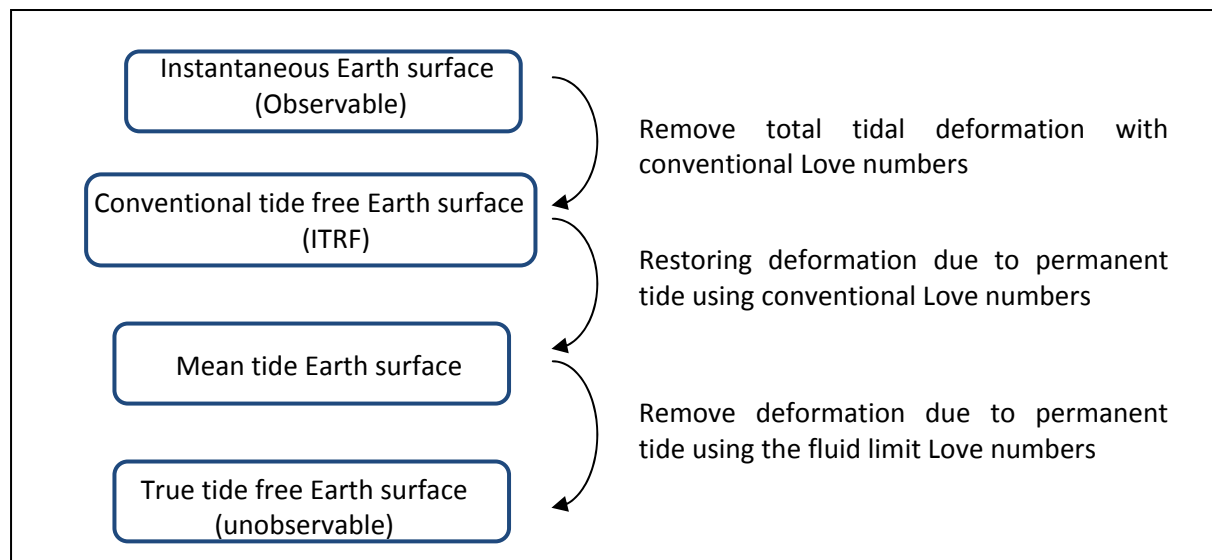
Figure 3.4 –Tidal surfaces used in geodetic analyse (adapted from IERS, 2010).

3.4.2. Rotational deformation due to polar motion

Polar motion is caused by the variation in position of the Earth's rotation axis. This variation causes deformations on the radial and horizontal position of points on the Earth's surface and is big enough to affect the geodetic position of a single point.

The Earth's flattening, combined with the obliquity of the ecliptic, results in a slow turning of the equator on the ecliptic, due to the differential gravitational effect of the Moon and the Sun. The slow circular motion, with a period of 26000 years is called precession and the other quicker motion with periods from 14 days to 18.6 years is called nutation. The nutation includes the Chandler wobble period of the Earth, about 14 months, with 9 m variation. [Vaníček and Krakiwsky, 1995].

From IERS (2010), the pole tide displacement (in milimetres) at given latitude (φ) and longitude (λ) is given by the following relations:

$$S_r = -33 \sin(2\varphi) \left(m_1 \cos(\lambda) + m_2 \sin(\lambda) \right)$$
$$S_\varphi = -9 \cos(2\varphi) \left(m_1 \cos(\lambda) + m_2 \sin(\lambda) \right) \qquad (3.47)$$
$$S_\lambda = 9 \cos(\varphi) \left(m_1 \sin(\lambda) - m_2 \cos(\lambda) \right)$$

Where S_r is the radial component (positive upwards);

S_φ is the meridian component (positive southwards);

S_λ is the parallel component (positive eastwards);

m_1 and m_2 are the time dependent offset of the instantaneous rotation pole from the mean, in arcseconds. More explicitly:

$$m_1 = x_p - \bar{x}_p \qquad \text{and} \qquad m_2 = -\left(y_p - \bar{y}_p\right)$$

Where $\bar{x}_p$ and $\bar{y}_p$ (in arcseconds) represent the IERS conventional mean pole position;

x_p and y_p (in arcseconds) represent the pole instantaneous position.

For a given epoch, these parameters can be downloaded from the IERS website. Taking into account that m_1 and m_2 vary at most 0.8 , the maximum radial displacement is approximately 25 mm and the maximum horizontal displacement is 7 mm in the horizontal component, for a single point [IERS, 2010].

3.4.3. Earth deformation due to mass loading

In addition to the solid Earth tide and pole tide, temporal variations of the mass distribution of the oceanic, atmospheric and hydrologic masses load and deform the Earth's surface, introducing site displacements effects. Since the Earth is not completely rigid, it deforms under this mass load variation. One can observe it as variations at the station in vertical and horizontal displacement, in gravity, tilt and in strain. This deformation is large enough to be detected with space based techniques as well as with terrestrial gravity observations.

The IERS Global Geophysical Fluid Center provides the geodetic community with models of geodetic effects (rotation, gravity and deformation) driven by the temporal variation of the Earth fluids. The fluids include fluid motions within the Earth such as the core and mantle, as well as the motions of surface fluids (oceans, atmosphere and continental water).

3.4.3.1. Ocean tide loading

The motion of ocean water mass caused by the ocean tides moves back and forth and these mass redistributions cause periodic loading of the ocean bottom. The displacement of the Earth's surface due to the load caused by the ocean tide is called the ocean tide loading. This loading effect can reach up to 10 cm at some coastal regions [IERS, 2010].

Computation of the displacements caused by the ocean tide loading depends on which tide model is used. Because of the strong dependence of the loading on the coast near tide, besides a global ocean tide model, a model near the coastlines will improve the estimates. The ocean

loading perturbation at a given location due to a given tidal harmonic is computed by integrating the tide height with a weighting function [Farrell, 1972], for all the ocean masses. Generally only 11 tidal harmonics are taken into account: the semi-diurnal harmonics M_2, S_2, K_2 and N_2, the diurnal harmonics O_1, K_1, P_1 and Q_1, and the long-period harmonics M_f, M_m, and M_{sa}. The total loading may be obtained by summing the effect of all harmonics. The displacement due to ocean tide loading for a given position and time is computed as a summation of the 11 significant harmonics (amplitude and phase) with corrections for the modulating effect of the 18.6 year lunar node [IERS, 2010]:

$$\Delta c = \sum_{k=1}^{11} f_k A_{ck} \cos(\omega_k t + \chi_k + u_k - \phi_{ck}) \tag{3.48}$$

Where Δc is the displacement component (north, south or west);

A_{ck} and ϕ_{ck} are the tidal amplitude and phase describing the loading response for a given site c and harmonic k;

f_k and u_k depend on the longitude of the lunar node;

ω_k is the angular velocity for harmonic k;

χ_k is the astronomical argument for harmonic k;

t represents the time.

For more information about the computation of f_k, u_k, ω_k and χ_k see Scherneck (1999) and Doodson and Warburg (1941).

An automated loading service is available at http://froste.oso.chalmers.se/loading// (accessed September 2012) which allows the computation of OTL parameters (amplitudes and phases) for the 11 most significant tidal harmonics at a given position and with the option to choose among 23 ocean tide models.

3.4.3.2. Environment loading effects

The loading effects caused by the environment also deform the surface of the Earth and may affect geodetic observations. These effects are caused by [van Dam and Wahr, 1998]:

- Variations in the horizontal distribution of atmospheric pressure;

- Non tidal ocean loading caused by the sea surface height variability as well as by density changes in the water column;

- Variations in the load of ground water, soil moisture, surface water (both in liquid form and as snow and glacial ice.

Atmospheric loading

Atmospheric pressure variations with periods of some days and months can be considered as loading functions on the Earth's surface and can induce quasi-periodic surface deformations. The largest variations are those associated with the passage of synoptic scale pressure systems. At the upper limit, displacements in the vertical component of 20-30 mm were observed with the passage of a 50 hPa variation in the atmospheric pressure. The corresponding deformation at the horizontal plan was observed at 2-3 mm, a factor of ten smaller in magnitude [Sun *et al.*, 1995].

The approach used to model atmospheric loading is based on the standard approach for deformation of the Earth by surface loads [Farrell, 1972]. It involves the convolution of Green's functions with a global surface pressure field. The source of global pressure fields derived from products by meteorological centers such as the European Center for Medium Weather Forecast (ECMWF) or the National Centres for Weather Prediction (NCEP).

The diurnal heating at the atmosphere causes surface pressure oscillations at diurnal S_1 and S_2 and higher harmonics. The recommendation is to calculate the station displacement using the Ray and Ponte (2003) atmospheric tidal model. Gridded values of the three-dimensional predicted surface displacements from the above model may be found at http://geophy.uni.lu/ggfc-atmosphere/tide-loading-calculator.html [IERS, 2010].

Non tidal ocean loading

The effects of non tidal ocean loading were investigated by van Dam *et al.* (1997). This effect is caused by density variations in the water columns that induce variations in the ocean bottom pressure. Ocean Global Circulation Models were used to compute the vertical surface displacements. The results show a maximum displacement as large as 20 mm with an average value of 3-6 mm for the other stations. However, errors in the Ocean Global Circulation Models make it difficult to accurately characterize the non tidal ocean loading.

More recently, Williams and Penna (2011) investigated this effect on GPS geodetic height data series. They found that the displacements are comparable in size to the atmospheric tide loading. Also, the combined correction reduced the error of the final static station height solution by 20-30%, to about 12-22 mm.

Hydrological loading

Changes in the soil moisture and groundwater volume, in addition to ice, introduce variations in mass load and lead to site displacement. The magnitude of this effect at a given position depends on the total surface load averaged over few hundred kilometers. A monthly model for the global variation of water storage and resultant Earth's displacement showed that this effect can cause vertical displacements up to 30 mm in some regions [van Dam *et al.*, 2001].

This page was intentionally left blank

Chapter 4. The concept of Precise Point Positioning

As in any positioning methodology, PPP comprises three components: the observations, the correction models and the adjustment procedure. The basic observations are the raw pseudorange and carrier phase, which are usually combined to form an ionosphere free observation. The correction models must be considered to eliminate or reduce undesirable effects and are applied to the observations, to the satellite clock and position and to the receiver station position. The adjustment procedure is implemented in the form of a sequential filter that adapts to varying receiver kinematic state.

The basic positioning model for PPP is the same as the one used in the standalone GPS receivers, available for users with unrestricted access to the Standard Positioning Service (SPS) for general purpose navigation. The most significant feature of PPP is the replacement of the satellite coordinates and satellite clock corrections being broadcasted with more accurate data from *e.g.* the IGS and the use of both pseudorange and carrier phase observations. Further refinements in PPP include the use of dual frequency code and carrier observations, taking into account receiver errors, satellite errors, relativity effects, propagation effects and site displacement effects. The primary observables are un-differenced code and carrier phase observations from a single receiver

PPP methodology is a two step procedure. Firstly, a global network provides control data that is processed by a global analysis centre. Secondly, the user receiver data is processed using the more precise products provided by the analysis centre. In this way PPP may be interpreted as a positioning method based on a GNSS service using corrections provided by a global network of tracking stations.

4.1. Observation space and state space GNSS corrections

Precise positioning is only possible when all the relevant error sources influencing the observations (above the centimetre level error) are corrected or mitigated. Various solutions are possible in relative positioning. One widely used is through observation differencing, which eliminates or significantly reduce all station or satellite correlated errors, allowing carrier phase ambiguity resolution.

The computation of a differencing solution using simultaneous observations from one or a network of reference receivers, as in Differential GNSS (DGNSS) estimates the corrections to the observation (usually the pseudorange) of each satellite observation or to the position of the observer as the lump sum of all the errors. This means that the sum of all the error effects, or the position error, at a reference station is computed and transmitted to the user as a single correction value. The user applies this correction value directly to its own observations or to the position coordinates, thus improving the positioning accuracy. In this way the correction is implemented in the observations space. The Differential method using correction to the observations is termed to use an Observation Space Representation (OSR), where the correction value represents the lump sum of GNSS errors for each observation [Wübbena, 2012].

Instead of computing only one correction for the observation, as a lump sum of all the errors at a reference station, as in the OSR, the state of the system, separated in individual error components, is determined from the observations of a network of reference stations. This information is transmitted to the user, so that a precise absolute position can be computed, taking into account that the provided information allows the correction of individual error terms on the user observation equations. An example of the application of this approach is the use of precise ephemeris and clock corrections. Most of the terms given in the observation equation can be treated as state parameters. This is termed as State Space Representation (SSR), where each error term is represented individually. In this way, PPP is a methodology based on SSR of GNSS errors.

4.2. Background

The term "Precise Point Positioning" was used for the first time by Héroux and Kouba [1995], when they proposed the use of "precise" satellite clock orbits and clocks for point positioning. Other works have been reported in this field based only on pseudorange observations [Lachapelle *et al.*, 1996; Elenriksen *et al.*, 1996; Gao *et al.*, 1997]. Their results are at the metre level accuracy, with the dominant error caused by the ionosphere, which could result in errors of several metres if not modelled or mitigated using dual frequency observations.

The theoretical foundation of PPP is documented in Zumberge *et al.* (1997a), a research group of the Jet Propulsion Laboratory (JPL) as a more efficient method to process and

analyze GNSS data from the IGS stations network, as the volume of GNSS reference stations data to analyze was huge and growing rapidly, and *"means to analyze this volume in a consistent, robust and economical manner is essential"*. This new data processing method, requires less computational effort, and makes the accuracy achieved at IGS for global solutions available to other users.

In Zumberge *et al.* (1997b) they computed orbits and clock information from a subset of a global GNSS network, with many of its stations equipped with an atomic clock. This was crucial when estimating 30 s interval satellite clock corrections, particularly when Selective Availability (SA) was active. With these high rate satellite clock corrections (when compared to the 15 min interval on standard IGS precise products), the kinematic positioning of moving receivers was achieved with an accuracy of approximately 7 cm (3D RMS), by comparison with static stations. At the time, the use of PPP was limited to static applications, because GPS data could be used only if collected at the exact same epochs for which there were high-quality clock corrections. This was so because the satellite clocks were dithered with a pseudo-random signal that made the clock errors unpredictable at other epochs. This was known as SA and was intended to limit the access to the more precise real-time positioning information only to authorized users.

In 1 May 2000 the US government changed its policy, and SA was turned off. This had an advantageous effect in PPP, allowing interpolation of the precise orbits and satellite clock corrections with significant less error. Witchayangkoon (2000) investigated PPP and achieved similar results to Zumberge *et al.* (1997a). He also investigated ambiguity fixing, error mitigation, the use of single frequency measurements and compared the results before and after SA was turned off. Bisnath and Langley [2001] and Bisnath [2004] proposed a geometric approach based on a kinematic sequential least squares filter to be used with data from LEO satellites equipped with GPS receivers for the purpose of Precise Orbit Determination (POD). GPS precise orbits and clock corrections were provided by the IGS. The achieved accuracy was at the submetre level.

Kouba and Heroux [2001] described a PPP approach using dual-frequency pseudorange and carrier phase observations along with IGS precise orbit products, with cm level accuracy. They emphasized error mitigation especially those related to the un-differenced observations. The data processing methodology was based on the ionospheric free combination and the troposphere zenith delay estimated as an additional unknown using mapping functions.

Additional correction terms were added to account for satellite antenna offsets, carrier phase wind-up, and site displacement effects (solid Earth tides, ocean tide loading and polar motion). This fundamental work provided the basic PPP methodology that can be implemented for static or kinematic positioning and may be considered as a traditional approach.

While early works focused primarily on static applications, there has been a continuous effort to extend PPP to kinematic applications addressing the convergence time and carrier phase ambiguity resolution.

Later works reported centimetre to decimetre accuracy by addressing these two aspects. Gao and Shen [2001] and Shen [2002] developed a new observation model based on the code-phase combination and addressed the problem of convergence time and ambiguity resolution by a "partial ambiguity fixing method".

Colombo *et al.* (2004) applied PPP to positioning mobile ground vehicles with an accuracy of 10 cm RMS. The convergence time tends to be slow in kinematic mode, about 30-40 min. They noticed an improvement in the consistency of point positioning when using more frequent clock corrections.

Chen *et al.* (2004) used PPP for sea level monitoring with a GPS buoy. They implemented a recursive least squares method to separate the variables that do not change or change slowly with time (ambiguities and tropospheric delay) from those parameters that change more rapidly with time. The estimated accuracy by comparison with relative positioning solution was 20 cm RMS.

Abdel-salam (2005) investigated ambiguity resolution and biases in PPP and used a new approach for estimating the absolute ionospheric delay. The application to kinematic ground, marine and airborne positioning was at the 20-30 cm accuracy level.

Zhang and Fosberg (2007) investigated the use of PPP for airborne LIDAR positioning and compared the results with satellite altimetry. The horizontal accuracies were not provided but for the aircraft height an accuracy of 10 cm RMS was estimated.

4.3. The traditional method

By "traditional method for PPP" the implementation similar to the one presented by Kouba and Héroux (2001) is meant, which is able to process kinematic data. This method can be summarized as follows:

- Use precise satellite and clock products;
- Combine un-differenced dual frequency pseudorange and carrier phase observations to form ionosphere free observation (IF);
- Implement in a sequential filter for the adjustment procedure;
- Estimate the zenith troposphere delay as an additional variable;
- Use correction models to estimate the value of the remaining error sources.

The vector of unknowns is formed by:

- Receiver position (3 variables per station): x_r, y_r, z_r
- Receiver clock error (1 variable per station): δt_r
- Wet zenith troposphere delay (1 variable per station): $\delta_{wet,z}$
- Carrier phase ambiguities (1 variable per satellite): N_{IF}

After the satellite clock corrections, and neglecting or correcting all remaining errors sources, the observation model results in the following simplified observation equations:

$$
\begin{aligned}
P_{IF} &= \rho_r^s(x,y,z) + c \cdot \delta t_r + m_{wet} \cdot \delta_{wet,z} = \\
&= \sqrt{(x^s - x_r)^2 + (y^s - y_r)^2 + (z^s - z_r)^2} + c \cdot \delta t_r + m_{wet} \cdot \delta_{wet,z} \\
\Phi_{IF} &= \rho_r^s(x,y,z) + c \cdot \delta t_r + m_{wet} \cdot \delta_{wet,z} + \lambda_{IF} N_{IF} = \\
&= \sqrt{(x^s - x_r)^2 + (y^s - y_r)^2 + (z^s - z_r)^2} + c \cdot \delta t_r + m_{wet} \cdot \delta_{wet,z} + \lambda_{IF} N_{IF}
\end{aligned}
\tag{4.1}
$$

This model is non-linear and thus makes it difficult to solve for the variables in the adjustment process using redundant observations. The observation model can be expanded in a Taylor's series [Kurtz, 1991] using a nominal receiver position $(x_{r,0}, y_{r,0}, z_{r,0})$:

$$
\begin{aligned}
P_{IF}(x_r, y_r, z_r, \delta t_r, \delta_{wet}) &= P_{IF}(x_0, y_0, z_0, \delta t_r, \delta_{wet,z}) + \\
&+ (x_r - x_0)\frac{\partial P_{IF}}{\partial x} + (y_r - y_0)\frac{\partial P_{IF}}{\partial y} + (z_r - z_0)\frac{\partial P_{IF}}{\partial z} + c \cdot \delta t_r + m_{wet} \cdot \delta_{wet,z} \\
\Phi_{IF}(x_r, y_r, z_r, \delta t_r, \delta_{wet}, N_{IF}) &= \Phi_{IF}(x_0, y_0, z_0, \delta t_{r,0}, \delta_{wet,0}, N_{IF,0}) + \\
&+ (x_r - x_0)\frac{\partial \Phi_{IF}}{\partial x} + (y_r - y_0)\frac{\partial \Phi_{IF}}{\partial y} + (z_r - z_0)\frac{\partial \Phi_{IF}}{\partial z} + c \cdot \delta t_r + m_{wet} \cdot \delta_{wet,z} + \lambda_{IF} N_{IF}
\end{aligned}
\tag{4.2}
$$

The partial derivatives for each one of the coordinates are:

$$\frac{\partial P_{IF}}{\partial x} = \frac{\partial \Phi_{IF}}{\partial x} = -\frac{x^s - x_{r,0}}{\sqrt{(x^s - x_{r,0})^2 + (y^s - y_{r,0})^2 + (z^s - z_{r,0})^2}} = -\frac{x^s - x_{r,0}}{\rho_0}$$

$$\frac{\partial P_{IF}}{\partial y} = \frac{\partial \Phi_{IF}}{\partial y} = -\frac{y^s - y_{r,0}}{\rho_0} \tag{4.3}$$

$$\frac{\partial P_{IF}}{\partial z} = \frac{\partial \Phi_{IF}}{\partial z} = -\frac{z^s - z_{r,0}}{\rho_0}$$

Each observation is equal to the observation model plus an error. For example, for the pseudorange: $P_{observed} = P_{model}(x_r, y_r, z_r, \delta t_r, \delta_{wet}) + \varepsilon_P$.

Taking the partial derivatives as above we form the following equations:

$$P_{IF,obs} - P_{IF}(x_0, y_0, z_0) = -\frac{x^s - x_{r,0}}{\rho_0} dx - \frac{y^s - y_{r,0}}{\rho_0} dy - \frac{z^s - z_{r,0}}{\rho_0} dz + c \cdot \delta t_r + m_{wet} \cdot \delta_{wet} + \varepsilon_P$$

$$\Phi_{IF,obs} - \Phi_{IF}(x_0, y_0, z_0) = -\frac{x^s - x_{r,0}}{\rho_0} dx - \frac{y^s - y_{r,0}}{\rho_0} dy - \frac{z^s - z_{r,0}}{\rho_0} dz + c \cdot \delta t_r + m_{wet} \cdot \delta_{wet} + \tag{4.4}$$

$$+ N_{IF} + \varepsilon_\Phi$$

The observation model can now be expressed using matrices $W = A \cdot dx + v$ for each satellite, where:

$$W = \begin{bmatrix} P_{IF,obs} - P_{IF}(x_0, y_0, z_0) \\ \Phi_{IF,obs} - \Phi_{IF}(x_0, y_0, z_0) \end{bmatrix} \text{ misclosure vector (observation - model)} \tag{4.5}$$

$$A = \begin{bmatrix} -\dfrac{x^s - x_{r,0}}{\rho_0} & -\dfrac{y^s - y_{r,0}}{\rho_0} & -\dfrac{z^s - z_{r,0}}{\rho_0} & 1 & m_{wet} & 0 \\ -\dfrac{x^s - x_{r,0}}{\rho_0} & -\dfrac{y^s - y_{r,0}}{\rho_0} & -\dfrac{z^s - z_{r,0}}{\rho_0} & 1 & m_{wet} & 1 \end{bmatrix} \text{ design matrix} \tag{4.6}$$

$$dx = \begin{bmatrix} dx \\ dy \\ dz \\ \delta t_r \\ \delta_{wet,z} \\ N_{IF} \end{bmatrix} \text{ vector of unknowns} \tag{4.7}$$

$$v = \begin{bmatrix} \varepsilon_P \\ \varepsilon_\Phi \end{bmatrix} \text{ vector of the error of the observations} \tag{4.8}$$

4.4. Adjustment procedure

The adjustment procedure is based on a sequential filter considering that each one of the different parameters has a different process noise model. When applying a sequential filter in PPP processing, an adaptation should be made on the parameter variance-covariance matrix to reflect this time variation. Two approaches will be described: the first is based on a least squares sequential filter [Kouba and Héroux, 2001; Shen, 2002] and the other is based on a discrete Kalman filter [Witchayangkoon, 2000; Abdel-salam, 2005; Tolman, 2008].

4.4.1. Least squares sequential filter

Sequential filter in least squares treats the parameters as pseudo-observations with the corresponding variance-covariance matrix. After linearization of the observation equations, the solution for the first epoch is estimated using the least squares solution, with *a priori* weighted constraints, for the unknowns:

$$\mathbf{X_1} = \mathbf{X_0} + \mathbf{dx_1} \qquad\qquad \mathbf{dx_1} = \left(\mathbf{P_{x,0}} + \mathbf{A^T P_{obs} A}\right)^{-1} \mathbf{A^T P_{obs} W} \qquad\qquad (4.9)$$

where $\mathbf{P_{x,0}} = \mathbf{C_{x,0}}^{-1}$ is the *a priori* weight matrix, which is the inverse of the *a priori* covariance matrix of the unknowns;

$\mathbf{P_{obs}}$ is the observations weight matrix. As a general rule the pseudorange accuracy may be assumed as 1 m and the carrier phase as 1 cm. Also satellite weighting should be applied to each observation.

The estimated covariance matrix is:

$$\mathbf{C_{x,1}} = \mathbf{P_{x,1}}^{-1} = \left(\mathbf{P_{x,0}} + \mathbf{A^T P_{obs} A}\right)^{-1} \qquad\qquad (4.10)$$

The estimated unknowns are given by:

$$\mathbf{X} = \mathbf{X_0} - \mathbf{dx} = \begin{bmatrix} x_0 - dx \\ y_0 - dy \\ z_0 - dz \\ \delta t_r \\ \delta_{wet,z} \\ N_{IF} \end{bmatrix} \qquad\qquad (4.11)$$

Starting with this first estimated solution, the adjustment procedure is implemented as a sequential filter that adapts to varying receiver antenna dynamics. The implementation considers the variations in the states of the unknowns between observation epochs and uses appropriate stochastic processes to update their variance. The dynamic model (process) which relates the vector of the parameters at a specific epoch, i, with the next epoch, $i+1$, is a simple one:

$$\mathbf{X_{i+1}} = \mathbf{X_i} + \boldsymbol{\varepsilon}_{\Delta t} \tag{4.12}$$

where $\boldsymbol{\varepsilon}_{\Delta t}$ is the process noise vector.

The covariance information has to be updated to include the process noise:

$$\mathbf{C_{x,i}} = \mathbf{P_{x,i}^{-1}} = \mathbf{C_{x,i-1}} + \mathbf{C_{\Delta t}} \tag{4.13}$$

Where $\mathbf{C_{\Delta t}}$ is the process noise covariance matrix, given as:

$$\mathbf{C_{\Delta t}} = \begin{bmatrix} \sigma_{\Delta t}^2(x) & 0 & 0 & 0 & 0 & 0 \\ 0 & \sigma_{\Delta t}^2(y) & 0 & 0 & 0 & 0 \\ 0 & 0 & \sigma_{\Delta t}^2(z) & 0 & 0 & 0 \\ 0 & 0 & 0 & \sigma_{\Delta t}^2(\delta t_r) & 0 & 0 \\ 0 & 0 & 0 & 0 & \sigma_{\Delta t}^2(\delta_{wet,z}) & 0 \\ 0 & 0 & 0 & 0 & 0 & \sigma_{\Delta t}^2(N_{IF}) \end{bmatrix} \tag{4.14}$$

The stochastic models for the unknowns are:

- For the coordinates x_r, y_r, z_r: station position may be constant (static receiver) or change over time depending on the receiver dynamics (kinematic receiver). If the receiver is static $\sigma_{\Delta t}^2(x) = \sigma_{\Delta t}^2(y) = \sigma_{\Delta t}^2(z) = 0$. If the receiver is on board a ship the process noise may be modelled as white noise with a variance of 100 m^2.

- For the receiver clock error δt_r: the receiver clock will drift according to the quality of its oscillator. For a quartz oscillator, the accuracy (difference from the true value after a given time interval) is about 1 s/day, and the frequency stability (how well a device keeps its frequency over a given time interval) is about 10^{-8} [Lombardi, 2008]. In order to accommodate for receiver clock jumps or if receiver clock steering was not enabled,

the clock error model should be set to white noise with a large value, which can amount to a few ms.

- For the zenith wet tropospheric delay, $\delta_{wet,z}$: its variation in time is considered relatively small, in the order of a few cm/hour and may be modelled as a random walk process with process noise of 1 cm^2/s.

- For the ambiguities, N_{IF} : it is assumed that its value remains constant as long as the carrier phases are free of cycle slips, which means $\sigma_{\Delta t}^2(N_{IF}) = 0$.

For the solution at epoch *i*, the parameters are computed from:

$$\mathbf{X_i} = \mathbf{X_{i-1}} - \mathbf{dx_i} \qquad \mathbf{dx_i} = \left(\mathbf{C_{x,i}}^{-1} + \mathbf{A^T P_{obs} A} \right)^{-1} \mathbf{A^T P_{obs} W} \qquad (4.15)$$

4.4.2. Extended Kalman filter

The origin of the Kalman filter lies in a famous paper published by Kalman (1960) describing a recursive solution to the discrete data linear filtering problem. The Kalman filter is a recursive optimal estimator that addresses the problem of estimating the state of a process that is governed by the linear stochastic difference equation. It is composed by a set of equations that provide an efficient computational method to estimate the state of a process in an optimal way in the statistical sense, *i.e.* minimizes the mean square of the error. The key of the Kalman filter is updating. As new observations are received sequentially, they are used to change the optimal estimate, in a least squares sense, of the process state vector. The Kalman filter has been used extensively in various applications related with positioning and navigation, showing its versatility in a large variety of noisy environments.

The filtering technique is based on a first order linear differential equation, which represents the dynamics of the linear system. Considering the discrete sampling of a random process, it can be modelled as [Brown and Hwang, 1997]:

$$\mathbf{x_{k+1}} = \mathbf{F_k x_k} + \mathbf{w_k}$$

$$\mathbf{b_k} = \mathbf{H_k x_k} + \mathbf{v_k}$$

$$(4.16)$$

Where $\mathbf{x_k}$ is the process state vector $(n \times 1)$ at epoch *k*;

$\mathbf{F_k}$ is the state transition matrix $(n \times n)$ relating the parameter from one epoch to the next;

$\mathbf{w_k}$ is the system error vector $(n \times 1)$, assumed as a white sequence with known covariance matrix $\mathbf{Q_k}$ $(n \times n)$;

$\mathbf{b_k}$ is the vector $(m \times 1)$ measurement at epoch k:

$\mathbf{H_k}$ is the matrix $(m \times n)$ is the design matrix;

$\mathbf{v_k}$ is the measurement error vector $(m \times 1)$, assumed to be a white sequence, having zero correlation with the system error vector and with known covariance matrix $\mathbf{R_k}$ $(m \times m)$;

n is the number of parameters;

m is the number of measurements.

The general formula of the Kalman filter is based on a linear combination of the state vector old estimate, $\hat{\mathbf{x}}_{old}$, with the new observation, $\mathbf{b}_{new}$:

$$\hat{\mathbf{x}}_{new} = \hat{\mathbf{x}}_{old} + \mathbf{K}(\mathbf{b}_{new} - \mathbf{A}_{new}\hat{\mathbf{x}}_{old}) \qquad (4.17)$$

The difference between the prediction and the actual observation is multiplied by a gain matrix, $\mathbf{K}$, to give the correction to the state vector. This gain matrix involves the statistics of $\hat{\mathbf{x}}_{old}$ and $\mathbf{b}_{new}$ to weight that mismatch.

The Kalman filter recursive equations are summarized in the following five steps:

1. Input initial estimates of the state vector $\hat{\mathbf{x}}_0^-$ and its error covariance $\mathbf{P}_0^-$.

2. Compute the Kalman gain matrix: $\mathbf{K_k} = \mathbf{P_k^-}\mathbf{H_k}^{\mathbf{T}}\left(\mathbf{H_k}\mathbf{P_k^-}\mathbf{H_k}^{\mathbf{T}} + \mathbf{R_k}\right)^{-1}$ (4.18)

3. Input the new observations and update the estimate of the state vector and the covariance matrix:

$$\hat{\mathbf{x}}_k = \hat{\mathbf{x}}_k^- + \mathbf{K_k}\left(\mathbf{z_k} - \mathbf{H_k}\hat{\mathbf{x}}_k^-\right)$$
(4.19)
$$\mathbf{P_k} = \left(\mathbf{I} - \mathbf{K_k}\mathbf{H_k}\right)\mathbf{P_k^-} \qquad (\mathbf{I} \text{ is the identity matrix})$$

4. Project ahead: $\hat{\mathbf{x}}_{k+1}^{-} = \mathbf{F}_k \hat{\mathbf{x}}_k$ and $\mathbf{P}_{k+1}^{-} = \mathbf{F}_k \mathbf{P}_k \mathbf{F}_k^{\mathbf{T}} + \mathbf{Q}_k$ \hfill (4.20)

5. Go to the next epoch, input the state vector and its error covariance and start a new loop from step 2.

The observation equations for positioning with GNSS have nonlinear dynamics and nonlinear measurement relationships. In order to apply Kalman filtering the equations must be linearized. There are two methods of linearizing the problem. One is to linearize about some nominal trajectory, not depending on measurement data, the Linearized Kalman Filter (LKF). The other method is to linearize about a trajectory that is continually updated with the state estimates resulting from the measurements, the Extended Kalman Filter (EKF). This is similar to a LKF, except that the linearization takes place around the filter's estimated trajectory rather than using a precomputed nominal trajectory [Brown and Hwang, 1997].

Due to the difficulty to model the trajectory of a floating platform at sea, with enough accuracy, the EKF was used in this study. This filter is similar to the one presented in the previous section (Discrete Kalman Filter), with the difference of dealing with a nonlinear process. Considering the discrete sampling of a nonlinear random process, it can be modelled as [Brown and Hwang, 1997]:

$$\mathbf{x}_{k+1} = \mathbf{f}(\mathbf{x}_k, \mathbf{k}) + \mathbf{w}_k$$

$$\mathbf{b}_k = \mathbf{h}(\mathbf{x}_k, \mathbf{k}) + \mathbf{v}_k$$

(4.21)

where: $\mathbf{x}_i$ is the process state vector $(n \times 1)$ at epoch k;

$\mathbf{f}(\mathbf{x}_k, \mathbf{k})$ is the nonlinear system model function;

$\mathbf{w}_k$ is the system error vector $(n \times 1)$, assumed as a white noise sequence with known covariance matrix $\mathbf{Q}_k (n \times n)$, with n as the number of parameters;

$\mathbf{b}_k$ is the vector $(m \times 1)$ measurement at epoch k;

$\mathbf{h}(\mathbf{x}_k, \mathbf{k})$ is a nonlinear measurements model function;

$\mathbf{v_k}$ is the measurement error vector $(m \times 1)$, assumed to be a white noise sequence, having zero correlation with the system error vector and with known covariance matrix $\mathbf{R_k}(m \times m)$, with m as the number of parameters;

The EKF recursive equations are similar with the ones described previously for the DKF, with the introduction of an additional step to linearize the system model function and the measurements model function:

1. Input initial estimates of the state vector $\hat{\mathbf{x}}_0^-$ and its error covariance $\hat{\mathbf{P}}_0^-$.

2. Compute the linear approximation terms, given by the Jacobian of the system model function, $\mathbf{f(x_k,k)}$, and the measurements model function, $\mathbf{h(x_k,k)}$:

$$\mathbf{F_k} = \left.\frac{\partial \mathbf{f(x_k,k)}}{\partial \mathbf{x}}\right|_{\mathbf{x}=\hat{\mathbf{x}}_k^-} \qquad \mathbf{H_k} = \left.\frac{\partial \mathbf{h(x_k,k)}}{\partial \mathbf{x}}\right|_{\mathbf{x}=\hat{\mathbf{x}}_k^-} \qquad (4.22)$$

3. Compute the Kalman gain matrix:

$$\mathbf{K_k} = \mathbf{P_k^- H_k}^{\mathbf{T}}\left(\mathbf{H_k P_k^- H_k}^{\mathbf{T}} + \mathbf{R_k}\right)^{-1} \qquad (4.23)$$

4. Input the new observations and update the estimate of the state vector and the covariance matrix:

$$\hat{\mathbf{x}}_\mathbf{k} = \hat{\mathbf{x}}_\mathbf{k}^- + \mathbf{K_k}\left(\mathbf{z_k} - \mathbf{h_k(x_k^-)}\right)$$

$$\mathbf{P_k} = \left(\mathbf{I} - \mathbf{K_k H_k}\right)\mathbf{P_k^-} \qquad (\mathbf{I} \text{ is the identity matrix}) \qquad (4.24)$$

5. Project ahead:

$$\hat{\mathbf{x}}_{\mathbf{k+1}}^- = \mathbf{f_k}(\hat{\mathbf{x}}_\mathbf{k})$$

$$\mathbf{P_{k+1}^-} = \mathbf{F_k P_k F_k}^{\mathbf{T}} + \mathbf{Q_k} \qquad (4.25)$$

6. Go to the next epoch, input the state vector and its error covariance and start a new loop from step 2.

The application of the EKF for the adjustment in PPP is implemented as follows:

- The state vector parameters are: $\mathbf{x} = \begin{bmatrix} x \\ y \\ z \\ \delta t_r \\ \delta_{wet,z} \\ N_{IF} \end{bmatrix}$ with initial covariance P_0^-;

- The system model is $\mathbf{x_{i+1}} = \mathbf{x_i}$, this means that the process model is $\mathbf{F} = \mathbf{I}$ ($\mathbf{I}$ is the identity matrix), with system error covariance $\mathbf{Q_k} = \mathbf{C_{\Delta t}}$, as defined by equation 4.14.

- For each satellite, the observations are: $\begin{bmatrix} P_{IF,obs} \\ \Phi_{IF,obs} \end{bmatrix}$

- For each satellite, the design matrix $\mathbf{H(x_k,k)}$ is defined by equation 4.6, for the pseudorange and code carrier phase ionospheric free Observation with measurement error covariance $\mathbf{R_k}$. This matrix will be diagonal, assuming that there is no correlation between pseudorange and carrier phase observations, with the carrier phase observations accurate at the cm level and the pseudorange at the metre level. It is recommended to apply a weighting function for each satellite since the quality of the observations depends on various influences that affect the observation accuracy, which are related with the signal propagation and the receiver quality.

4.5. Precise GNSS products

The GPS broadcast ephemerides have a standard based on the Keplerian orbital parameters and their changing rates. They are derived from observations at Earth fixed monitoring stations. These stations are positioned with respect to some ITRF (International Terrestrial Reference Frame) realization. Therefore GPS positions are defined in the same coordinate system. These ephemerides allow limited positioning accuracy in standalone mode, at the 1 m level (see annex B).

An increasing number of users demands high-quality GNSS products for their applications (hydrographic surveying, ocean studies, weather services, farming, etc) that require more precise information than the one broadcasted by the GNSS satellites. PPP is one methodology that depends on the availability of precise products related with the SSR of corrections, in particular precise satellite positions and clock corrections.

The designated precise ephemerides are provided by the International GNSS Service (IGS). The IGS is a service with international multi-agency membership to support geodetic and geophysical activities. Such service is accomplished through a global network of tracking stations equipped with high quality GNSS receivers. The IGS provides precise satellite ephemeris and clock corrections products that are currently made available at no cost in different forms that vary in latency and accuracy (see annex B).

4.6. PPP Performance

The standard metrics used to describe the performance of a positioning service are: accuracy, availability, continuity, coverage, integrity, reliability and initialization period [U.S. Government, 2008]:

- Accuracy is defined as the statistical difference between the estimate or measurement of a quantity and the true value of that quantity;
- Availability is defined as the percentage of time that the service is available to the user;
- Continuity is defined to be the probability that a healthy positioning service continue to be healthy without unscheduled interruption over a specified interval of time;
- Integrity is a measure of the trust which can be placed in the correctness of the information supplied by positioning system;
- Reliability is the ability of a positioning system to perform its required functions over a specified time interval;
- Initialization period is the minimum time required for a positioning system to provide a valid solution with a given accuracy.

Much of the PPP performance inherits the standards for GNSS services based only on the signal broadcasted by the satellites, but also depends on the performance standards for the service providing the corrections, in the same way that Differential GNSS depends on the performance of the reference stations. In this way the availability and continuity of PPP depends on the services providing the corrections.

Since PPP is based on information of a global network of GNSS ground stations, additional integrity assurance and error corrections are provided to the user. However as a standalone positioning system, it is recommended that PPP has autonomous integrity capacity.

The initialization period considered in PPP is longer than the one considered for standard GNSS positioning (below one minute), since it requires more time for the solution to converge or achieve a high accuracy level, mainly due to the time needed to decorrelate the phase ambiguity. This additional time, the convergence period, is the length of time required from a cold start to a decimetre-level position solution. It is presently about 30 min to a few minutes, under normal conditions, but may vary depending on the methodology used to determine the ambiguities, the quality of the observations, satellite geometry and availability of redundant observations [Bisnath and Gao, 2009].

4.7. Software using PPP

Several software products implementing a PPP processing strategy have been developed in the last years by government agencies, universities and individuals, such as:

- BERNESE (by the University of Bern), http://www.bernese.unibe.ch/index.html;
- GIPSY-OASIS II (by the Jet Propulsion Laboratory), https://gipsy-oasis.jpl.nasa.gov;
- TerraPos (by TerraTec and the Norwegian Hydrographic Service), http://www.terrapos.no/index.html;
- RTKLIB (by Tomoji Takasu at Tokyo University Marine Science and Technology), http://www.rtklib.com/;
- GPSTk (by the Space and Geophysics Laboratory within the Applied Research Laboratories at The University of Texas at Austin), http://www.gpstk.org/.

Currently available post-processing online services are listed at the Precise Point Positioning Software Centre (http://gge.unb.ca/Resources/PPP/). These services are open without costs for any user, and may be found at:

- Canadian Spatial Reference System PPP (CSRS-PPP) by Natural Resources Canada (NRCan), http://www.geod.nrcan.gc.ca/products-produits/ppp_e.php.
- GPS Analysis and Positioning Software (GAPS) by University of New Brunswick, http://gaps.gge.unb.ca/;
- Automatic Precise Positioning Service (APPS) by Jet Propulsion Laboratory, http://apps.gdgps.net/;
- magicGNSS by GMV, http://magicgnss.gmv.com/ppp/.

Martín *et al.* (2012), compared the results of kinematic GNSS-PPP using most of these different online post-processing services. Three trajectories with different kinematic

properties were tested: light airplane flight, standard car and man walking. The reference trajectory was first computed in GNSS carrier phase relative positioning mode. The differences of the PPP with respect to the reference trajectory show that kinematic PPP can achieve an accuracy (standard deviation) level better than 10 cm for planimetric measurements and better than 20 cm for the altimetric measurements. Based on an average of all kinematic scenarios, the most favourable online software was for the MagicGNSS, followed by NRCan with only slightly worst results.

Chapter 5. PPP methodology used in this study

The traditional model for Precise Point Positioning as given by Kouba and Héroux (2001) and described in the previous chapter was the basic reference used in this study. Some modifications were implemented to adapt the method for kinematic positioning of a platform at sea and test further developments towards enhanced data processing strategies to improve convergence time, reduce pseudorange noise influence in the solution and use more efficient stochastic models for the observations from each satellite.

The developed PPP methodology is based on the requirements to position a floating platform at sea, either a buoy or a ship. The GNSS observations are processed sequentially and all the corrections are computed epoch by epoch, based on the time of observation and on the pseudorange based approximate point position. It was thought to be adequate for use in real time processing, provided that precise products are available (satellite positions and clock corrections). In addition, the software is based on a modular approach, allowing extensible and maintainable programming code.

5.1. Parameters to be determined in kinematic positioning

Using the GPS+ Toolkit C++ library [Tolman *et al.*, 2004] (see Annex D), based on the traditional PPP method, several modifications and new routines were implemented when required, to improve and complement the existing software.

One of the implemented modifications is related with the parameters to be estimated. In a moving platform, we are also interested in determining the velocity vector. Also the carrier phase ambiguities while being estimated as float numbers; its integer nature was kept to allow ambiguity fixing. These functionalities were implemented in the context of the GPSTk library. Thus, the parameters to be determined in this model are:

- Position;
- Velocity;
- Receiver clock error;
- Receiver clock rate;
- Wet zenith troposphere delay;
- Carrier phase ambiguity for L1;
- Carrier phase ambiguity for L2;

5.2. Observation data files

The data acquired by the receivers is first converted to the standard format RINEX (Receiver Independent Exchange) observation and navigation files. Usually each manufacturer provides an utility to convert from proprietary format to RINEX. This format was first defined by Gurtner *et al.* (1989). Several versions have been developed as a consequence of revisions made to meet the evolving requirements of the GNSS community. The latest version, 3.1, was published in June 2009 [Gurtner and Estey, 2009]. The format consists of three types of ASCII files:

- The observation data file containing the pseudorange and carrier phase for each of the satellites tracked by the station receiver, among other receiver related information;
- The navigation file containing the navigation message broadcasted by the satellites;
- The meteorological data file containing information from meteorological sensors that may be installed at the receiver station. This information is useful to model the troposphere effect on the observations.

5.3. Additional files to implement the corrections

To correct for all the possible error sources, PPP requires additional information to account for the following effects:

- Satellite position corrections;
- Satellite precise clock corrections;
- Satellite and receiver antenna offsets;
- Tidal constituents (also called harmonics) to compute the ocean loading tide displacement for a given position;
- Polar motion parameters;

5.3.1. Satellite positions and clock corrections

The satellite positions and clock corrections can be downloaded from a precise products provider. The correction files are given in SP3 format [Hilla, 2010]. The SP3 files used in this study were downloaded from the IGS (see annex B), containing correction values regularly spaced at 15 min interval, which is not dense enough to interpolate the clock correction at 1 s interval, as required for kinematic applications due to the negative impact of satellite clock corrections on PPP.

In contrast to the satellite orbital positions, which have a smooth trend, satellite clock interpolation may not be accurate enough, due to the high level of irregularity on its trend. Montenbruck *et al.* (2005) showed that linear interpolation of satellite clock corrections at 300 s is not adequate to achieve centimetre level accuracy. This conclusion was also verified in this study using Lagrange polynomials as an interpolation method. The results show an accuracy of 0.5 m (3D RMS). Thus, for static positioning it is advantageous to avoid interpolation and decimate the GPS receiver data in order to coincide with precise ephemeris and clock corrections epochs. However this is not feasible in kinematic positioning whose sampling rate is usually higher than 1 Hz.

The influence of sampling rate when using IGS 5 min, 30 s and 5 s interval satellite clock corrections in PPP was investigated by Fei *et al.* (2010). The results show that satellite clock sampling rate has very little effect on the static PPP solution, provided that the observations are decimated to the epochs of the satellite clock corrections. However, the satellite clock sampling rate has a significant impact on the kinematic PPP, solution when a solution is required every second or even smaller intervals, when interpolation is mandatory. The error caused by interpolation for intermediate epochs depends on the sampling rate. The 5 min interval satellite clock corrections reduce the accuracy by 30-50 percent when compared to the 30 s and 5 s interval satellite clock corrections. The 30 s and 5 s interval satellite clock corrections interpolation produce the same results and satisfy the requirements for cm level accuracy in PPP.

Satellite clock correction files, at 30 s interval, are available for download from the IGS (ftp://igscb.jpl.nasa.gov/pub/product/), in the RINEX CLK format [Ray and Gurtner, 2006]. The information from the SP3 and CLK files is combined by the software in a data structure, where the satellite positions and clock corrections are given both at 30 s interval, by interpolating the satellite positions of the SP3 file (at 900 s interval) to the epochs of the CLK file (at 30 s interval). In this way, both satellite and clock parameters are provided at 30 s intervals, suitable for kinematic applications, as required for this study.

5.3.2. Satellite and antenna information

The information for the satellite and receiver antenna phase centre correction is provided in the form of ANTEX files [Rothacher and Schmid, 2010]. These files contain azimuth and elevation dependent Phase Centre Variation (PCV) as a result of a calibration process for

each antenna model (both for satellite and receivers). These files can be downloaded from the IGS website at ftp://igscb.jpl.nasa.gov/pub/station/general/.

5.3.3. Ocean tide loading constituents

The tidal constituents to compute the ocean tide loading displacement are provided in the form of BLQ format as given by an open service, the "Ocean tide loading provider" at http://froste.oso.chalmers.se/loading//, for a single position. For kinematic positioning, instead of using this online service, which is restricted to a single position per submission, it is recommended to have files with spatial grid information for each one of the tidal constituents and interpolate for each position as the platform moves.

5.3.4. Polar motion parameters

The daily polar motion parameters can be downloaded from the International Earth Rotation Service (IERS) under the form of a time series of the so-called Earth Orientation Parameters at http://www.iers.org/nn_10968/IERS/EN/DataProducts/EarthOrientationData/.

5.4. Data verification and cleaning

The PPP method developed in this study uses dual frequency pseudorange, dual frequency carrier phase and also Doppler observations. Considering the current status of the GNSS constellations and the usual GNSS receiver performance, the observations recorded at each epoch, for each satellite should normally provide five independent observations: carrier phase on two frequencies, pseudorange on two frequencies and Doppler on a single frequency.

Data verification and data cleaning of the observations is a relevant step in the preparation of the processing with PPP algorithms. Since the observations are processed sequentially, any error in the data series will induce erroneous solutions, and should be detected before starting the processing. This task is performed sequentially at each single epoch GNSS observation epoch by applying the following detection rules:

1. For each satellite, verify if pseudorange and carrier phase observations are present for both frequencies L1 and L2. If not ignore this satellite in the data record.
2. For each satellite, verify if there are gross errors in the pseudorange observations. A gross error for a pseudorange observation is considered as one value that is above or below reasonable limits. Considering the receiver antenna on the Earth's surface, the height of one GPS satellite, for example, is approximately 20200 km, a reasonable

domain for pseudorange observations should be between 15000 and 25000 km, accounting for all the errors included on the raw observations. If an erroneous value is flagged, ignore this satellite in the data record.

3. For each satellite, verify if there are gross errors in the carrier phase observations. Some RINEX observation files signal a "0" if there is no observation. This cannot be interpreted as a valid observation and if it occurs, we must ignore this satellite in the data record.

4. For each satellite, verify if it is above a given elevation threshold. If not ignore this satellite in the data record.

5. Verify if, after passing by all the previous simple filters, a given GNSS data record still has enough satellites to compute the positioning solution.

5.5. Cycle slip detection

Cycle slips occur if the receiver loses phase lock of the satellite signal. This may be caused by obstructions, high signal noise (caused by multipath and ionospheric scintillation), interference and receiver signal processing. In a cycle slip the carrier phase shows a sudden jump by an integer number of cycles. The fractional part of the phase is not affected by this discontinuity in the observation sequence. The cycle slip may be as small as one or a few cycles, or contain millions of cycles. As soon as the cycle slips have been detected, there are two ways to deal with them: one is to repair or remove the data; the other is to set a new ambiguity unknown in the GNSS observation equations [Seeber, 2003].

With two frequency signals it is possible to combine the observations to enhance cycle-slip detection. The goal is to create an observable where the variations due to cycle slips are greater, making them easily detected. This requires that high variation effects, such as the geometry, clock errors, troposphere effect and ionosphere effect are previously removed. Two kinds of data combinations are used: one based in carrier phase measurements only and another based on the combination of carrier phase and pseudorange measurements. Among the possible combinations the ones used in this study and already provided in the GPSTk library are [Blewitt, 1990]:

- Use the carrier phase geometry-free (see annex C) combination in order to remove the geometry and all non-dispersive effects. This provides a low-noise signal (multipath and noise less than 1 cm). It is affected by ionospheric refraction but this effect varies as a smooth function. Any unusual variation may indicate cycle slips in one or the two

frequencies. However, two special cycle slips can lead to very small variations, and the cycle slip may remain undetected [Wellenhof *et al.*, 1997].

- Use the Melbourne-Wübbena combination of code and carrier phase (see annex C). This combination cancels all the non-dispersive effects and also the ionosphere refraction. However the combined observable is affected by multipath and its performance is worse than the carrier phase ionospheric combination. The noise level is in the range of a few cycles, mainly dependent on the noise of the pseudorange observations and it is used as a secondary test.

A time series of phase data which has no cycle slips is called a "phase connected arc". After a cycle slip is detected a new phase connected arc is marked, for the purpose of initializing a new carrier phase ambiguity. The Loss of Lock Indicator (LLI) indexes of carrier phase observations contained in the RINEX observation files are also used to detect cycle slips.

5.6. Weighting satellite observations

The noise level of the GNSS signal at the receiver depends on the influences through the propagation path and also on the receiver performance. It is known that satellite observations with lower elevation angles have the lowest SNR and are more affected by tropospheric effects, when compared to observation from satellites with higher elevation angles. This means that there are two potential and simple ways of weighting the observations, either derived from the satellite elevation angle or from the SNR. Experimental results with GNSS observations from a static station showed little difference when comparing the cosecant of the elevation angle weighting function with the SNR weighting function [Collins and Langley, 1999].

The weighting function used in this study is based on the MOPS (Minimum Operational Performance Standards) of the Radio Technical Commission for Aeronautics (RTCA) of the document RTCA DO-229D [RTCA, 2006]. The algorithm of the MOPS weighting function is implemented in the GPSTk library as a C++ class. This algorithm combines the influence of several effects to estimate the weight of each satellite:

$$w^s = \frac{1}{\sigma^2_{recv} + \sigma^2_{URA} + \sigma^2_{mult} + \sigma^2_{trop} + \sigma^2_{ion}} \tag{5.1}$$

Where σ^2_{recv} is the estimated noise due to the receiver performance;

σ_{URA}^2 is the estimated noise due to the User Range Accuracy (URA) indicator provided in the navigation message and represents the 1-sigma range error due to satellite and control segment errors;

σ_{mult}^2 is the estimated noise due to multipath;

σ_{trop}^2 is the estimated noise due to the troposphere effect;

σ_{ion}^2 is the estimated noise due to the ionosphere effect.

5.7. Data combinations

The methodology implemented in this study allows the use of a set of known GNSS observation data combinations, seeking improvements when compared to the use of the traditional Ionospheric Free (IF) combination. The primary goal is to reduce the noise level of the combined observable, mitigate the ionospheric effect and keep the integer nature of the ambiguities.

In the scope of this study, GNSS data combinations were implemented to perform specific tasks, either to mitigate the ionospheric effect, for cycle slip detection and ambiguity determination (see annex C), as listed:

- Inter-frequency combinations:
    - Ionospheric Free (IF)
    - Geometry Free (GF)
    - Wide-lane (WL)
    - Narrow-lane (NL)

- Pseudorange and phase combinations:
    - Code (pseudorange)-phase average (CP)
    - Melbourne-Wübbena (MW)
    - Divergence-free (DF)

The data combinations CP and DF were introduced to GPSTk in the scope of this work.

5.8. Ambiguity determination

The methodology used in this study allows the estimation of the initial GNSS carrier phase ambiguities before solving the model equations using a recursive filter. These initial ambiguities are approximate values that are contaminated by the noise of pseudorange measurements and are useful as a first approximation of the initial ambiguity value for the solution estimation process using a recursive filter. These approximate initial values reduce significantly the initial variance and process noise that must be considered for the ambiguities stochastic modelling and also improve the convergence time.

The initial ambiguities are estimated directly using the DF combination (see annex C):

$$
\begin{aligned}
C_{DF,1} &= P_1 + \frac{f_1^2 + f_2^2}{f_1^2 - f_2^2}\,\Phi_1 - \frac{2f_2^2}{f_1^2 - f_2^2}\,\Phi_2 \\
C_{DF,2} &= P_2 + \frac{2f_2^2}{f_1^2 - f_2^2}\,\Phi_1 - \frac{f_1^2 + f_2^2}{f_1^2 - f_2^2}\,\Phi_2
\end{aligned}
\tag{5.2}
$$

The DF combination cancels the terms that are of equal magnitude for the pseudorange and carrier phase observations, such as the receiver-satellite geometric range, receiver clock error, ionosphere, troposphere, and antenna offset. At this initial stage, all the remaining terms (multipath, phase windup, receiver hardware delay and satellite hardware delay) are lumped to the noise term. The initial carrier phase ambiguities are estimated directly from the equation system 5.2. No attempt was made to fix the ambiguities, due to the influence of the pseudorange noise, which is too high when compared to the carrier phase wavelength.

5.9. Deterministic model

The deterministic model relates the observations with the parameters to be determined. This study uses the model based on the one described by Gao and Shen (2001). This model uses the CP combination for each frequency (see annex C) instead of the IF combination for code:

$$
\begin{aligned}
C_{CP,1} &= 0.5P_1 + 0.5\Phi_1 \\
C_{CP,2} &= 0.5P_2 + 0.5\Phi_2
\end{aligned}
\tag{5.3}
$$

The CP combination also eliminates the ionosphere effect, but has three times smaller noise when compared to the IF code combination and allows to keep the integer nature of the ambiguities. The already mentioned carrier phase IF combination (equation 3.25) completes the equation system.

This approach forms a set of three of three linearly independent equations for each satellite and has the following advantages when compared to the traditional approach:

- All the data combinations are ionospheric free, with one additional observation per satellite;
- The data combinations involving pseudorange observations have smaller noise;
- It keeps the integer nature of the ambiguities and each ambiguity can be estimated individually, which means that the ambiguity fixing techniques can be implemented.

The resulting observation equations for each satellite are the following:

$$
\begin{aligned}
C_{CP,1} &= \rho + c \cdot dt + Trop + \quad 0.5 \cdot \lambda_1 N_1 + \quad\quad 0 \quad\quad + noise \\
C_{CP,2} &= \rho + c \cdot dt + Trop + \quad\quad 0 \quad\quad + \quad 0.5 \cdot \lambda_2 N_2 + noise \\
C_{IF,\Phi} &= \rho + c \cdot dt + Trop + \frac{f_1^2}{f_1^2 - f_2^2} \lambda_1 N_1 - \frac{f_2^2}{f_1^2 - f_2^2} \lambda_2 N_2 + noise
\end{aligned}
\tag{5.4}
$$

When using only ionospheric free data combinations, remain three linearly independent equations from the four raw observations (based on dual frequency pseudorange and carrier phase observations). Then, the minimum number of satellites required for computing a single epoch solution is:

- A minimum of four satellites are required to compute the instantaneous velocity vector the receiver clock rate, using Doppler observations;
- The other parameters (position, receiver clock error, zenith troposphere delay and carrier phase ambiguities) are computed using the pseudorange and carrier phase observations. The number of unknowns is five plus two times the number of satellites. If only four satellites are visible, there are 13 unknowns for 12 observations and the system cannot be solved in a single epoch. Thus, to compute a positioning solution at least five satellites are required, *i.e.* 15 observations for 15 unknowns.

5.10. Stochastic model

The influence of random processes should be stochastically modelled in the parameter estimation process along with its deterministic component. Three components of stochastic modelling must be considered: observations, system dynamics and parameters.

5.10.1. Observations stochastic model

The noise term in the observation equation model is the sum of measurement noise and any other error not properly corrected. The stochastic model of the observations includes information about the accuracy of the equation model.

This study considers the influence of the measurement process and the linear combination of observations. The standard deviation of the measurement noise is assumed to be 1 cm for carrier phase measurements and 1 m for pseudorange measurements. Using the error propagation law, assuming a normal distribution, the CP combination has an error of 1 m and the carrier phase IF combination has an error of 3 cm.

As mentioned in section 5.6, each observation is also weighted by a function that depends on the satellite elevation angle and is based on the MOPS observation weighting algorithm [RTCA, 2006].

5.10.2. Parameters stochastic model

Recalling the deterministic model, mentioned in section 5.9, observation equations contain parameters that correspond to the position coordinates, receiver clock error, zenith tropospheric wet delay and carrier phase ambiguity. The random behaviour of these parameters can be modelled taking in consideration the kinematic motion onboard a ship or on a buoy, as described on table 5.1.

Table 5.1 – Parameters stochastic models used for kinematic motion onboard a ship or on a buoy.

	Initial Variance	Model (variance)
Position coordinates	100 m^2	White noise (100 m^2)
Receiver clock error	100 m^2	White noise (100 m^2)
Zenith troposphere wet delay	0.1 m^2	Random walk (0.01 m^2/hour)
Carrier phase ambiguity	100 m^2	Constant if no cycle slips

Chapter 6. Software development

Software development is a crucial part of this study. The software should be reusable, adaptable and easily readable, for further upgrade and improvements in a flexible way. This task was highly facilitated through the use of the open source GPSTk abbreviation for "GPS Toolkit") library.

The general structure of any software used for GNSS positioning requires the input of observations and user options. Then this input information is used to compute the solution. The final solution is prepared to send for output, either in the form of a string for a display or to a file. This general structure may be divided into three basic components [Xu, 2007]:

- Functional library – consisting of physical models, algorithms and tools;
- Data platform – to prepare the data for use in a time loop;
- Data processing core – to construct the observation equations, accumulates them within the time loop and computes the solution.

The GNSS software developed as part of this study was designated as SAPPos (Satellite Absolute Precise Positioning) and obeys to this general structure. The development of SAPPos will be described next, with reference to the GPSTk C++ classes that were used to solve specific tasks, the modified GPSTk classes and the new classes required to introduce in order to solve specific problems of kinematic precise positioning of marine platforms.

6.1. The GPS Toolkit (GPSTk)

The GPSTk library is being extensively used by the GNSS community to rapidly and easily develop, implement and solve GNSS related problems. The GPSTk is an advanced GNSS Open Source Software initiated by the Applied Research Laboratories of the University of Texas, to provide a world class GNSS library computing suite to the satellite navigation community. It is written in C++ programming language and the first version of the GPSTk was presented by Tolman *et al.* (2004).

The GPSTk library is being continuously improved and is open to the participation for the benefit of all users in the following ways: bug reports, new algorithms, suggestions for improvements and contributions of additional applications. The latest stable version, version 2.0, is available for download since 27th June 2012. For more information consult the

website, http://www.gpstk.org/bin/view/Documentation/WebHome. Annex D provides additional information concerning with the installation and how to use the library under Microsoft Windows XP operating system, as a result of the experience achieved during the development of this study.

6.2. Functional Library

The SAPPos functional library includes the following physical models, algorithms and tools required to compute a PPP solution, much of them inherited from the GPSTk, such as:

- Physical models:
  - Tropospheric model;
  - Relativity model;
  - Satellite antenna offset model;
  - Solid Earth tide model;
  - Sun and Moon orbital model.
- Algorithms.
  - Data pre-processing;
  - Cycle slip detection;
  - Satellite weighting;
  - Single point positioning;
  - Single point velocity determination;
  - Geometric precision;
  - Adjustment algorithms.
- Tools:
  - Data structures;
  - Data input and output.
  - Coordinates transformation (from ECEF XYZ to geodetic);
  - Time systems transformation;
  - Broadcast orbit transformation (from keplerian elements to ECEF XYZ);
  - Interpolation methods;
  - Matrix operations;
  - Statistical analysis.

Most of the models, algorithms and tools are already part of the GPSTk C++ library, such as the data structures, cycle slip detection, times systems transformations, relativity model, Solid Earth tide model, satellite antenna offset model, Sun and Moon orbital model, broadcast orbits transformation, adjustment algorithms. Therefore it is considered unnecessary to describe each one. Only the modifications and new C++ classes introduced in the scope of this thesis will be described on the next sub-section. The C++ code is described in annex E.

6.2.1. Precise clock files

As mentioned in section 5.3, precise clock corrections contained on IGS standard SP3 files, are given in a 15 min interval, which is not adequate for kinematic applications. In the scope of this thesis, focused in standalone precise kinematic positioning, it was required to develop the ability to deal with 30 s interval CLK files, which is not available from the GPSTk library.

The new class `PreciseCLK` simply reads data parameters from a CLK file data parameters organizing them into a CLK-header and CLK-data streams. The 30 s satellite clock corrections are added to the satellite positions and clock corrections data structure by a new function"addClock" in GPSTk `TabularEphemerisStore` class. Satellite positions for the epochs of the CLK data stream are interpolated from the 15 min interval positions derived from SP3 files, using Lagrange interpolation of order 10. In this way a tabular data structure with 30 s satellite position and clock corrections is created at data pre-processing stage which is then ready for use during the sequential loop stage.

6.2.2. Tropospheric model

Several tropospheric models are available on the GPSTk library, all derived from an abstract base class `TropModel`. However the GMF's [Boehm *et al.*, 2006b] and the GPT [Boehm, 2007] models (see section 3.5) are not available. New classes were developed for the specific purpose to implement the GMF's and GPT. These new classes are based on the Fortran versions available for download at http://ggosatm.hg.tuwien.ac.at/DELAY/ and programmed in C++ according with the GPSTk guidelines for programmers, using the same abstract base class as used for the others tropospheric models.

The new class `GMFTropModel` requires the input of the approximate receiver position, observation date and satellite elevation angle. This information is provided in the GNSS data

measurements and by the pseudorange position solution. The air temperature and pressure may be input by the user or automatically computed for the observation position using the GPT model. The output consists of the dry zenith troposphere delay and the mapping functions values, both for the wet and hydrostatic component.

6.2.3. Solid Earth tide

The displacement caused by the solid Earth tide is computed using the GNSS pseudorange approximate solution. It was used the GPSTk class `SolidTides`. This class uses the equation for the displacement of the station due to degree two, as described in 3.4.1. The displacement is given with respect to the "conventional tide-free" surface.

An additional correction for the permanent tide was added to the software, in order to convert the tidal reference from the "conventional tide-free" to the mean-tide surface. This was required whenever GNSS coordinates used to derive SSH were compared to satellite altimetry SSH.

6.3. Data platform

The program structure developed in this study is based on "Example 9" given at GPSTk API (Application Programming Interface) http://www.gpstk.org/doxygen/example9_8cpp-example.html. Also the physical models, algorithms and tools used in the software were copied from the GPSTk library. Proper modifications to the GPSTk routines were made whenever necessary.

The data platform is dedicated to the preparation of all possibly needed data for use and performing the preparation in a time loop:

- Common part:
  - Program start;
  - Read user input parameters;
  - Read all the data files necessary to run of the software (*e.g.* satellite data file, station data file, etc);
  - Data pre-processing;
  - Transform satellite orbit data;

- Sequential time loop:

  o Get the needed data for use at related epoch (*e.g.* initial coordinates of the receivers, etc);

  o Compute all possible parameters and model values for use at related epoch (*e.g.* transformation matrices, orbit data, correcting models, etc);

  o Read the observation data and transform it to a suitable form for use;

  o Single point positioning;

  o Single point velocity determination;

- Summary part:

  o Statistic analysis of the results;

  o Quality control;

  o Results output.

6.4. Data processing core

The data processing core forms the observations equations and solves the problem in accordance with specific user options previously defined. The EKF from the GPSTk was modified to allow the input of initial conditions for the receiver coordinates receiver clock error and L1 and L2 ambiguities for initialization of the filter.

The initial conditions for the receiver coordinates and clock error are estimated using the IF pseudorange LMS (Least Mean Squares) solution. In this way, these parameters initial error are reduced when compared with a completely unknown initialization. The initial condition for the ambiguity is based on the method described at section 5.8, using the DF data combination.

A different data processing core can be chosen depending on the user option. As an example the SAPPos can be configured for standard point positioning that uses the LMS algorithm to compute the solution. In the future if new requirements are defined, the data processing core may be easily adapted to perform new tasks, taking advantage of the modularity and modifiability of OOP. A flowchart of the SAPPOS is represented on figure 6.1.

START

File input:
- OBS, NAV, SP3, CLK, Antex and BLQ.

Define:
- Elevation angle mask;
- Antenna site offset;
- Observation equations;
- Measurement errors;
- Process noise.

Read data epoch by epoch

Data pre-processing:
- Filter gros errors in observations;
- Compute an approximate pseudorange based LMS solution.

Compute corrections:
- Relativistic effects;
- Antenna phase center variation;
- Windup (for satellite only);
- Tropo hydrost. and map. functions;
- Site dependent corrections;

Compute satellite weights:
- MOPS, Elevation angle and URA.

Compute data combinations:
- NL, WL, IF, MW, DF, CP and GF.

Detect and mark cycle slips.

Def. initial cond.:
- LMS pos and rcv clk err;
- L1 and L2 ambiguities.

Data processing:
- Form equations;
- Extended Kalman filter.

Summary part:
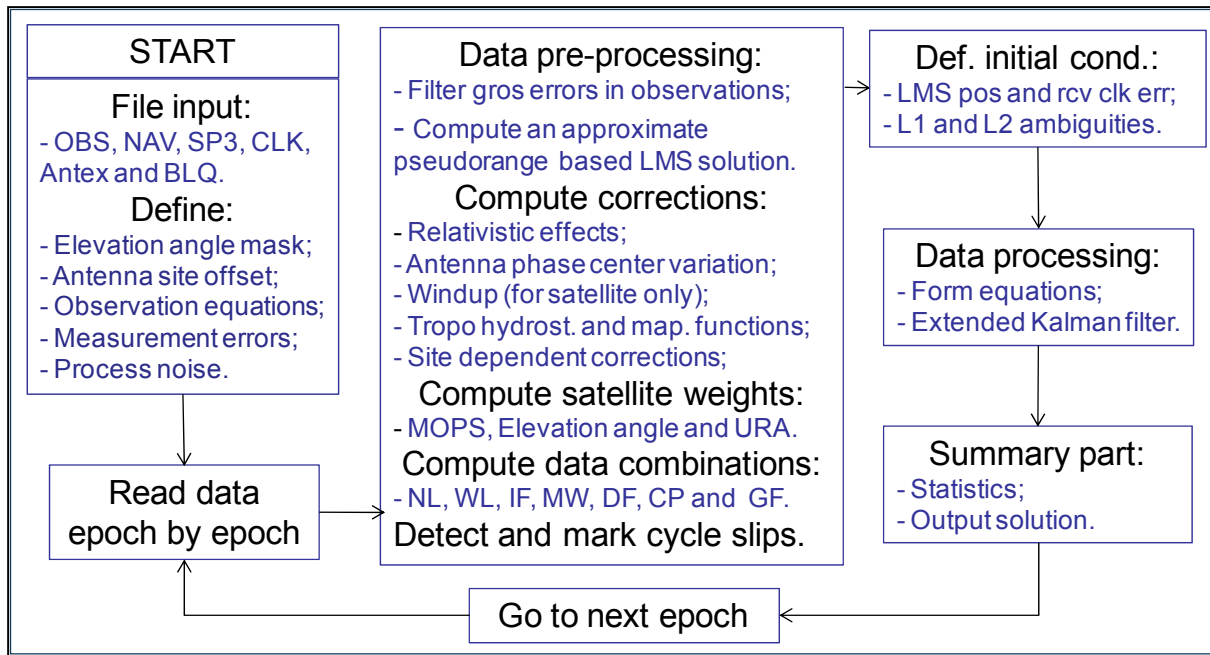- Statistics;
- Output solution.

Go to next epoch

Figure 6.1 – Flowchart of the program SAPPos (Satellite Absolute Precise Positioning) developed in this study.

Chapter 7. Experiments and results

The PPP methodology and the software developed in this study was tested using GNSS data collected by receivers installed on static stations and also on a survey ship. This chapter describes how the data was collected, presents the results and analyses the performance of the PPP methodology developed.

The chapter is divided into three main sections. The first section is devoted to the analysis of the PPP performance by comparing with a static position with known coordinates. The second section is devoted to the analysis of PPP performance for kinematic positioning in marine platforms by comparing with a reference trajectory computed by carrier phase GNSS relative positioning. The third section compares SSH derived from PPP with satellite altimetry data. Different processing options are considered for the analysis of its influence on the positioning quality.

7.1. PPP on a static station

7.1.1. Using PPP in static mode

As mentioned in section 5.10, PPP can be used for static positioning simply by changing the stochastic model of the station coordinates, which are assumed to be constant with an initial error. The initial approximate position is based on the standard point positioning solution, with may be assumed to have a conservative estimated accuracy of 10 m (standard deviation) for each coordinate.

Observations from an EUREF permanent network station, LEON, were used to evaluate the performance of SAPPos for static PPP. GNSS observations at 30 s interval were first decimated for the epochs of the IGS SP3 files.

The result is plotted on figure 7.1, for the time series of the three coordinates. The solution converged after 5 epochs, which are 15 min apart, and the 95% confidence spheroid of the differences for the final solution, when compared to the station true position, is 0.9 cm. As expected the accuracy of the vertical coordinate is worst when compared with the horizontal coordinates, due to geometric influence of the satellite configuration on the position solution.

Figure 7.1 – Result of static PPP processing by SAPPos using data from EUREF permanent network station LEON with reference to its true position.

7.1.2. Using PPP in kinematic mode

Another data set from the EUREF station LEON, with observations at 1 s interval, was processed by SAPPos, in kinematic mode. Now, CLK 30 s clock corrections were used in conjunction with SP3 files to allow interpolation with a reasonable accuracy for all observation epochs. The results of the kinematic solution agree with the static one, with a bias of 5 cm and 3D RMS error of 7 cm, considering only the results after convergence.

Table 7.1 – Summary statistics of the SAPPos kinematic solution with reference to the true position of a fixed station (in metres).

	bias	std. dev.	max.
North	-0.02	0.02	0.08
East	0.00	0.03	0.07
Up	0.05	0.05	0.09

Since the horizontal coordinates have better accuracy that the vertical component and to enhance plot readability, only the geodetic height difference is plotted on figure 7.2. The time series shows some variations which are related with the influence of the satellite geometry, or PDOP (. In good visibility conditions the PDOP is around 2 or 3. The observed higher PDOP values are explained by obstruction, interference or missing data in satellite precise ephemeris files (SP3) or high data rate clock correction files (CLK). Also, due to the geometry influence in the position accuracy the horizontal coordinates have smaller

differences than the height as in the example on table 7.1. However, it should be remembered that, for marine applications, the vertical component is the one that is requires the highest accuracy level.
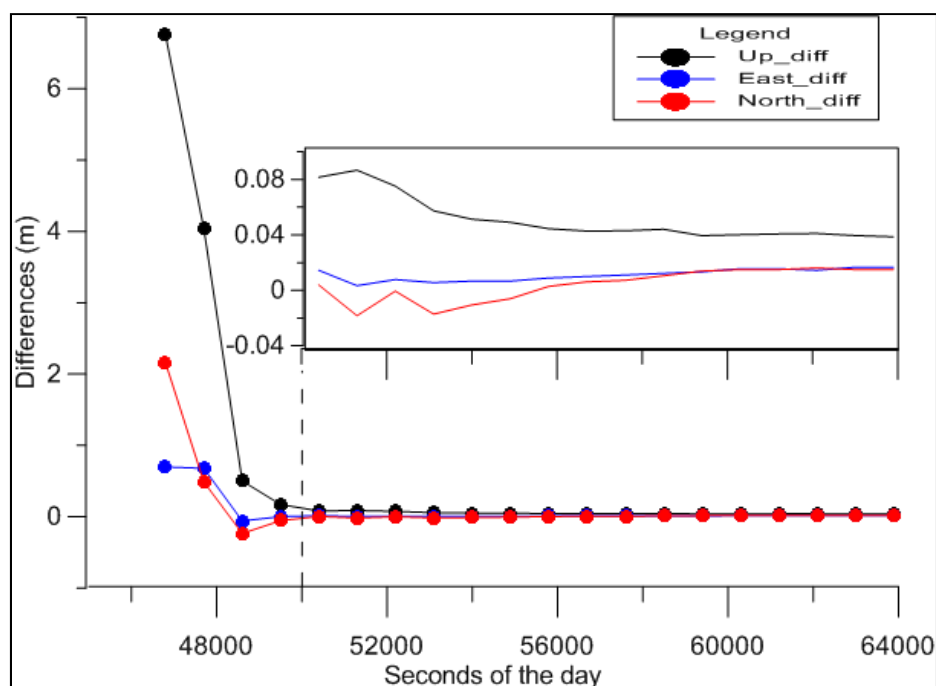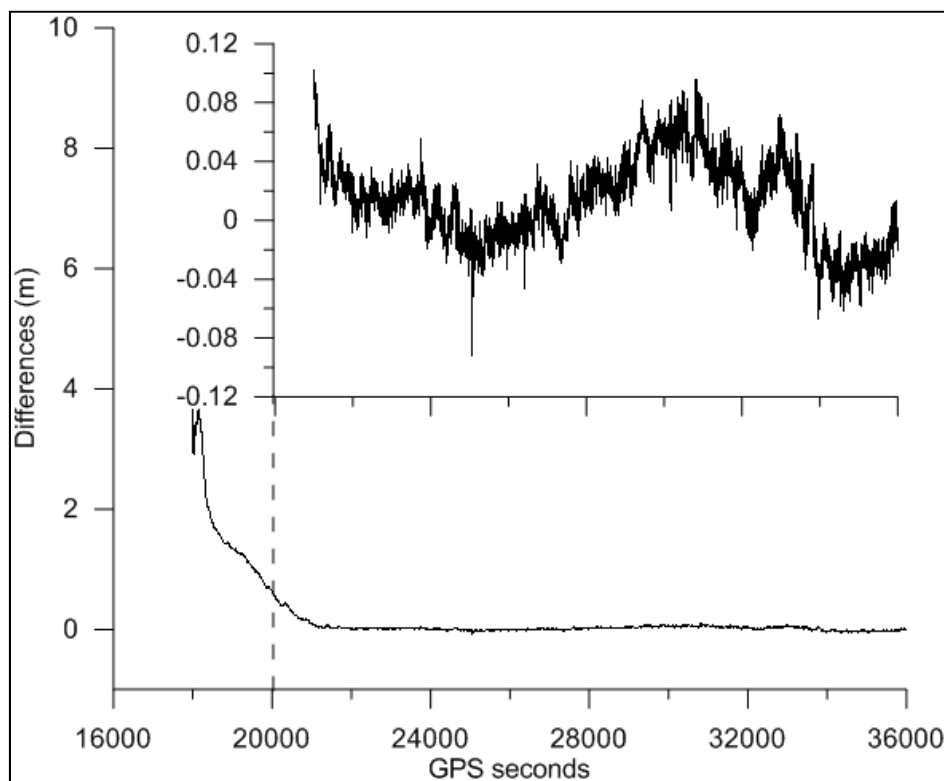

Figure 7.2– Result of kinematic PPP processing by SAPPos using data from EUREF permanent network station LEON with reference to its true position.

The time required for the solution to converge depends on the system model and stochastic parameters used in the recursive filter to estimate the solution. The convergence criterion was a 3D error less than 10 cm with reference to the known station position. SAPPos uses a Kalman filter formulation, already implemented in the GPSTk library. In the example above a simple system model as white noise was assumed for the coordinates. The convergence period was about 2000 s. This period may be reduced by estimating the carrier phase ambiguities, but this option was not intentionally considered for processing a static station.

7.2. PPP on a marine platform

One of the problems of the performance evaluation of PPP in a marine environment, at the open sea is due to lack of a good reference. In this study it was used GPS data already collected at sea and processed in relative positioning mode, which is proved to be accurate enough to serve as reference trajectory.

In the scope of project "study of the Portuguese Oceanic Coastal zone Using remote Sensing data" (POCUS), a test campaign was prepared, using a survey vessel, NRP Auriga. The aim of this study was to evaluate the feasibility of GPS measurements of SSH on board a ship by comparing it with satellite altimetry SSH [Marreiros *et al.*, 2012]. The GPS data acquired during this campaign was used to evaluate the performance of SAPPos on board a ship.

7.2.1. Equipment installation

The data collection campaign was previously planned to occur on the 16 and 17 June 2007 in order to coincide with the altimetric satellite JASON and ENVISAT passes. All the equipment was installed on board the Portuguese Navy coastal survey ship NRP Auriga, with a length of 31 m (see Figure 7.3).

Two shore stations were used as reference for relative carrier phase GPS positioning in post-processing. Relative carrier phase GPS positioning can achieve centimetre level accuracy in kinematic platforms (Xu, 2007). The use of kinematic relative positioning is feasible in the vicinity (few tens of kilometres) of a single reference station. The range of the kinematic solution can be increased significantly by using multiple reference stations near the planned trajectory. It is advisable to fix the carrier phase integer ambiguities prior to the mission start, in the vicinity of one reference station. The lock to the GPS signals, as the ship follows its planned track, will be maintained with careful installation of the antennas in order to have good visibility to satellites and no electromagnetic interferences. In normal sea state conditions, ship motion may cause antenna height variations of a few metres. The determination of SSH requires an additional care for the compensation of vessel motion and draught variations during the mission, as described on section 2.4.

The following equipment was installed on board the NRP Auriga:

- Two GPS receivers TRIMBLE 4000 SSE each one with a dedicated antenna TRIMBLE Compact L1/L2 with groundplane. The two antennas were installed on a base with 2 m length, in the port-starboard direction, fixed to the passage between the two chimneys of the ship. The two antennas were used to determine independent GPS OTF positioning solutions.

- The ship was already equipped with a GPS/INS used for motion compensation of multibeam surveys, the SEAPATH 200. This system is composed by two antennas and an Inertial Measurement Unit (IMU). The accuracy of its measurements are (RMS):

- o Roll: 0.1º;
- o Pitch: 0.1º;
- o Heave: 5 cm or 5% whichever is higher.

The IMU was installed in a fixed position near the ship's gravity centre. This position is not exactly defined and may change during the mission period due to changes in load, such as fuel and water consumption. An approximate location may be found from the ship's drawings. Any displacement error of the IMU's location from the ship's gravity centre may induce non-existent heave measurements due to roll or pitch motion effects on the vertical displacement of the IMU.

Raw data from the dual frequency GPS receivers were recorded at a 1Hz data rate. One raw data file was created every 2 hours. Raw data from the Seapath 200 were recorded using a serial logger and configured for 10 Hz data rate output.

The two GPS antennas of the Seapath 200 were installed in the longitudinal direction of the ship, making a cross with the other two standalone GPS antennas (see figure 7.3).
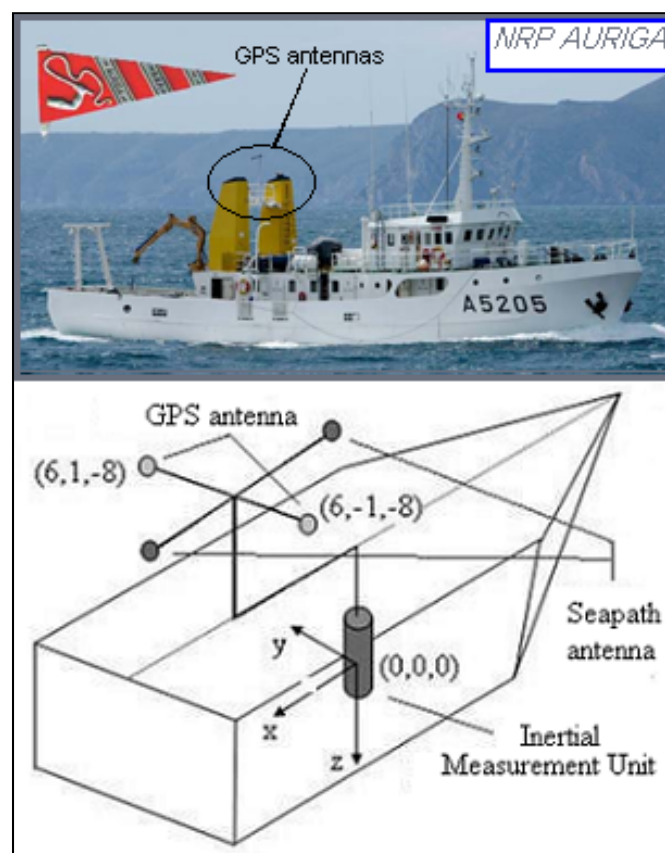
Figure 7.3 – Portuguese navy survey ship NRP Auriga and equipment configuration with approximate body frame coordinates, in metres.

Two coastal reference stations were installed as close as possible to the ships planned track in order to allow good quality relative positioning results for the entire test period. One reference station was installed at the extreme north of the navigation plan (Gaia) and the other at the extreme south (Carvoeiro). The maximum distance of the ship's position from the closest reference station was 110 km (see figure 7.4).
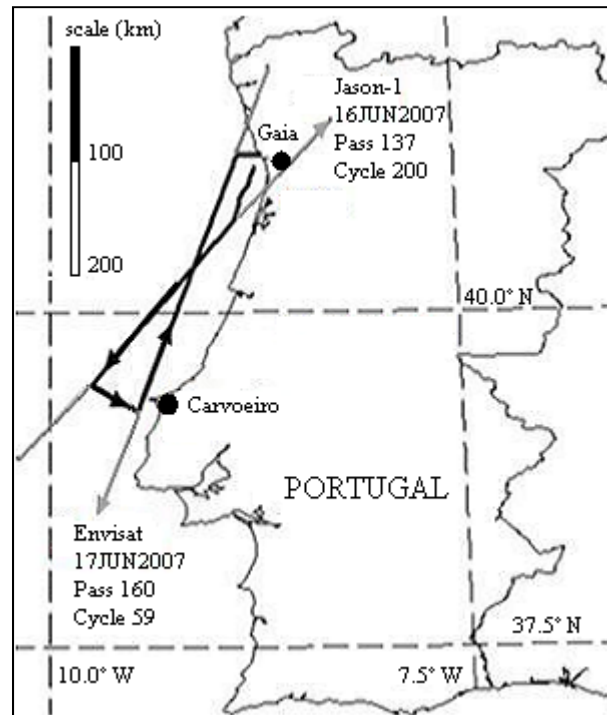
Figure 7.4 – Mission navigation plan (black line), satellites track (gray line) and reference stations (black dots).

The data collection campaign took place between 16 0830 UTC and 17 1810 UTC of June 2007 in order to coincide with the ENVISAT and JASON-1 passes along the Portuguese coast (see figure 7.4) during a navigation period of 33 hours. GPS measurements of SSH were computed along ENVISAT pass 160 (cycle 59) and JASON-1 pass 137 (cycle 200). The collected GPS and IMU data sets were recently reprocessed using PPP and compared with satellite altimetry data processed with improved coastal corrections [Marrreiros *et al.*, 2012]

7.2.2. Determination of the antenna position in the ship's body frame

The body frame coordinates given in figure 7.3 are a first approximation based on the ships drawings. An error in the Trimble GPS antennas body frame coordinates will induce an error in the determination of ship motion effects. It was found that more accurate body frame coordinates must be estimated for each one of the Trimble GPS antennas.

For the estimation of accurate body frame coordinates of each GPS antenna, a simple procedure was implemented based on the assumption that the instantaneous SSH may be considered constant from one epoch to the next, 1 s interval, along the ships track. This estimation procedure was implemented sequentially in a search space centered on the approximate solution, for a given consecutive set of GPS ships positions without gaps and outliers, as follows:

1. Firstly, approximate values are assumed as a potential solution for the antenna position in the ships body frame, from the ships drawings.

2. The Trimble GPS antenna geodetic height is estimated and corrected for pitch, roll and heave using the ships assumed body frame coordinates.

3. The motion corrected (correction for pitch, roll and heave) GPS geodetic height variation (from one epoch to the next) is computed.

4. The sum of the GPS geodetic height variations for all the data set is accumulated and stored.

5. Another potential solution for the body frame coordinates is tested. A grid of potential solutions is given by a small variation (5 cm) applied to each one of the antenna coordinates (x, y or z) in the body frame, within a reasonable range (in this case, +/- 1 m). The process in steps 2 and 3 is repeated, and another sum of GPS geodetic height variations is stored.

6. If the sum of new accumulated GPS geodetic height variations is smaller than the one previously stored, then replace the stored value and assume the new potential solution as the best one.

7. Continue this process within the grid of potential solutions.

8. Finally, the most accurate solution is the one that corresponds to the smallest accumulated value of GPS geodetic height variations for all the potential solutions.

This methodology was applied to two subsets, one for each antenna, where all GPS ships position solutions were validated as good. The data sets should be long enough in order to minimize the influence of positioning errors in this estimation procedure. In this case, each data set is about 1 hour long (contains 3600 consecutive epochs) for each one of the antennas without gaps and outliers. The final result for the antenna position is shown in table 7.2.

Table 7.2 - GPS antennas coordinates in the ships body frame (in metres).

	X Longitudinal (positive backwards)	Y port-starboard (positive to port)	Z vertical (positive downwards)
Port antenna	6.11	0.85	-8.19
Starboard antenna	6.10	-1.16	-8.00

Note that the distance between the two GPS Trimble antennas is 2.01 m, in the port-starboard direction as computed from the estimated coordinates, which is in agreement with the true value observed with a tape during the installation on the on board antennas.

7.2.3. Determination of a reference trajectory

GNSS raw data from each receiver was converted and merged into a single RINEX file. Each one of the two TRIMBLE GPS receivers data installed on board was processed in OTF mode independently for each reference station. OTF is an abbreviation for "On-The-Fly" and stands for a processing method that does not requires static initialization of GPS carrier phase ambiguity resolution and is used for kinematic applications that require a centimetre level accuracy. More information about this method may be found in the specialized literature such as Leick (1995) and Xu (2007).

The commercial software package TRIMBLE Total Control v 2.73 was used to process the GNSS data. Since two antennas were installed on board and two reference stations were available, four independent baselines were computed:

- Gaia – Port antenna;
- Gaia – Starboard antenna;
- Carvoeiro – Port antenna;
- Carvoeiro – Starboard antenna.

The results of RTK data processing for each one of the baselines are summarized in the plots of height versus time for each one of the four baselines, after correcting for ship motion effects (roll, pitch and heave). From the RTK derived height time series plotted in figure 7.6 it is observed that:

- Some outliers are visible mainly when the ship is at longer distances from the reference station.
- The starboard GPS antenna gives the best results and has less data gaps, when compared to the port antenna. It was found this was cause by malfunction of the GPS receiver connected to the port antenna.

- The baseline Carvoeiro-Starboard antenna is the one that shows overall the most consistent results.

- Near Gaia reference station the baseline Gaia-Starboard seems to be the one with the most consistent results.

From these observations the final solution was based on a combination of the Carvoeiro-Starboard antenna and Gaia-Starboard antenna, taking in consideration the criteria of minimum distance of the Starboard antenna to each one of the reference stations. A mixed solution set was created using results from each one of the above mentioned baselines. See figure 7.6, where the vertical dashed lines indicates the period that corresponds to each one of the baselines:

- Baseline Gaia – Starboard is used from the start to epoch 58000 s;

- Baseline Carvoeiro – Starboard is used from epoch 58001 to 125000 s;

- Baseline Gaia – Gaia Starboard is used again from epoch 125001 to the end.
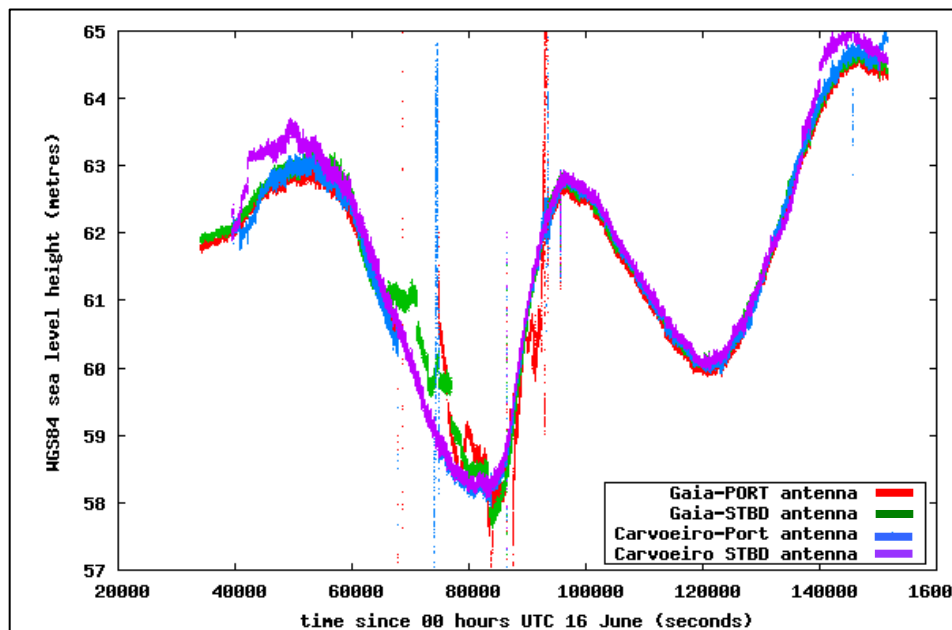
Figure 7.5 – RTK derived height time series for each one of the two antenna of the ship using the two reference stations (four baselines).

The final reference trajectory solution for the ship's trajectory was based in a mixed solution using the two reference stations for the starboard GPS antenna. The criteria for selecting the reference station was the minimum baseline distance. Using this criterion the maximum distance to a reference station is 110 km. The height plot of the final data set is represented in figure 7.6.
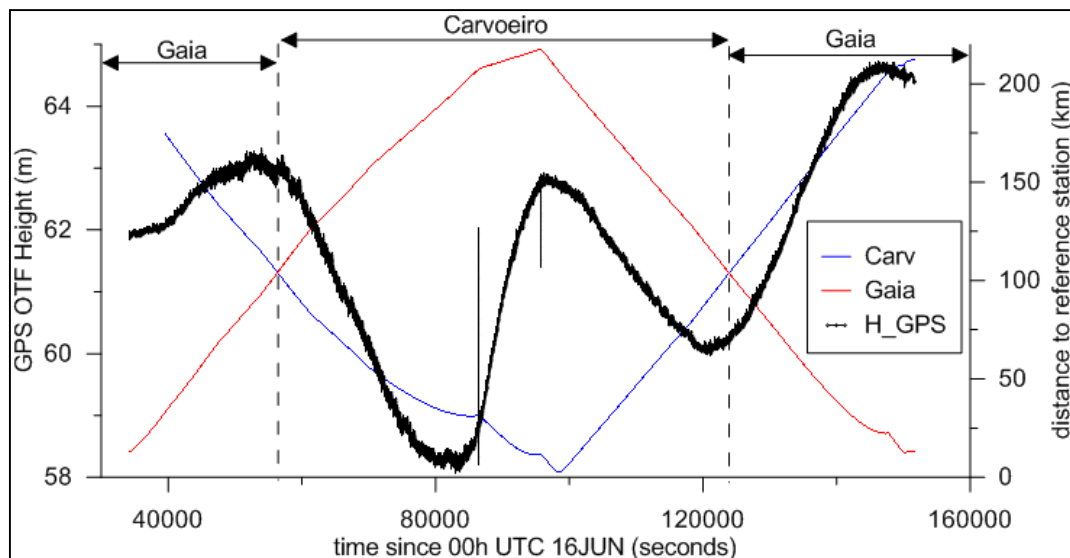
Figure 7.6 – Final GPS OTF height derived from the ship reference trajectory heights, using both reference stations. The distance to each reference station is also represented.

7.2.4. Performance analysis of the developed PPP software

The RINEX data files from the ship starboard antenna were used for processing in PPP mode, using the software developed under the scope of this study, SAPPos. Additionally the same RINEX data files were used for processing with the open source software RTKLIB [Takasu, 2010]. The RTKLIB (http://www.rtklib.com/rtklib.htm) is an open source software for GNSS positioning that can be used, among other functionalities, for PPP.

The satellite positions were derived from IGS precise ephemeris SP3 files. The satellite clock errors were interpolated from IGS 30 s CLK files. The estimated coordinates consider the antenna phase centre offset. Solid Earth, ocean loading and pole tidal effects have also been applied. The tropospheric zenith path delay was estimated as an additional unknown and a dual frequency combination was used to eliminate the ionospheric effect.

PPP results from SAPPos were first compared to the OTF solution using a reference station for the entire trajectory, the baseline Gaia-starboard antenna (figures 7.7 and 7.8). The main conclusions of this analysis are:

- Near the reference station, the two time series are highly correlated and both show the same high frequency variations due to ships motion (figure 7.7).

- As the ship moves away, the OTF solution seems to reduce its accuracy, while the PPP solution keeps the expected trend. The largest differences occur between 62000

and 85000 s, when the ship was at the greatest distance from both the reference station and the PPP solution seems to keep its centimetre accuracy (figure 7.8).

- The PPP convergence time was 300 s (figure 7.8).
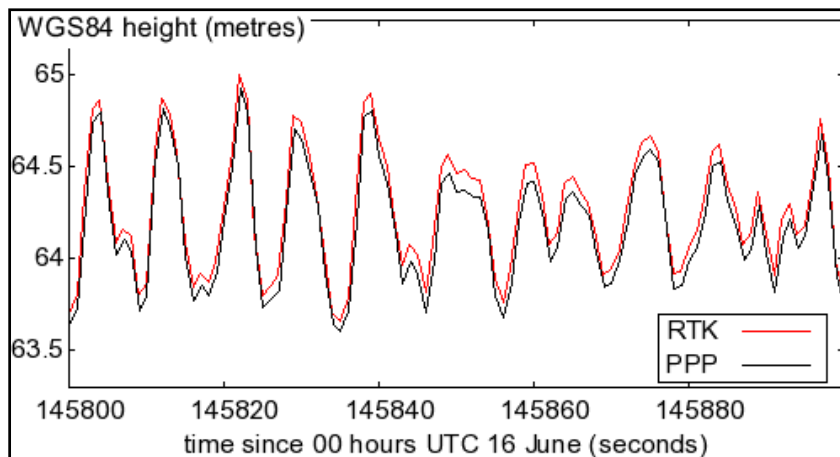
Figure 7.7 - Detail of PPP vs OTF height series, near the reference station, Gaia.
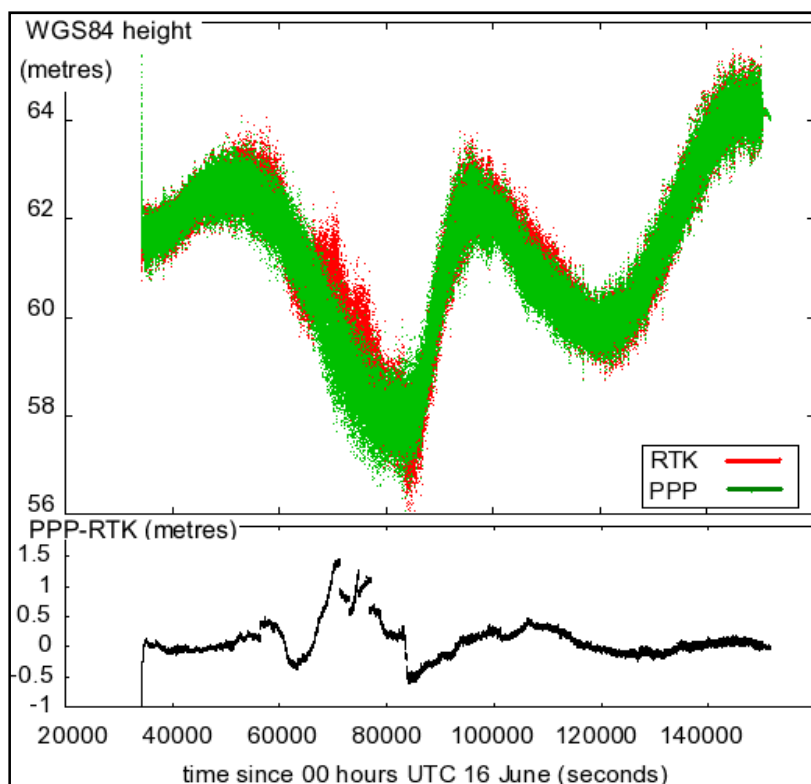
Figure 7.8 – SAPPos PPP vs OTF height full time series. The lower plot represents the differences.

Next, the more accurate OTF reference trajectory, resulting from the combination of using the two reference stations, was used to evaluate the performance of both SAPPos and RTKLIB (figure 7.9).
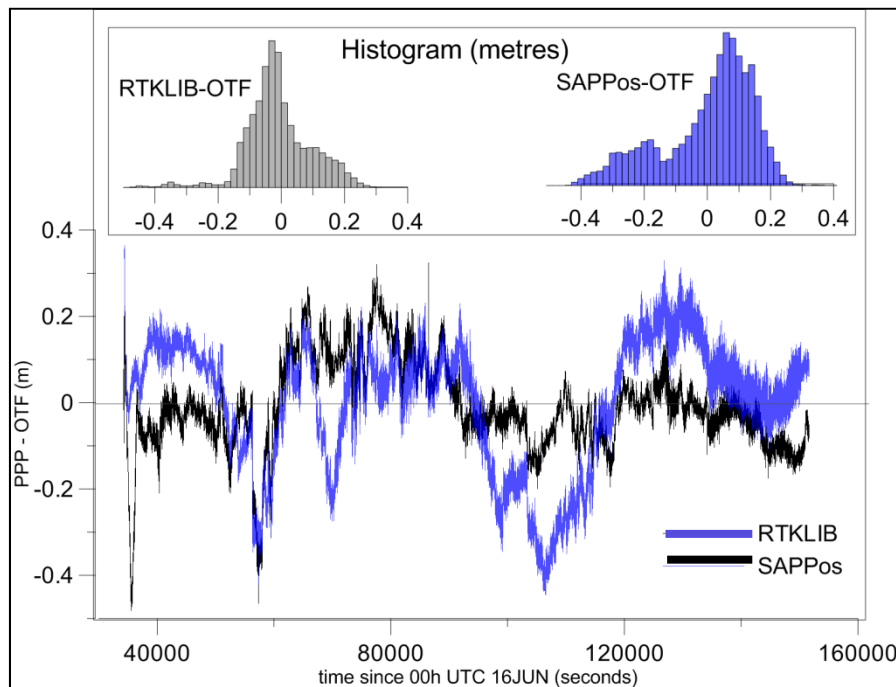
Figure 7.9 – PPP height differences for SAPPos – OTF and RTKLIB – OTF (lower graph) and respective histograms (top graph).

The statistical analysis of the height differences time series indicates that the RTKLIB solution seems to be more accurate, with a standard deviation of 10 cm, when compared to the SAPPos solution, with a standard deviation of 14 cm. The average value of the differences is 1.8 cm. The slightly better results with RTKLIB when compared with SAPPos are due, probably, to the functionally available on the RTKLIB to fix the carrier phase ambiguities.

The convergence time, however seems to be slightly better for the SAPPos, about 300 s, when compared with the RTKLIB. The assumption for this faster convergence is probably due to the preliminary ambiguity determination based on the DF combination implemented in the SAPPos.

7.3. Comparison of satellite versus ship based SSH

The SSH derived in the previous section is now compared with coastal altimetry. The processing of coastal satellite altimetry data in this specific project, using state-of-the-art methodologies, is described in Marreiros *et al.* (2012).

The results for the comparison between ship-based and satellite altimetry SSH show that both measurement systems are able to capture the main signals present in the SSH along the observed profiles. The standard deviation of the differences for the ENVISAT is 9 cm, while for JASON-1 is 13 cm. These results are within the expected values, considering that they have been derived with 20 Hz altimeter data and that the satellite and ship measurements span different time periods. The GPS derived SSH results seem to be more accurate along the ENVISAT path than along the JASON-1 path (figures 7.10 and 7.11). This may be explained by an increased wave motion when the ship was moving southwards along the JASON-1 track. As ship´s roll, pitch and heave increases, errors in lever arms calibration and GPS satellite cycle slips causes a loss of accuracy in the position solution.

It should also be recalled that, although the ship cruise was planned to coincide as close as possible with the passage of the satellites in the middle point of ship's track plan, there is a maximum time difference between ship and satellite measurements of 8 and 6 hours at the start and end of the data collection period for the ENVISAT and JASON-1, respectively. Therefore, patterns of ocean variability in the study region may have contributed to the residual differences shown in figures 7.10 and 7.11.

Figure 7.10 - GNSS derived and satellite altimetry SSH, using the GPD wet tropospheric correction and WITM ocean tide model, along ENVISAT pass 160, cycle 59. The two data series were intentionally offset from each other. The lower plot represents the differences between the two data series.
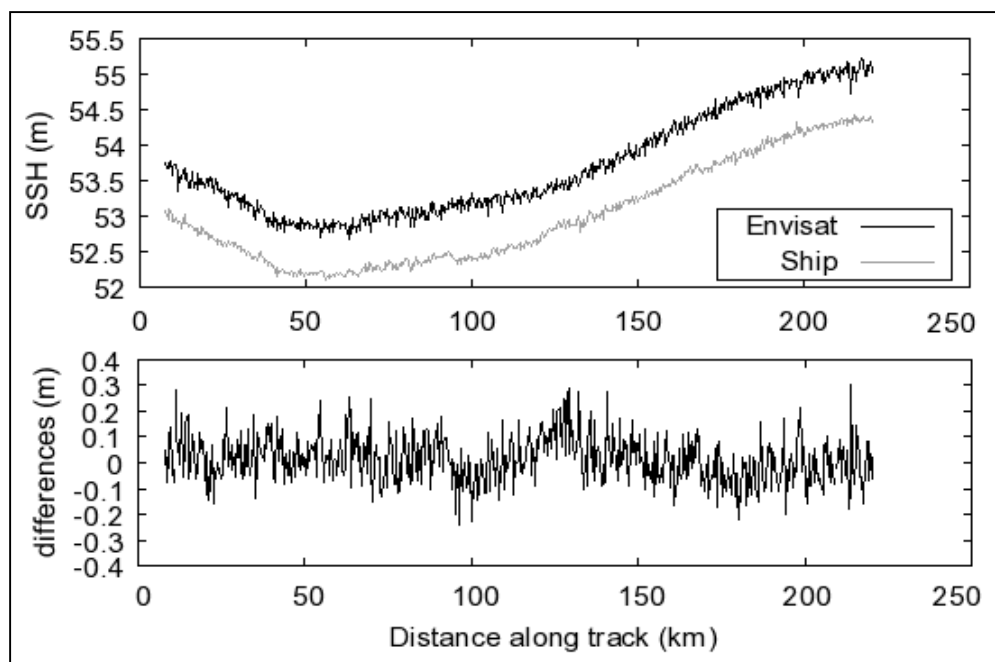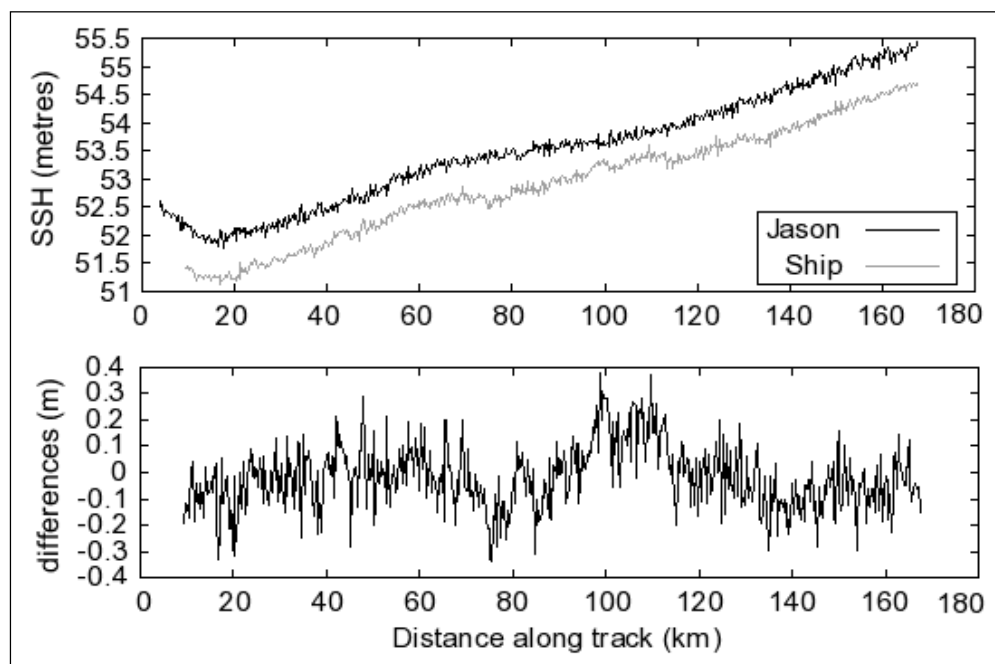

Figure 7.11 - GNSS derived and satellite altimetry SSH using the GPD wet tropospheric correction and the WITM ocean tide model, along JASON-1, pass 137, cycle 200. The two data series were intentionally offset from each other. The lower plot represents the differences between the two data series.

Chapter 8. Conclusions and recommendations

The study carried out during this investigation has shown that PPP can be used for precise positioning of marine platforms and all objectives set forth at the Introduction of this thesis were generally achieved. The analysis done through this investigation have contributed towards a better understanding of several specific problems in PPP involving the use of the most appropriate physical models, selection of the best data combinations and the improvement of performance, including the convergence time.

The specific contributions of this study can be summarized as follows:

1. Development of a positioning methodology that can be used for kinematic positioning with a single GNSS receiver;
2. Assessment of the quality of the resulting PPP estimate accuracy in a marine environment and comparison to the derived ship based PPP with SSH estimates obtained from satellite altimetry;
3. New routines were programmed to implement methods not available at the GPSTk library. The software implementation, based on the GPSTk library, is standard and as portable between platforms as possible;
4. As a result of this thesis, a new PPP software suite that can be used in real life, both for static and kinematic applications in the domain of hydrography and oceanography, is freely available, and can integrate further developments. This has the potential to avoid the dependence of commercial software packages, reducing costs;
5. The comparison with satellite altimetry demonstrated the feasibility of GNSS measurements of SSH on board ships for collecting in situ data for validation of coastal altimetry products.

8.1. Conclusions

PPP is capable of achieving centimeter accuracy level in the case of static positioning. By comparison with a reference trajectory computed by RTK, the accuracy of kinematic PPP was accessed to be also at decimetre level.

The accuracy of kinematic PPP was accessed to be also at decimetre accuracy level by comparing with a reference trajectory computed by RTK.

Precise satellite clock errors cannot be interpolated for a long period interval (900 s) without significant error. For kinematic PPP, when the solutions are estimated along the trajectory at 1 s interval, high data rate (no higher than 30 sec interval) clock corrections are required.

The modifications made to the PPP software by introducing new data combinations, troposphere model and satellite weighting, significantly improved the accuracy and convergence time when compared to the traditional PPP model. The comparison with the RTK solution, near the reference station, shows the same accuracy, at centimetre level. This study shows that PPP allows offshore marine precise positioning where reference stations are not available for a reliable RTK solution.

The best performance for PPP was achieved with the IF carrier phase combination and CP combination for each frequency. The MW combination was used to estimate the ambiguities and also improved the convergence time to 300 s in kinematic positioning.

The comparison between ship-based and satellite altimetry measurements of SSH along two satellite tracks on the west Iberian coast showed that the difference between the various ENVISAT and JASON-1 SSH data sets derived by using appropriate models for the wet tropospheric correction and for the ocean tides are smaller than the differences between the SSH captured by the two measurements systems: altimeter and GPS installed on a vessel. In part this can be explained by the particular conditions of the study area with moderate ocean tide variability and low to moderate variability in the wet path delay.

8.2. Recommendations for future work

The methodology presented in this study can be applied to any GNSS system, such as GPS, GLONASS, etc. However, only GPS data was processed and the software is not yet able to process observations from another GNSS. This is a relevant topic that requires further investigation and will certainly improve the performance of PPP.

The developed PPP methodology estimates the ambiguities as float numbers and keeps its integer nature allowing ambiguity fixing, in theory. Further development will be dedicated to this pending issue.

Concerning with the GNSS-derived SSH two types of improvement can be performed. First, implement more accurate ship dynamic models in order to estimate the influence of

hydrodynamics, squat or load variation effects. Secondly, improved methodologies to reduce error sources derived from lever arms calibration and ship draught variation shall be adopted.

This page was intentionally left blank

References

Abdel-salam, M. A. (2005) *Precise Point Positioning Using Un-Differenced Code and Carrier Phase Observations*, Ph.D. dissertation, Geomatics Engineering Department, University of Calgary, Alberta, September 2005.

Banville, S., Santerre, R., Cocard, M. and Langley, R.B. (2008) "Satellite and receiver phase bias calibration for undifferenced ambiguity resolution" Institute of Navigation National Technical Meeting 2008.

Bisnath, S.B. and Langley, R.B. (2001) "Precise Orbit Determination of Low Earth Orbiters with GPS Point Positioning". *Proceedings of ION National Technical Meeting*, January 22-24, Long Beach, 2001.

Bisnath S. (2004) *Precise orbit determination of low Earth orbiters with a single GPS receive-based, geometry strategy*, Ph.D. dissertation, Department of Geodesy and Geomatics Engineering, Technical Report No. 220, University of New Brunswick, Fredericton, New Brunswick, Canada.

Bisnath, S.B. and Gao, Y. (2009) "Innovation: Precise Point Positioning", *GPS World*, April, 2009.

Blewitt, G. (1990) "An automatic editing Algorithms for GPS data", *Geophys. Res. Lett.*, 17(3), 199-202.

Boehm, J., Werl, B., and Schuh, H. (2006a) "Troposphere mapping functions for GPS and very long baseline interferometry from European Centre for Medium-Range Weather Forecasts operational analysis data", *J. Geophys. Res.*, 111, B02406.

Boehm, J., Niell, A. E., Tregoning, P. and Schuh, H., (2006b) "Global Mapping Function (GMF): A new empirical mapping function based on numerical weather model data," *Geophys. Res. Lett.*, 33, L07304.

Boehm, J., Heinkelmann, R., and Schuh, H. (2007) "Short Note: A global model of pressure and temperature for geodetic applications", *J. Geod.*, 81(10), 679-683.

Brown, R.G., Hwang, P.Y. (1997) *Introduction to random signals and applied Kalman filter*, 3rd edition, Wiley.

References

Cannon, M.E. and Schwarz, K.P. (1989) "GPS semi-kinematic positioning along a well-controlled traverse", *Proceedings of the 5ᵗʰ International Geodetic Symposium on Satellite Positioning*, Las Cruces, New Mexico, March 13-17, vol 2, 621-630.

Casaca, J., Matos, J. and Baio, M. (2000) *Topografia geral*, Lidel – Edições Técnicas Lda.

Chen, W., Hu, C., Li, Z., Chen, Y., Ding, X., Gao, S. And Ji, S. (2004) "Kinematic GPS Precise Point Positioning for Sea level Monitoring with GPS buoy", *J. Global Pos. Syst. ,* vol. 3, nº 1-2, 302-307.

Cheng, K.-C. (2005) *Analysis of water level measurement using GPS*, Report No. 476, Geodetic Science and Surveying, Department of Geological Sciences, The Ohio State University, Columbus, Ohio, USA.

Collins, J.P. (1999) "An overview of inter-frequency carrier phase combinations", unpublished. Available for download: http://gauss.gge.unb.ca/papers.pdf/L1L2combinations.collins.pdf (accessed 7 June 2012).

Collins, J.P. and Langley, R.B. (1999) *Possible weighting schemes for GPS carrier phase observations in the presence of multipath.* Geodetic Research Laboratory, Depatment of Geodesy and Geomatics Engineering, University of New Brunswick, Fredericton N.B., Canada.

Colombo, O.L., Sutter, A.W., Evans, A.G. (2004) "Evaluation of precise, kinematic GPS point positioning", Proceedings of the Institute of Navigation (ION) GGSS-2004 Meeting, Long Beach, California, September 2004.

Dach, R., Hugentobler, U., Fridez, P., Meidl and M. (2007) *Bernese GPS software*, version 5.0, Astronomical Institute, University of Bern, January 2007. Available for download: http://www.bernese.unibe.ch/docs/DOCU50.pdf (accessed 14 May 2012).

Davies, K. (1989) *Ionospheric Radio*, Peter Peregrinus, Ltd., London,

Davis, J. L., Herring, T. A., Shapiro, I. I., Rogers, A. E. E., and Elgered, G. (1985) "Geodesy by radio interferometry: effects of atmospheric modelling errors on estimates of baseline length", *Radio Sci*., 20(6), 1593-1607.

Deurloo, R. (2011) *Development of a Kalman filter integrated system and measurement models for a low-cost strapdown airborne gravimetry system*, Ph.D. Dissertation in Surveying Engineering, Department of Geosciences, Environment and Spatial Planning, Faculty of Sciences, University of Porto, March 2011.

References

Doong, D.-J., Lee, B.-C. and Kao, C.C. (2011) "Wave measurements using GPS velocity signals", *Sensors*, 11, 1043-1058.

Doodson, A.T., and Warburg, H.D. (1941) *Admiralty Manual of Tides*, Her Majesty's Stationery Office, London, 270 pp.

Dufau, C., Martin-Puig, C. and Moreno, L. (2011) "User requirements in the coastal ocean for satellite altimetry" in Vignudelli, S., Kostianov, A., Cippolini, P. And Benveniste, J. (eds), *Coastal altimetry*, Springer, Heidelberg, 51-60.

Elenriksen, J., Lachapelle, G., Raquet, J., Stephen, J. (1996) "Analysis of Stand-Alone GPS Positioning Using Post-Mission Information", *Proceedings of the 9th International Technical Meeting of the Satellite Division of The Institute of Navigation*, Kansas City, MO, September 1996, 251-259.

Farrell, W.E. (1972) "Deformation of the Earth by Surface Loads", *Rev. Geophys. Space Phys.*, 10(3), 761-797.

Fei, G., Xiaohong, Z., Xingxing, L. and Shixiang, C. (2010) "Impact of sampling rate of IGS clock on Precise Point Positioning", *Geo-spatial Inform. Sci.*, 13(2), June 2010.

Fernandes, M.J., C. Lázaro, A. Nunes, N. Pires, L. Bastos and V. Mendes (2010) "GNSS-Derived Path Delay: An approach to compute the wet tropospheric correction for coastal altimetry", in*: IEEE Geosci.Remote Sens. Lett.*, 7(3), 596-600.

Gao, Y., McLellan, J.F. and Abousalem, M.A. (1997) "Single-point GPS accuracy using precise GPS data" *The Australian Surveyor*, 42(4), 185-192.

Gao, Y. and Shen, X. (2001) "Improving Ambiguity Convergence in Carrier Phase-Based Precise Point Positioning" *Proceedings of the ION GPS 2001*, 11-14 September 2001, Salt Lake City, UT, 1532-1539.

Garcia-Fernandez M., M. Markgraf and O. Montenbruck (2005) "Estimation of rocket spin rates from GPS phase wind-up" TN 05-06 version 1.0, Space Flight Technology, German Space Operations Center (GSOC), Dec. 27.

Gurtner, W., Mader, G., McArthur, D. (1990) "A common exchange format for GPS data", *CSTG GPS Bulletin*, 2 (3), May-June 1989, National geodetic Survey, Rockville.

References

Gurtner, W., Estey, L. (2009) *RINEX, The Receiver Independent Exchange format*, v3.1. Available for download from: http://igscb.jpl.nasa.gov/igscb/data/format/rinex301.pdf (accessed 20 June 2012).

Haines, B.J., Desai, S.D. and Born, G.H. (2010) "The Harvest Experiment, Calibration of the Climate data record from TOPEX/Poseidon, Jason-1 and the Ocean Surface Topography Mission", *Mar. Geod.*, 33(S1), 91-113.

Hatch, R. (1994) "Comparison of several AROF kinematic techniques", in *Proceedings of the 7th International Technical Meeting of the Satellite Division of the Institute of Navigation (ION GPS 1994),* September 20-23, Salt Lake City, Utah, 363-370.

Hein, G., Blomenhofer, H., Landau, H., and Taveira, E. (1992) "Measuring Sea Level changes using GPS in buoys" in *Sea Level Changes: Determnation and effects*, P.L. Woodworth, D.T. Pugh, J.G. DeRonde, R.D. Warrick and J, Hannah, eds., Geophysical Monograph Series, Volume 69, IUGG.

Herring, T. A. (1992) "Modeling atmospheric delays in the analysis of space geodetic data", in *Proceedings of refraction of transatmospheric signals in geodesy*, Netherlands Geodetic Commission Series, 36, The Hague, Netherlands, 157-164. Available for download from: http://www.ncg.knaw.nl/Publicaties/Geodesy/pdf/36DeMunck.pdf (accessed 15 June 2012).

Hernandez-Pajares M., Juan, J.M., Sanz, J., Orus, R., Garcia-Rodriguez, A. and Colombo, O.L. (2004) "Wide Area Real Time Kinematic with Galileo & GPS signals", *Proceedings of the ION GNSS 17th International Technical Meeting of the Satellite Division*, Long Beach, CA, September 21-24, 2541-2554.

Héroux, P. and Kouba, J. (1995) "GPS Precise Point Positioning with a Difference" Geomatics 95, Ottawa, Ontario, Canada, June 1995.

Hilla, S. (2010) "The Extended Standard Product 3 Orbit Format (SP3-c)". Available for download from: http://igscb.jpl.nasa.gov/igscb/data/format/sp3c.txt (accessed 13 May 2012).

Hofmann-Wellenhof, B., Lichtenegger, H. And Collins, J. (1992) *GPS Theory and Practice*, Springer-Verlag.

Holdridge, D.B. (1967) "An alternate expression for light time using general relativity", Jet Propolsion Laboratory, *Space program summary 37-48*, 3(2-4).

References

IAG (1984) *Resolutions of the XVIII General Assembly of the International Association of Geodesy*, Hamburg, Germany, August 15-27, J. Geod., 58(3), 309-323.

International Earth Rotation and Reference Systems Service – IERS Conventions 2010 (2010) *IERS Conventions (2010) - Technical note 36*. Available for download from: http://www.iers.org/nn_11216/IERS/EN/Publications/TechnicalNotes/tn36.html (accessed 12 March 2012).

IHO (2005) *Manual on Hydrography*, International Hydrographic Organization, Publication M-13, 1st edition, May 2005.

IOC - International Oceanographic Commission (2006) *Manual on seal level measurement and interpretation*, vol. IV, JCOMM technical report No 31, UNESCO.

IS-GPS-200F (2011) *Navstar GPS Space Segment/Navigation User Segment Interfaces*, IS-GPS-200, 21-Sep-2011, Global Positioning Systems directorate. Available for download from: http://www.gps.gov/technical/icwg/IS-GPS-200F.pdf (last accessed March 2012).

Kalman, R.E. (1960) "A new approach to linear filtering and prediction problems", *J. Basic Eng.*, 82D, 35-45, March 1960.

Kaplan, E. D. and Hegarthy, C. J. [editors] (2006) *Understanding GPS: principles and applications*, 2nd ed., Artech House.

Kato, T., Terada, Y., Ito, K., Hattori, R., Abe, T., Miyake, T., Koshimura, S. and Nagai, T. (2005) "Tsunami due to the 5 September 2004 off the Kii peninsula earthquake, Japan, recorded by a new GPS buoy", *Earth, Planets Space*, 57, 297-301.

Kelecy M.T., Born, G.H and Parke, M.E. (1994) "Precise mean sea level measurements using the Global Positioning System", *J. Geophys. Res.*, 99(2C), April 15, 7951-7959.

Klobuchar, J.A. (1996) "Ionospheric effects on GPS" in *Global Positioning System: Theory and applications*, vol I, edited by Parkinson and Spilker, Progress in Astronautics and Aeronautics, vol 163, The American Institute of Aeronautics and Astronautics, Washington, 1996, 679-862.

Kouba, J. and Héroux, P. (2001) "Precise point positioning using IGS orbit and clock products", *GPS Solutions*, 5(2), 12-28. Available for download from: http://www.geod.rncan.gc.ca/publications/papers/pdf/final.pdf (accessed 10 June 2012).

References

Kouba, J. (2009) "A guide to using International GNSS Service (IGS) Products". Available for download from: http://igscb.jpl.nasa.gov/components/usage.html (accessed 16 May 2012).

Kurtz, M. (1991) *Handbook of applied mathematics for engineers and scientists*, MacGraw-Hill.

Lachapelle, G., Cannon, M.E., Qiu, W., and Varner, C. (1996) "Precise aircraft single-point positioning using GPS post-mission orbits and satellite clock corrections", J. Geod., 70(9), 562-571.

Leick, A. (1995) *GPS Satellite surveying*, 2nd edition, Wiley-Interscience.

Lombardi, M. (2008) "The accuracy and stability of quartz watchs", *Horological J.*, February 2008, 57-59. Available for download from: http://tf.nist.gov/general/pdf/2276.pdf (accessed 10 June 2012).

Marshall, A. and Denys, Paul (2008) "Water level measurement tidal datum transfer using high rate GPS buoys", FIG Working Week 2008, Stockholm, Sweden 14-19 June.

Marreiros, P., Fernandes, M.J., and Bastos, L. (2012) "Evaluating the feasibility of GPS measurements of SSH on board a ship along the Portuguese West Coast*", J. Adv. Space Res.*, in press.

Martín, A., Anquela, A.B., Berné, J.L., Sanmartin, M. (2012) "Kinematic GNSS-PPP results from various software packages and raw data configurations", *Sci. Res. and Essays*, 7(3), 419-431, January, 2012. Available for download from: http://www.academicjournals.org/SRE (accessed 29 May 2012).

Mendes, V. (1999) *Modelling the neutral-atmosphere propagation delay in radiometric space techniques*, Technical Report 199, Department of Geodesy and Geomatics Engineering, University of New Brunswick. Fredericton N.B., Canada.

Montenbruck, O., Gill, E., Kroes, R. (2005) "Rapid orbit determination of LEO satellites using IGS clock and ephemeris products*", GPS Solutions*, 9, 226-235.

Mourad, A.G., Frazier, N.A., Holdahl, J.H., Someroski. F.W. and Hopper, A.T. (1969) *Satellite applications to marine geodesy*, prepared by Batelle Memorial Institute, Columbus, Ohio for National Aeronautics and Space Administration, Washington D.C., January, 1969.

References

Niell, A.E. (1996) "Global mapping functions for the atmosphere delay at radio wavelengths", *J. Geophys. Res.*, 101(B2), 3227-3246.

Parker, H. (2007) *Accuracy Analysis of Height Transfer and Calibration Verification of Bottom Mounted Tide Gauges using GPS Buoys*, Dissertation, School of Surveying, University of Otago, Dunedin.

Paulo, S., (1997) *Squat – Previsão do comportamento dos navios da Marinha*, Relatório 000/DG-820/972287, Direcção de Navios, Marinha.

Ray, J. and Gurtner, W. (2006) "RINEX extensions to handle clock information", v3.00, 14 November 2006. Available for download from: http://igscb.jpl.nasa.gov/igscb/data/format/rinex_clock300.txt (accessed 2 June 2012).

Ray, R.D. and Ponte, R.M., (2003) "Barometric tides from ECMWF operational analyses" *Ann. Geophys.*, 21(8), 1897-1910.

Rocken, C., Kelecy, T.M., Born, G.H., Young, L.E., Purcell, G.H., and Wolf, S.K. (1990) "Measuring Precise Sea Level from a Buoy using the Global Positioning System", *Geophys. Res. Lett.*, 17(12), 2145-2148.

Rothacher, M. and Schmid, R. (2010) "ANTEX: The Antenna Exchange Format, v1.4", 15 September 2010. Available for download from: http://igscb.jpl.nasa.gov/igscb/station/general/antex14.txt (accessed 2 June 2012).

Remondi, B.W. (1984) "Using the Global Positioning System (GPS) phase observable for relative geodesy: modelling, processing and results", University of Texas at Austin, Center of Space Recearch.

Remondi, B.W. (1985) "Global Positioning System carrier phase: description and use", *Bulletin Géodésique*, 59, 361-377.

Remondi, B.W. (1988) "Kinematic and pseudo-kinematic GPS", *Proceedings of the Satellite Division Conference of the Institute of Navigation*, Colorado Springs, Colorado, September 21-23.

RTCA (2006) *Minimum operational Performance Standards for Global Positioning System/Wide Area Augmentation System Airborne Equipment*, SC-159 DO-229D, issued 12/13/2006.

References

Saastamoinen, J. (1972) "Atmospheric correction for the troposphere and stratosphere in radio ranging of satellites", *The Use of Artificial Satellites for Geodesy, Geophysical Monograph Series*, 15, Henriksen, S. W., Mancini, A.,Chovitz, B. H. (eds.), 247-251.

Scherneck, H.-G. (1999) "Explanatory supplement to the section Local site displacement due to ocean loading of the IERS Conventions (1996) Chapters 6 and 7, Schuh, H. (ed.)", *DGFI Report 71*, 19-23.

Schmid, R., Steigenberger, P., Gendt, G., Ge, M. and Rothacher, M. (2007) "Generation of a consistent absolute phase center correction model for GPS receiver and satellite antennas", *J. Geod.*, 81(12), 781-798.

Schöne, T., Pandoe, W., Mudita, I., Roemer, S., Illigner, J., Zech, C. and Galas, R. (2011) "GPS water level measurements for Indonesia's Tsunami Early Warning System", *Nat. Hazards Earth Syst. Sci.*, 11, 741-749. Available for download from www.nat-hazards-earth-syst-sci.net/11/741/2011/ (accessed 17 February 2012).

Seeber. G. (2003*) Satellite geodesy*, de Gruyter.

Shen, X. (2002) *Improving ambiguity convergence in carrier phase-based precise point positioning*, Ph.D. dissertation, Department of Geomatics Engineering, University of Calgary, Calgary, Alberta, Canada.

Spilker, J.J. (1996) "Tropospheric effects on GPS" in *Global Positioning System: Theory and applications*, vol I, edited by Parkinson and Spilker, Progress in Astronautics and Aeronautics, vol 163.

Stewart, R.H. (2008) *Introduction to physical oceanography*, Department of oceanography, Texas A&M University. Available for download from: http://oceanworld.tamu.edu/home/course_book.htm (accessed 2 June 2012).

Sun H.P., Ducarne, B., Dehant, V. (1995) "Effect of the Atmospheric Pressure on Surface Displacements", *J. Geod.*, 70, 131-139.

Takasu, T. (2010) "Real-time PPP with RTKLIB and IGS real-time satellite orbit and clock", IGS Workshop, Newcastle upon Tyne, England, June 28 - July 2, 2010.

Tolman, B., Harris, R. B., Gaussiran, T., Munton, D., Little, J., Mach, R., Nelsen, S., Renfro, B., Schlossberg, D. (2004) "The GPS Toolkit -- Open Source GPS Software." *Proceedings of the 17th International Technical Meeting of the Satellite Division of the Institute of Navigation*, Long Beach, California, September 2004

References

Tolman, B.W. (2008) "GPS precise absolute positioning via Kalman filtering", *Proceedings of the ION GNSS International Technical Meeting of the Satellite Division*, 16-19, September 2008, Savannah, GA.

Tolman, B.W., A. Kerkhoff, D. Rainwater, D. Munton and J. Banks (2010) "Absolute Precise Kinematic Positioning with GPS and GLONASS", *Proceedings of the 23rd International Technical Meeting of the Satellite Division of the ION*, Portland, OR, September, 2010.

U.S. Government (2008) *GPS SPS performance standard*, 4th edition, September 2008. Available for download from: http://www.gps.gov/technical/ps/2008-SPS-performance-standard.pdf (accessed 12 March 2012).

Van Dam, T.M., Wahr, J., Chao, Y., Leuliette, E. (1997) "Predictions of crustal deformation and geoid and sea level variability caused by oceanic and atmospheric", *Geophys. J. Int.*, 129, 507-517.

Van Dam, T.M. and Wahr, J. (1998) "Modeling environment loading effects: a review", *Phys. Chem. Earth*, 23(9-10), 1077-1087.

Van Dam, T.M., Wahr, J., Milly, P.C.D., Shmakin, A.B., Blewitt, G., Lavallée, D., Larson. K.M. (2001) "Crustal displacements due to continental water loading", *Geophys. Res. Lett.*, 28(24), 651-654.

Vaníček, P. and E.J. Krakiwsky (1995) *Geodesy: The concepts*, Elsevier 2nd edition, 5th printing.

Vignudelli, S., P. Cipollini, C. Gommenginger, S. Gleason, H. Snaith, H. Coelho, J. Fernandes, C. Lázaro, A.L. Nunes, J. Gómez-Enri, C. Martin-Puig, P. Woodworth, S. Dinardo and J. Benveniste (2011) "Satellite Altimetry: Sailing Closer to the Coast", in D.L. Tang (ed.), *Remote Sensing of the Changing Oceans*, Springer-Verlag Berlin Heidelberg, 217-238.

Wahr, J.M. (1985) "Deformation Induced by Polar Motion", *J. Geophys. Res.*, 90(B11), September 30, 9363-9368.

Watson, C.S. (2005) *Satellite altimeter calibration and validation using GPS buoy technology*, Ph.D. dissertation, Centre for Spatial Information Science, University of Tasmania, July 2005.

Wells, D., Beck, N., Delikaraoglou, D., Kleusberg, A., Krakiwsky, E., Lachapelle, G., Langley, R., Nakiboglu, M., Scharwz, K., Tranquilla, J., and Vaníček, P. (1987). *Guide to

GPS Positioning, Canadian GPS Associates, Fredericton, New Brunswick, Canada, 2nd edition. 600 pp. Reprinted as UNB GGE Lecture Notes No. 58. Available for download from: http://gge.unb.ca/Pubs/LN58.pdf (accessed 15 April 2012).

Williams, S.D.P., Penna, N.T. (2011) "Non-tidal ocean loading effects on geodetic GPS heights", *Geophys. Res. Lett.*, 38, L09314.

Witchayangkoon, B. (2000) *Elements of GPS Precise Point Positioning*, PhD Dissertation, Spatial Information Science and Engineering, University of Maine, December 2000.

Wu J.T., Wu, S.C., Hajj, G.A., Bertiger, W.I. and Lichten, S.M. (1993) "Effects on antenna orientation on GPS carrier phase", *Manuscripta Geodaetica*, 18, 91-98.

Wübbena, G. (2012) "RTCM State Space Representation (SSR) Overall concepts towards PPP-RTK", presentation at PPP-RTK & Open Standards Symposium, March 12-13. 2012, Frankfurt, Germany.

Xu, G. (2007) *GPS Theory, algorithms and applications*, 2nd edition, Springer.

Zhang, X. and Forsberg, R. (2007) "Assessment of long-range kinematic GPS positioning errors by comparison with airborne altimetry and satellite altimetry", *J. Geod.*, 81, 201-2011.

Zumberge, J.F., Heflin, M.B., Jefferson, D.C., Watkins M.M. and Webb F.H. (1997a) "Precise Point Positioning for the efficient and Robust Analysis of GPS Data from Large Networks*", J. Geophys. Res.*, 102, 5005-5017, 1997.

Zumberge, J.F., Watkins, M.M. and Webb F.H. (1997b) "Characteristics and Applications of Precise GPS Clock Solutions Every 30 Seconds", *Navigation: Journal of the Institute of Navigation*, (44)4, 449-456, Winter 1997-1998.

Annex A. Status and future of GNSS

A.1. Introduction

This annex is devoted to the description of Satellite Navigation Systems. A Satellite Navigation System (SatNav) is a system of satellites that provides autonomous geo-spatial positioning. Satellite methods utilize artificial satellites to which ranges, range differences and any other measurement that may be used for the purpose of determining the coordinates of the observer.

In standard point positioning mode, SatNav allows small electronic receivers to determine their location (longitude, latitude, and altitude) to within a few metres using radio signals transmitted along the line-of-sight to the satellites. The receivers calculate the precise time as well as the antenna position.

One SatNav with global coverage is designated as Global Navigation Satellite System (GNSS). The following GNSS are operational or in development phase:
- GPS – Global Positioning System (United Sates of America);
- GLONASS – Russian Federation´s Global Navigation Satellite System (Russia);
- GALILEO – European Satellite Navigation System (Europe);
- BEIDOU – Chinese word for compass (China).

Some nations are developing regional coverage SatNav, such as:
- QZSS – Quasi-Zenith Satellite System (Japan);
- IRNSS – Indian Regional Navigation Satellite System (India);

A Satellite Based Augmentation System (SBAS) consists of widely dispersed reference stations that monitor and gather GNSS data. These data are forwarded to a master station for processing to determine the integrity and differential corrections for each monitored satellite. The integrity information and corrections to observations are then send to an Earth station and uplinked to a geostationary satellite. The geostationary satellites downlink the integrity and differential corrections for each monitored satellite using a frequency with a modulation similar to that used by GNSS. The geostationary satellite also can serve as an additional ranging signal. Currently the following SBAS are available:
- WAAS – Wide Area Augmentation System (United Sates of America);

- EGNOS - European Geostationary Navigation Overlay Service (Europe);

- GAGAN – GPS Aided Geosynchronous Augmented Navigation System (India);

- SDCM – System for Differential Corrections and Monitoring (Russia);

- MSAS - Multi-functional Transport Satellite (MTSAT) Satellite-based Augmentation System (Japan);

- SNAS (China);

In general, a SatNav is composed of three segments:

- The space segment, consisting of a constellation of satellites transmitting radio signals to the users;

- The user segment, consisting of the worldwide user receiver and antenna sets. It performs signal reception, data demodulation and computation of the navigation solution. The variety of applications requires development of specific methods for ground, sea, aviation and space applications;

- The control segment, consisting of a global network of ground facilities, that track the satellites, monitor their transmissions, perform analyses and send command and data to the satellites.

A.2. GPS: Global Positioning System (USA)

The GPS is a satellite radio navigation system developed by the Department of Defense (DoD) of the USA. This system uses a Medium Earth Orbit (MEO) satellite constellation transmitting microwave signals allowing a GPS receiver to determine its position, velocity and time.

The roots of GPS are closely connected to the dawn of the space age when the launch of the Sputnik satellite by the Soviet Union in 1957, since the satellite orbit could be determined by observing the Doppler Effect. Using this knowledge the USA developed the first satellite positioning system, called TRANSIT. This system was developed by the confluence of a vital need and advanced technology. The vital need was to have accurate navigation systems for the new class of submarines developed to carry Polaris missiles [Parkinson *et al.*, 1996].

With Transit, the horizontal position of a moving vehicle can be determined by measuring the Doppler shift of satellite signals, with an horizontal accuracy of 80 to 100 m (2D RMS). This system had no precise timing aboard the satellites, the calculation of a position took about 15

min and it was not fully global and available. Transit has been continuously operational since January 1964 (when the first position fix was computed on board of a submarine) until the end of 1996.

The concept of GPS was born in 1973 when the DoD decided to develop a satellite navigation system based on previous systems (like TRANSIT). In 1977 the first receiver tests were performed using pseudolites. The first operational GPS satellite was launched in 1978. Till 1985 a total of 11 block 1 satellites were launched. In 1993 the system reached full 24-satellite constellation. In this year it was also decided to allow the world wide civilian use.

In 17th July 1995 the Full Operational Capability (FOC) was achieved (http://www.navcen.uscg.gov). Five years later, on 1st May 2000, the deactivation of the SA was announced by the U.S. President Bill Clinton (http://clinton.nara.gov/WH/EOP/OSTP/html/0053_2.html), leading to an immediate improvement of the accuracy for civilian users from 100 m to 20 m. In September 2007 the U.S. Government announced its decision to produce the future generation of GPS satellite, known as GPS III, without the SA feature and permanently eliminate this source of uncertainty in GPS that was a concern for worldwide civil users (http://georgewbush-whitehouse.archives.gov/news/releases/2007/09/20070918-2.html).

A.2.1. Space segment and signals

The GPS baseline constellation consists of 24 satellites distributed in 6 orbital planes, with four slots per plane. Three of the 24 slots are expandable. Any surplus satellites that exist on orbit will occupy other locations in the orbital planes. There are no a priori specified slots for surplus satellites. The reference orbit parameters are [DoD, 2008]:

- Semi-major axis: 26559.7 km:
    - Altitude: 20200 km;
    - Period: 11 hours 58 min (aprox.12 sidereal hours);
- Eccentricity: 0.01º;
- Inclination: 55º

These orbits are nearly circular and have a period of approximately 12 sidereal hours. As of 11 August 2012 the space segment was built-up by 32 satellites: 10 satellites of block IIA, 12 satellites of block IIR, 7 satellites of block IIR(M) and 2 satellites of block IIF (University of

New   Brunswick   GPS   constellation   status: http://gge.unb.ca/Resources/GPSConstellationStatus.txt).

The original GPS design contains two ranging codes; the C/A (Coarse Acquisition) code, which is freely available to the public, and the restricted P (Precision) code, which is reserved for military applications and is encrypted, forming the P(Y) code.

After the launch of satellites IIR(M), two new signals were added on both frequencies L1 and L2: A new civil signal (L2C) and a new military signal (L1M and L2M). The new satellites IIF transmit another signal, on a new frequency, the L5C.

As part of the modernization plan, the satellites model III, still under production and planned to start launch after 2014, will include a new civil signal (L1C).

GPS uses Code Division Multiple Access (CDMA) technique to send different signals on the same frequency. The modulation method used for these basic GPS signals is the Binary Shift Phase Keying (BPSK). The new signals L2C and L5C are also BPSK modulated, the L1M and L2C are Binary Offset Carrier (BOC) modulated and the L1C is Multiplexed Binary Offset Carrier (MBOC) modulated (see table A.1).

Table A.1 – GPS frequency and signal plan (see http://www.gps.gov).

Satellites	Frequency and Signals							
	L1 (1575,45 MHz)				L2 (1227.60 MHz)			L5 (1176.45 MHz)
	L1C/A BPSK	L1P(Y) BPSK	L1M BOC	L1C MBOC	L2P2(Y) BPSK	L2M BOC	L2C BPSK	L5C BPSK
IIA 1990-1997	X	X			X			
IIR 1997-2004	X	X			X			
IIR(M) 2005-2009	X	X	X		X	X	X	
IIF 2010-...	X	X	X		X	X	X	X
III 2014-...	X	X	X	X	X	X	X	X

A.2.2. Control segment

The Operational Control Segment (OCS) began operation in 1985, consisting of five monitor stations, four ground antennas for upload and the Operational Control Center. The master

control station is in Colorado Springs, EUA, and the others are located on Ascension Island (Atlantic Ocean), Diego Garcia (Indian Ocean), Kwajalein and Hawaii (both Pacific Ocean) [The current OCS includes a master control station, an alternate master control station, 12 command and control antennas and 16 monitoring stations. The locations of these facilities are shown in the map bellow:
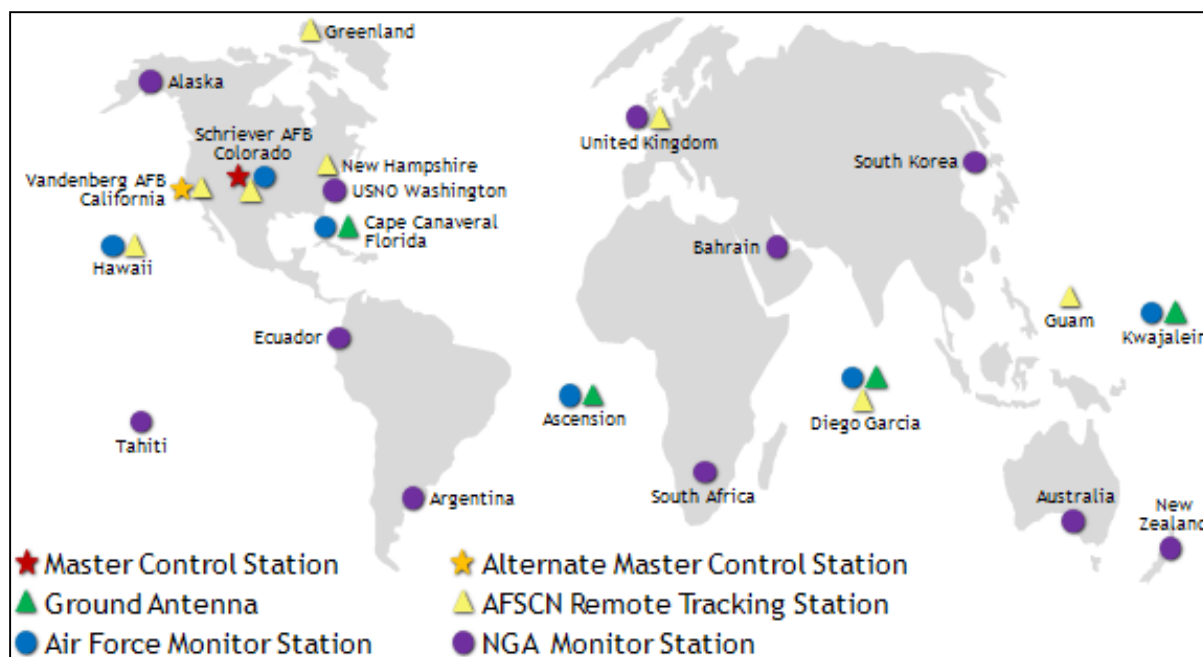
Figure A.1 – GPS control segment (from http://www.gps.gov/systems/gps/control/).

A.3. GLONASS (Russia)

GLONASS (stands for GLObal Navigation Satellite System) is a satellite navigation system developed by the former Soviet Union for military use. It was soviet second generation satellite navigation system, improving their Tsikada system which required one or two hours of signal processing to determine a position with high accuracy. The system is operated by the Coordination Scientific Information Centre (KNIT's) of the Ministry of Defense of the Russian Federation.

For a long time since, the start of GLONASS, the periods for observing more than four satellites were limited because GLONASS was not fully operational. Development of GLONASS began in 1976 with a goal of a global coverage predicted for 1991. In 1995 the constellation was completed, but the system fell rapidly into decay with the collapse of the Russian economy. Older satellites were taken out of service after their life time has been exceeded. The satellite replacement did not occurred and only 8 satellites remain in orbit in

2001. To have uninterrupted working conditions it is essential that a minimum of 18 satellites are in orbit, which was achieved by 2008-2009 and the complete 24 operational satellites constellation was achieved on May 2012 [Oleynik, 2012].

GLONASS was first planned to broadcast two types of signal: a standard precision (SP) signal and an encrypted high precision (HP) signal. All satellites transmit the same SP signal, however each satellite transmits on a slightly different frequency using a 25-channel Frequency Division Multiple Access (FDMA) technique. Due to interference with radio astronomy, the frequency band had already to be modified, more than once. Like GPS, GLONASS transmits navigational data at 50 bits/s. The wavelengths of the carrier are different for each satellite due to the different frequencies used. The knowledge of the wavelength is crucial for ambiguity resolution. The wavelength difference between the two extremes is 0.15 cm, which is less than 0.01 carrier cycle.

Second generation GLONASS satellites started deployment in 2003 also broadcast an additional frequency and an additional code base on CDMA. It is intended to follow the direction of signal modernization, to improve accuracy of phase and range measurements and interoperability with other GNSS [Oleynik, 2012].

A.3.1.   Space segment and signals

The first GLONASS satellite was launched into orbit in 1982. A fully functional GLONASS constellation consists of 24 satellites deployed in 3 almost circular orbits. As of 16 November 2012, 31 satellites were in orbit with 24 operational (http://www.glonass-center.ru/en/archive/). The reference orbit parameters are [ICD-GLONASS, 2008]:

- Semi-major axis: 25510 km:
  - o   Altitude: 19100 km;
  - o   Period: 11 hours and 16 min.
- Eccentricity: 0.01º;
- Inclination: 64.8º;

A characteristic of the GLONASS constellation is that any given satellite only passes over the exact same spot over the Earth every eighth sidereal day. The system is designed in such a way, that constellation, and therefore DOP-values will repeat each sidereal day, but with different satellites. For comparison each GPS satellite passes over the same spot twice every

sidereal day. Also, users in higher latitude areas obtain better GLONASS DOP-values than GPS, due to the higher inclination of satellite orbits.

The second, generation of satellites, known as GLONASS-M, were developed beginning in 1990 and first launched in 2003. These satellites possess a substantially increased design lifetime (7 years). Since 2003 the satellite type GLONASS-K1are being deployed, which has also increased design lifetime (10 years) and a new L-band frequency and new CDMA signal open for civil users. After 2013, a new GLONASS-K2 will start to be launched. These satellites have a reduced weight of only 750 kg and offer an additional L-band frequency with additional navigational signals at frequencies L1 and L2.

A fourth generation satellite, the GLONASS-KM is under design phase with the requirements to have higher life time and with twice the weight and onboard power supply, when compared with the GLONASS-K's. The deployment phase is planned to start in 2017.

A.3.2. Control segment

The GLONASS control segment is composed by (see figure A.2):

- SCC – System Control Center;
- TT&C – Telemetry, Tracking and Command station (5 stations);
- ULS – Uplink station (3 stations);
- MS – Monitoring station (10 stations);
- CC – Central Clock (2 stations);
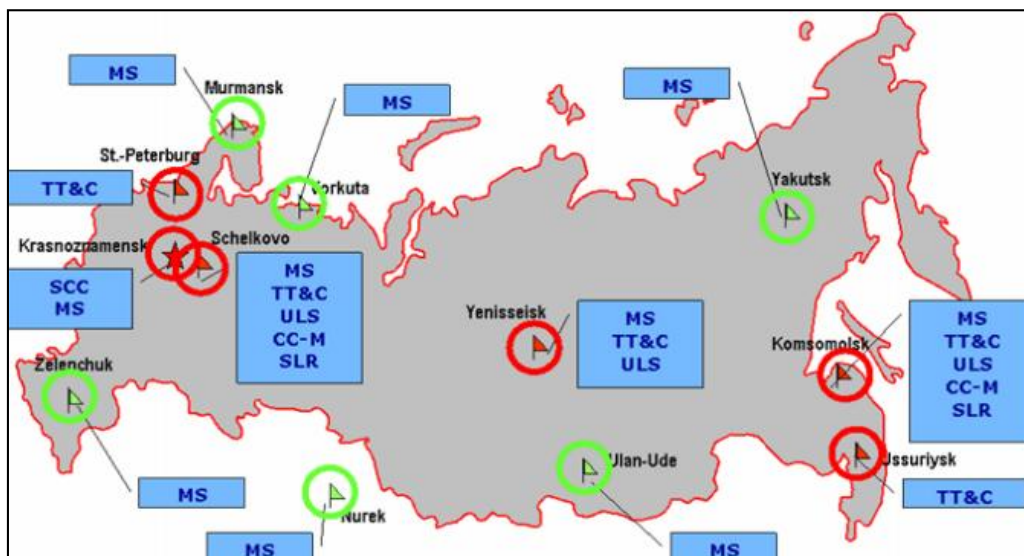- SLR – Laser Tracking Station (2 stations);

Figure A.2 – GLONASS control segment [Revnivykh, 2008].

A lack of a global coverage of ground stations is a drawback of the GLONAS system, since it may cause delays in the discovery of satellite anomalies and updating of satellite data.

A.3.3.   GPS vs GLONASS

GLONASS performance on position and velocity determination is comparable with GPS once the full system is operational [Oleynik, 2012].

GLONASS and GPS are not entirely compatible with each other however, they are generally interoperable.   Already available in the market, GNSS receivers already provide GPS and GLONASS measurements. The main advantages for the user community are increased accuracy and higher system integrity on a worldwide basis [Xu, 2007].

Table A.2 – Comparison of GPS and GLONASS.

	GLONASS	**GPS**
No of satellites	24	24
No of orbital plans	3	6
Inclination	64.8º	55º
Orbital radius	25510 km	26560 km
Fundamental frequency	5.011 MHz	10.23 MHz
Carriers		
L1	1606 to 1615.5 MHz	1575.42 MHz
L2	1246.0 to 1256.5 MHz	1227.60 MHz
Signals		
C/A	0.511 MHz	1.023 MHz
P	5.110 MHz	10.23 MHz
Geodetic reference	PZ 90	WGS 84
Time reference	GLONASS time	GPS time

A.4. GALILEO (Europe)

GALILEO is a GNSS initiated by the European Union and the European Space Agency for providing a highly accurate, guaranteed global positioning service under civilian control. It is inter-operable with GPS and GLONASS. A user will be able to take a position with the same receiver from any of the GNSS satellites in any combination. GALILEO will deliver real-time positioning for public use with metre level accuracy, will guarantee availability of the service under the most extreme circumstances and will inform users within seconds of a failure of any satellite.

A private company or a consortium of companies will establish the Ground Segment, takes responsibility for the launch of the satellites and will operate the system. The question of

financial founding and the formation of the private consortia slowed down the process of development. It seems that the deployment phase is fully paid by the public, while the funding of the operational and maintenance phase is still under discussion.

The development program comprises two main phases [ESA, 2013]:

- The In-Orbit Validation (IOV) phase. The IOV is concluded and consisted of assessing the system testes, the operation of two experimental satellites and a reduced constellation of four operational satellites and their ground infrastructure. Two of operational satellites were launched and positioned in one orbital plane on 21 October 2011. The other two operational satellites were launched on 12 October 2012 and positioned on another orbital plane on 12 October 2012.
- The Full Operational Capability (FOC). The FOC consists of the deployment of the remaining ground and space infrastructure, including an intermediate initial operational capability phase with 18 satellites in operation (the 4 IOV plus 14 others). By 2015, 18 satellites should be in place, followed by the rest until 2020.

A.4.1. Space segment and Signals

Fully functional GALILEO constellation consists of 27 satellites and 3 spares deployed in three almost circular orbits with a semi-major of 29600 km in a so-called Walker (27,3,1) configuration. This semi-major radius axis results in an orbit repetition time of 10 days. Each satellite will broadcast precise time signals, precise ephemeris and other data. The GALILEO satellite constellation has been optimised to the following constellation specifications:

- Semi-major axis: 29600 km:
  - o Altitude: 23222 km;
  - o Period: 14 hours;
- Eccentricity: 0.01º;
- Inclination: 56º.

The first GALILEO test satellite, Giove-A, was launched into orbit on 28 December 2005. A second test satellite, Giove-B, was launched on 27 April 2008. This satellite will incorporated some enhancements over GIOVE-A, allowing additional signals to be generated and received on the ground. The aim was to keep on providing early in-orbit experimentation with the common baseline L1 open service signals (see GALILEO homepage: http://www.esa.int/Our_Activities/Navigation/The_future_-_Galileo/What_is_Galileo).

The GALILEO navigation signals are transmitted in the four frequency bands:

Table A.3 – GALILEO carrier frequency per signal [ICD-GALILEO, 2010].

Signal	Frequency
E5a	1176.450 MHz
E5b	1207.140 MHz
E5 (E5a+E5b)	1191.795 MHz
E6	1278.750 MHz
E1	1575.420 MHz

The frequency bands have been selected in the allocated spectrum for Radio Navigation Satellite Services (RNSS), and in addition to that, E5a, E5b and L1 bands are included in the allocated spectrum for Aeronautical Radio Navigation Services (ARNS), employed by civil-aviation users, and allowing dedicated safety-critical applications.
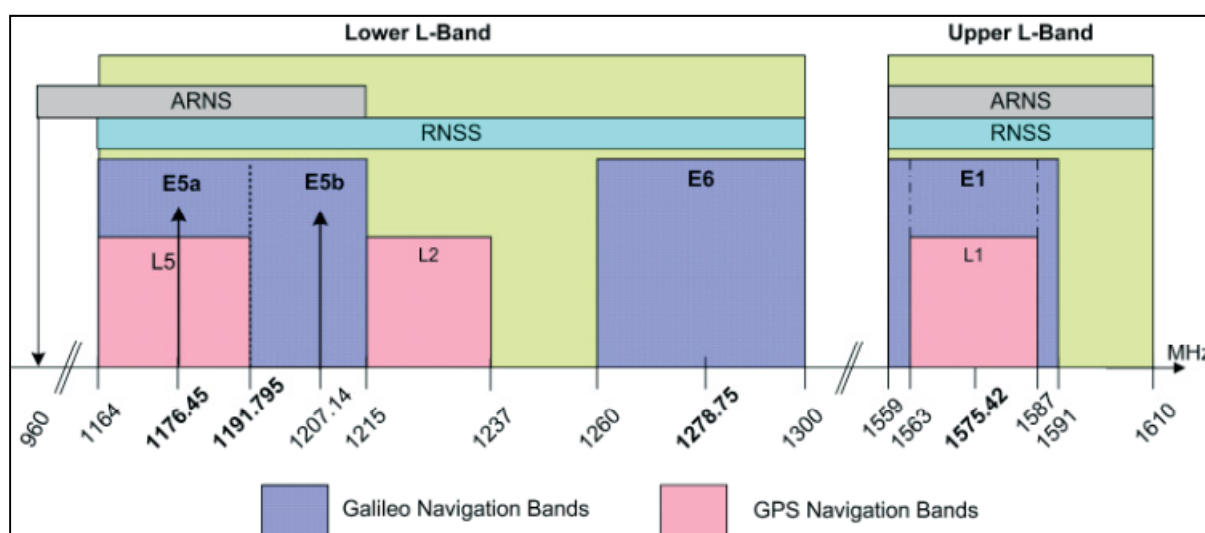
Figure A.3 – GALILEO frequency plan [ICD-GALILEO, 2010].

All GALILEO transmitting satellites share the same frequency bands, making use of the CDMA technique. Spread Spectrum signals are transmitted including different ranging codes per signal component, per signal, per frequency and per satellites.

A.4.2.   Control segment

The core of the GALILEO ground segment will be the two control centres. Each control centre will manage 'control' functions supported by a dedicated Ground Control Segment (GCS) and 'mission' functions, supported by a dedicated Ground Mission Segment (GMS). The GCS will use a global network of five transmitting stations to communicate with each satellite on regular contacts, long-term test campaigns and contingency contacts. A global network of thirty GALILEO Sensor Stations (GSS) will be used to monitor the navigation

signals of the satellites on a continuous basis. The prime element of the GSS is the reference receiver (see GALILEO homepage: http://www.esa.int/Our_Activities/Navigation/ The_future_-_Galileo/What_is_Galileo).

A.4.3.   Services

Like modernized GPS, GALILEO will also transmit freely on three frequencies with pseudorange codes modulated on each frequency. GALILEO will offer five different services to accommodate the needs of various users [ICD-GALILEO, 2010]:

- Open Service (OS): This service is free of charge. Receiver manufacturer's, however have to pay to implement *e.g.* patented memory codes. The OS is intended for mass market users such as cellular telephone, personal digital assistants (PDA's) and vehicle and pedestrian navigation.

- Commercial Service (CS): This service offers higher data rates than the OS and will lead to higher accuracy level. As the user has to pay for this service, access control via encryption of the data channels will be implemented.

- Safety of Life (SoL): This service will provide integrity information, i. e. within a certain "time to alarm" (6s) the user is warned if a certain satellite should not be used. This service is intended for users requiring guaranteed integrity such as CAT-1 aircraft landing, train guiding and marine applications.

- Public Regulated Service (PRS): This service is still under discussion within the European Union. It is intended for authorized public or strategic applications requiring a high level of continuity such as police, telecommunications networks and emergency services. The military use of GALILEO would also work with PRS. Its signal modulation and encryption will provide anti-spoofing and anti-jamming capabilities.

- Search and Rescue (SAR): Together with other satellite systems it will be possible to locate distress transmitters. For the first time, also a return channel will be implemented.

Table A.4 – GALILEO frequencies and services [ICD-GALILEO, 2010].

	E5a	E5b	E6	SAR	E1
OS	X	X			X
CS	X	X	X		X
SoL	X	X			X
PRS			X		X
SAR				X	

A.5. COMPASS (China)

In December 2011, China released a test version of the interface control document for the COMPASS [ICD-Beidou, 2011]. It is a small publication (with eleven pages) covering only the description of the open civil signal and gapping to describe information concerning with coordinate system, time scale and ephemeris data description. The official COMPASS website is available at http://en.beidou.gov.cn/index.html.

China started to build its independent GNSS in 1980's, the COMPASS (Beidou in Chinese). China decided to develop a GNSS starting with regional services and expanding to global services. A three step development strategy has been adopted [ICD-Beidou, 2020]:

- Phase I: Experimental, from 2000 until 2003, with the launch of 3 satellites;
- Phase II: Regional services for China and its surroundings, planned for 2012;
- Phase III: Global coverage, planned for 2020.

A.5.1. Frequency and signals

The positioning services will be transmitting signals using the following frequencies:

Table A.5 – Compass frequencies [Hegarty and Cartre, 2008].

Signal	Center frequency (MHz)	Bandwidth (MHz)
B1	1561.098	4.092
B1-2	1589.742	4.092
B2	1207.14	24
B3	1268.52	24

A.5.2. Services

Compass is being projected to incorporate two positioning services: an open service and an authorized service, the last with higher accuracy for use by the Chinese government and its military.

The open service will provide accuracies of 10 m in positioning, 0.2 m/s in velocity and 50 ns in time dissemination.

A.5.3. Orbital characteristics

The nominal constellation of the Compass regional system (Phase II) is composed of 14 satellites, including 5 Geostationary Earth Orbit (GEO), 4 Medium Earth Orbit (MEO) and 5

Inclined Geosynchronous Orbit (IGSO. The GEO satellites are positioned at longitudes: 58º.75 E, 80º E, 100º.5 E, 140º E and 160ª E [ICD-Beidou, 2011].

The first COMPASS experimental satellite was launched on October 2000 and the operational satellite was launched on April 2007 [Hegarty and Chatre, 2008].

A.5.4.   Control segment

The control segment, as with any GNSS, will consist of a master station, monitor stations and upload stations. No further information is available at present date.

References

Chen, J., Wu, B., Hu, X., Zu, S., Cao, Y., Wu, X., Xing, N. (2012) "Compass/Beidou: system status and initial service", presentation at IGS Workshop on GNSS Biases, 18-19 January, University of Bern, Switzerland.

DoD (2008) *Global Positioning System Standard Positioning Service Performance Standard*, 4th edition, U.S.A Department of Defense, September 2008. Available for download from: http://www.gps.gov/technical/ps/2008-SPS-performance-standard.pdf.

ESA (2013) *GALILEO Fact sheet*, European Space Agency. Available for download from: http://download.esa.int/docs/Galileo_IOV_Launch/Galileo_factsheet_2012.pdf.

Hegarty and Chatre (2008) "Evolution of the Global Navigation Satellite System (GNSS)", *Proceedings of the IEEE*, 96, No 12, December 2008.

ICD-Beidou (2011) *Beidou Navigation Satellite System Signal in Space Interface Control Document* (test version), China satellite Navigation Office.

ICD-GALILEO (2010) *Galileo Open Service Signal-In-Space Interface Control Document*, issue 1.1, September 2010.

ICD-GLONASS (2008) *GLONASS Interface Control Document,* edition 5.1, Russian Institute of Space Device Engineering, English translation of russian document.

Parkinson, B.W., Stansell, T., Beard, R. and Gromov, K. (1995) "A history of satellite navigation" *Navigation: Journal of The Institute of Navigation*, 42(1), Special Issue, 109-164.

Oleynik, E. (2012) "GLONASS Status and modernization" presentation at the United Nations/Latvia Workshop of GNSS, 14-18 May 2012, Riga, Latvia.

Revnivykh, S. (2008) "GLONASS: status and progress", CGSIC meeting, 16th September 2008, Savannah, Georgia, USA. Available for download from: http://www.navcen.uscg.gov/pdf/cgsicMeetings/48/Reports/International%20Subcommittee/%5B24%5D%20GLONASS%20CGSIC%2016.09.2008.pdf.

Spilker, J.J., Parkinson, B.W. (1996) "Overview of GPS operation and design", *Global Positioning System: Theory and applications, Volume I*, , Progress in Astronautics and Aeronautics, Vol 163, The American Institute of Aeronautics and Astronautics, Washington, 1996, 29-55.

Turner, D.A. (2006) "Space–based PNS modernization update", Munich Satellite Navigation Summit 2006.

Annex B. GNSS Precise products providers

B.1. International GNSS Service (IGS)

The International GNSS Service (IGS) was officially established in January 1994, originally known as the "International GPS Service for Geodynamics, from 1999 as the "International GPS Service" and finally, since March 2005 with the current designation. It is an operational scientific service of the International Association of Geodesy (IAG) and one of several services contributing to the Global Geodetic Observing System (GGOS). The origins and early development of the IGS are described by Beutler *et al.* (2008).

The IGS operates is a voluntary, non-commercial confederation of about 200 institutions worldwide, self-governed by its members. As of 23 August 2012 the tracking network was composed by 440 stations with 369 active stations. It primarily supports scientific activities based on high accurate Earth observations using GNSS. The mission of the IGS is to provide "the highest quality data and products as the standard for global navigation satellite system (GNSS) in support of Earth science research, multidisciplinary applications and educations. These activities aim to advance scientific understanding of the Earth system components and their interactions, as well to facilitate other applications benefiting society (IGS, 2012).

The production plan of the IGS is organized into Stations that transmit GNSS and meteorological data to the Data Centres, where the data is archived and provided open access to IGS data and products. The IGS Data Centres fall into three categories: operational, regional and global. The Operational Data Centres are in direct contact with the stations. The Regional Data Centres collect data from operational data centres and/or stations, maintain a local archive of the data received, provide on-line access to these data to the users of the region and transmit data from a subset of their sites (minimally, IGS reference stations) to the Global Data Centres. The Global Data Centres are the main interfaces to the Analysis Centres and the user community.

The IGS products result from the processing of station data by the Analysis Centres which are combined at the Analysis Centre Coordinator (ACC). The IGS ACC has overall responsibility for generating the main official IGS combined products. For the period 2012-15, the ACC functions are performed by NOAA's National Geodetic Survey, in Silver Spring, Maryland, USA. The IGS Central Bureau is sponsored by the National Aeronautics

and Space Administration (NASA) Earth Surface and Interior Focus Area and hosted by the Jet Propulsion Laboratory (JPL) of the California Institute of Technology(see figure B.1).
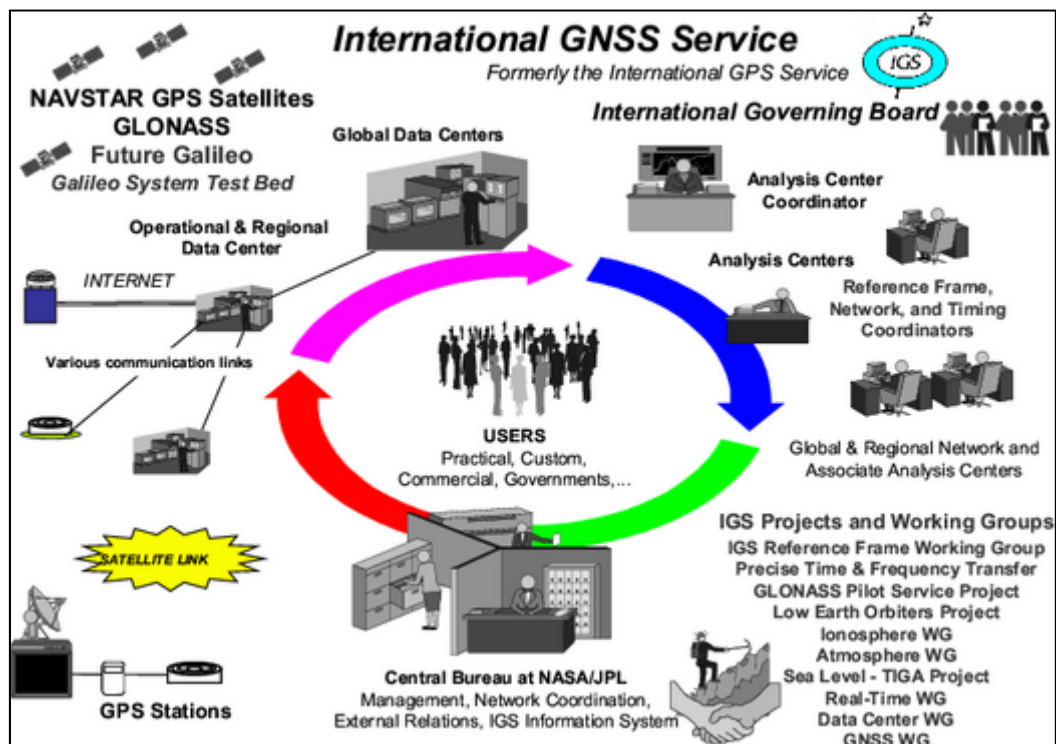

Figure B.1 – A diagram showing the organization of the IGS (from.
http://igscb.jpl.nasa.gov/organization/figure1.html accessed 15 May 2012)

The IGS collects archives and distributes GNSS observation data sets that are used to generate the following products (IGS, 2012):

- GPS satellite ephemerides;
- GLONASS satellite ephemerides;
- Earth rotation parameters;
- IGS tracking station coordinates and velocities
- GPS satellite and IGS tracking station clock information;
- Zenith tropospheric path delay estimates;
- Global ionospheric maps.

The IGS provides precise satellite ephemeris and clock products that are currently made available at no cost in different forms that vary in latency and accuracy, see table B.7. The IGS satellite ephemerides and clocks are provided in SP3 (a standardized orbit file format) and CLK (RINEX extension to handle clock information).

Table B.1 – Extract of IGS product table. Orbit accuracies are 1D mean RMS over the three XYZ geodetic components. Clock accuracies are relative to IGS time scale, which is linearly aligned to GPS time in one-day segments. The SDev values are computed by removing a separate bias for each satellite, whereas this is not done for the RMS values (IGS, 2012).

GPS satellite ephemerides and clocks						
		accuracy	latency	updates	Sample interval	
Broadcast	Orbits	~ 100 cm	real time		daily	
	Sat. clocks	~ 5 ns RMS ~ 2.5 ns SDev				
Ultra-rapid (predicted half)	Orbits	~ 5 cm	real time	at 03, 09, 15, 21 UTC	15 min	
	Sat. clocks	~ 3 ns RMS ~ 1.5 ns SDev			15 min	
Ultra-rapid (observed half)	Orbits	~ 3 cm	3 - 9 hours	at 03, 09, 15, 21 UTC	15 min	
	Sat. clocks	~ 150 ps RMS ~ 50 ps SDev			15 min	
Rapid	Orbits	~ 2.5 cm	17 - 41 hours	at 17 UTC daily	15 min	
	Sat. clocks	~ 75 ps RMS ~ 25 ps SDev			5 min	
Final	Orbits	< 2.5 cm	12 - 18 days	every thursday	15 min	
	Sat. clocks	~ 75 ps RMS ~ 25 ps SDev			30 s	
GLONASS satellite ephemerides						
Final	Orbits	~5 cm	12 - 18 days	weekly	15 min	

References

Beutler, G., Moore, A.W. and Mueller, I.I. (2009) "The International global navigation satellite systems service (IGS): development and achievements", *J. Geod.* 83, 297-307.

IGS (2012) http://igscb.jpl.nasa.gov/ (accessed 7 July 2012).

This page was intentionally left blank

Annex C. GNSS data combinations

C.1. Introduction

Data combinations are methods of combining GNSS data measured with the same receiver at the same station. It is different from data differentiations. Data differentiations are methods of combining GNSS data (of the same type) measured at different stations [Xu, 2007]. Data differentiations are not possible in PPP, by definition.

Data combinations can be advantageous for solving specific GNSS problems, most often used for three purposes:

- Provide an observable that has a wavelength greater that the raw observables, a wide-lane observable, which has advantages for ambiguity resolution;
- Reduce the ionosphere effect;
- Reduce noise and the effect of multipath;

It is not possible to have all these desirable characteristics at the same time in a single data combination. Each data combination has its advantages and drawbacks. Depending on the requirements, the optimal data combination will not always be the same.

This annex summarizes the data combinations for dual frequency observations used in the scope of this thesis. The following linear data combinations are considered, with the abbreviated notation:

- Linear combinations between observations of the same type:
  - o Ionosphere-free (IF);
  - o Geometry-free (GF);
  - o Wide-lane (WL);
  - o Narrow-lane (NL).
- Linear combinations between observations of different type:
  - o Code-phase (CP);
  - o Melbourne-Wübbena (MW);
  - o Divergence-Free (DF).

C.2. General equations for the combinations of two or more observables

A general combination of two observables, O_1 O_2, can be formed by $n_1 O_1 + n_2 O_2$ where n_1 and n_2 are arbitrary real numbers. However, to make such a combination in order to have the same physical meaning as the basic observables, the combination must be scaled by $n_1 + n_2$. A general formula for the combination of k observables is given as a weighted average [Xu, 2006]:

$$C = \begin{bmatrix} n_1 & \dots & n_k \end{bmatrix} \cdot \begin{bmatrix} O_1 \\ \dots \\ O_k \end{bmatrix} = n_1 O_1 + \dots + n_k O_k \tag{C.1}$$

However, order to make such a combination that still has the same meaning as a pseudorange or carrier phase observation, in a dimensional sense, the standardized combination has to be formed as a weighted average. This implies that:

$$n_1 + \dots + n_k = 1 \tag{C.2}$$

C.2.1. Standard deviation of the combined observable

Considering the standard deviation of each observable, σ_k, according with the covariance propagation law, the standard deviation of the combined observable is:

$$\sigma_C^2 = \begin{bmatrix} n_1 & \dots & n_k \end{bmatrix} \cdot \begin{bmatrix} \sigma_1^2 & \dots & 0 \\ \dots & \dots & \dots \\ 0 & \dots & \sigma_k^2 \end{bmatrix} \cdot \begin{bmatrix} n_1 \\ \dots \\ n_k \end{bmatrix} = n_1^2 \sigma_1^2 + \dots + n_k^2 \sigma_k^2 \tag{C.3}$$

It can be shown that $\sigma_C^2 \geq k \cdot \min\left(\sigma_1^2, \dots, \sigma_k^2\right)$. This means that data combination will degrade the data of the more accurate of the raw observables. The above equations are valid either for pseudorange and carrier phase observations.

C.2.2. Frequency and wavelength of the combined observable

The combination of k carrier phase observations of different frequency leads to the following expression for the combined carrier phase (from equation C.1):

$$\lambda_C \varphi_C = n_1 \lambda_1 \varphi_1 + \dots + n_k \lambda_k \varphi_k \qquad (\text{ in metric units}) \tag{C.4}$$

This equation can be expanded explicitly as [Collins, 1999]:

$$\lambda_C \varphi_C = \rho\left(n_1 + ... + n_k\right) + n_1 \lambda_1 N_1 + ... + n_k \lambda_k N_k = \rho + \lambda_C N_C \qquad \text{(C.5)}$$

Where ρ is the geometric distance;

   λ_C is the wavelength of the combined observable;

   N_C is ambiguity of the combined observable.

The above equation leads to:

$$\lambda_C N_C = n_1 \lambda_1 N_1 + ... + n_k \lambda_k N_k \Leftrightarrow$$
$$N_C = \frac{n_1 \lambda_1 N_1}{\lambda_C} + ... + \frac{n_k \lambda_k N_k}{\lambda_C} \qquad \text{(C.6)}$$

But for N_C to be an integer, the terms $\dfrac{n_1 \lambda_1}{\lambda_C} ... \dfrac{n_k \lambda_k}{\lambda_C}$ must also be integers and represent an equivalent linear combination in units of cycle, instead of units of cycle. It will be represented as *i* and *k*:

$$\left. \begin{array}{l} i_1 = \dfrac{n_1 \lambda_1}{\lambda_C} \Rightarrow n_1 = \dfrac{i_1 \cdot \lambda_C}{\lambda_1} = \dfrac{i \cdot f_1}{f_C} \\[2mm] i_k = \dfrac{n_k \lambda_k}{\lambda_C} \Rightarrow n_k = \dfrac{i_k \cdot \lambda_C}{\lambda_k} = \dfrac{i_k \cdot f_k}{f_C} \end{array} \right\} \Rightarrow \dfrac{i_1}{i_k} = \dfrac{n_1}{n_k} \cdot \dfrac{f_k}{f_1} \qquad \text{(C.7)}$$

The combined frequency is given by:

$$f_C = i_1 f_1 + ... + i_k f_k \qquad \text{(C.8)}$$

And the wavelength is given by:

$$\lambda_C = \frac{c}{f_C} = \frac{c}{i_1 f_1 + ... + i_k f_k} = \frac{1}{\dfrac{i_1}{\lambda_1} + ... + \dfrac{i_k}{\lambda_k}} \qquad \text{(C.9)}$$

C.2.3.   Ionosphere effect on a combined observable

The ionospheric delays of signals at different frequencies are different, and its linear combination is:

$$\delta_{ion,C} = \frac{n_1 \delta_{ion,1} + ... + n_k \delta_{ion,k}}{n_1 + ... + n_k} \qquad \text{(C.10)}$$

Assuming the dependency only on the frequency (the TEC only depends on the signal path), the ionospheric delay (see section 3.4) is given by the simplified expression:

$$\delta\phi_{ion} = -\frac{40.3 \cdot TEC}{f^2} = \frac{const}{f^2} \tag{C.11}$$

Using this relation, the combined ionospheric delay for the carrier phase is given as:

$$\delta\phi_{ion,C} = n_1\delta_{ion,1} + ... + n_k\delta_{ion,k} = -40.3 \cdot TEC\left(\frac{n_1}{f_1^2} + ... + \frac{n_k}{f_k^2}\right) \tag{C.12}$$

The ionosphere delay factor with reference to the L1 ionosphere delay is given as:

$$\frac{\delta\phi_{ion,C}}{\delta\phi_{ion,L_1}} = \frac{-40.3 \cdot TEC\left(\dfrac{n_1}{f_1^2} + ... + \dfrac{n_k}{f_k^2}\right)}{\dfrac{-40.3 \cdot TEC}{f_1^2}} = n_1 + ... + \frac{n_k \cdot f_1^2}{f_k^2} \tag{C.13}$$

C.3. Inter-frequency linear combinations

Given the coefficients for a linear combination in the units of cycles, the following can be derived as follows:

- Coefficients in the range domain (using equation C.7);
- Accuracy of the combined observable with reference to the L1 observable (using equation C.3);
- Wavelength of the combined observable (using equation C.9);
- Frequency of the combined observable (using equation C.8);
- Combined observable ionosphere factor (using C.13);

The following table summarizes the main properties for the most used linear combinations of observations, considering the GPS L1 and L2 frequencies with the same noise level.

Table C.1 – Summary of the main properties of some inter-frequency linear combinations.

	i_1	i_2	n_1	n_2	$\dfrac{\sigma_C}{\sigma_{L_1}}$	$\lambda_c(cm)$	$f_C(MHz)$	$\dfrac{\delta\phi_{ion,C}}{\delta\phi_{ion,L_1}}$
IF	1	$-\dfrac{f_2}{f_1}$	$\dfrac{f_1^2}{f_1^2-f_2^2}=2.546$	$-\dfrac{f_2^2}{f_1^2-f_2^2}=-1.546$	2.97	48.44	618.849	0
GF	1	$-\dfrac{f_1}{f_2}$	1	-1	1	-	-	-0.65
WL	1	-1	$\dfrac{f_1}{f_1-f_2}=4.529$	$-\dfrac{f_2}{f_1-f_2}=-3.529$	5.74	86.19	347.820	-1.28
NL	1	1	$\dfrac{f_1}{f_1+f_2}=0.562$	$\dfrac{f_2}{f_1+f_2}=0.438$	0.71	10.69	2803.020	1.28

The development of these combinations is given in the next sub-sections. The minus signal of the ionosphere factor of the GF and WL has the meaning of a delay, when compared to the L1 ionosphere effect.

C.3.1. Ionosphere-free combination (IF)

The simplified observation equation for the carrier phase, considering only the ionosphere effect is:

$$\varphi_{r,f}^s(t_r) = \frac{\rho(t_r)}{\lambda} + \frac{\delta t_r}{\lambda}\cdot\left(c-\frac{d\rho(t_r)}{dt}\right) - c\cdot\frac{\delta t^s}{\lambda} - \frac{\delta_{ion,f}}{\lambda} + N_{r,f}^s \qquad (C.14)$$

For a linear combination of two frequencies, the following condition must be fulfilled:

$$i\frac{\delta_{ion,1}}{\lambda_1} + j\frac{\delta_{ion,2}}{\lambda_2} = 0 \qquad (C.15)$$

Where i and j are two arbitrary numbers. However the choice is not completely arbitrary since the increase of the combined observation noise must be considered. A common choice derives from defining $i = 1$. This choice is the well known ionosphere free combination (IF), also referred as the L3 combination [Dach *et al.*, 2007], where:

$$i = 1$$

$$\frac{\delta_{ion,1}}{\lambda_1} + j\frac{\delta_{ion,2}}{\lambda_2} = 0 \Leftrightarrow j = -\frac{\delta_{ion,1}}{\lambda_1}\cdot\frac{\lambda_2}{\delta_{ion,2}} = -\frac{f_1}{f_1^2}\cdot\frac{f_2^2}{f_2} = -\frac{f_2}{f_1} \qquad (C.16)$$

The IF is based on the same observation type (carrier phase or pseudorange) at different frequencies. The error sources that are the same for both frequencies remain unchanged. The error sources that depend on the frequency are combined and do not cancel, except the ionosphere effect.

The observation equations for the pseudorange and carrier phase ionosphere free combination are:

$$P_{r,IF}^s(t_r) = \rho_r^s(t_r) + \delta t_r \cdot \left(c - \frac{d\rho(t_r)}{dt} \right) - c \cdot \delta t^s + \delta_{rel} + \delta_{trop} +$$
$$\delta P_{mult,IF} + \delta a_{r,IF} + \delta a^{s,IF} + bP_{r,IF} + bP^{s,IF} + \varepsilon_{P,IF}$$

$$\Phi_{r,IF}^s(t_r) = \rho(t_r) + \delta t_r \cdot \left(c - \frac{d\rho(t_r)}{dt} \right) - c \cdot \delta t^s + \delta_{rel} + \delta_{trop} +$$
$$\left(\lambda \cdot N_r^s \right)_{IF} + \delta\Phi_{mult,IF} + \lambda_{IF} \cdot \delta_{wnd} + \delta a_{r,IF} + \delta a^{s,IF} + b\Phi_{r,IF} + b\Phi^{s,IF} + \varepsilon_{\Phi,IF}$$

$$(C.17)$$

This combination has some weaknesses:

- It does not allow keeping the integer characteristics of the ambiguity parcel. The ambiguity can only be estimated as a float unknown;
- The measurement noise (standard deviation) is three times higher than the basic observations;
- It cannot remove the higher order effects, which, although covering less than 0.1% of the total effects, can be several tens of centimetres of range error during periods of high ionosphere activity [Klobuchar, 1996].

C.3.2. Geometry-free linear combination

The geometry component of the observation equations is the one that contains the terms referred to the geometric distance and the receiver and satellite clock errors. A geometry free combination linear combination removes the geometry component and can be formed by making differences between observables: code-code, code-phase and phase-phase.

The simplified carrier phase observation equation considering only the geometry terms, the ionosphere and the ambiguity is:

$$\varphi_{r,f}^s(t_r) = \frac{\rho(t_r)}{\lambda} + \frac{\delta t_r}{\lambda} \cdot \left(c - \frac{d\rho(t_r)}{dt} \right) - c \cdot \frac{\delta t^s}{\lambda} - \frac{\delta_{ion,f}}{\lambda} + N_{r,f}^s \qquad (C.18)$$

For a linear combination of two frequencies, the following condition must be fulfilled:

$$i\left(\frac{\rho(t_r)}{\lambda_1}+\frac{\delta t_r}{\lambda_1}\cdot\left(c-\frac{d\rho(t_r)}{dt}\right)-c\cdot\frac{\delta t^s}{\lambda_1}\right)+j\left(\frac{\rho(t_r)}{\lambda_2}+\frac{\delta t_r}{\lambda_2}\cdot\left(c-\frac{d\rho(t_r)}{dt}\right)-c\cdot\frac{\delta t^s}{\lambda_2}\right)=0 \Leftrightarrow$$

$$\frac{i}{\lambda_1}\left(\rho(t_r)+\delta t_r\cdot\left(c-\frac{d\rho(t_r)}{dt}\right)-c\cdot\delta t^s\right)+\frac{j}{\lambda_2}\left(\rho(t_r)+\delta t_r\cdot\left(c-\frac{d\rho(t_r)}{dt}\right)-c\cdot\delta t^s\right)=0 \Leftrightarrow \qquad \text{(C.19)}$$

$$\frac{i}{\lambda_1}+\frac{j}{\lambda_2}=0$$

Where i and j are two arbitrary numbers. However the choice is not completely arbitrary since the increase of the combined observation noise must be considered. A common choice derives from defining $i = 1$. This choice is the well known ionosphere free combination, also referred as the L4 combination [Dach *et al.*, 2007], where:

$$i = 1$$
$$\frac{1}{\lambda_1}+\frac{1}{\lambda_2}=0 \Leftrightarrow j = -\frac{\lambda_2}{\lambda_1}=-\frac{f_2}{f_1} \qquad \text{(C.20)}$$

The GF removes all the terms that are independent on the frequency.

C.3.3. Wide-lane linear combinations

The wide-lane is formed by the combination of two observations of the same type, in accordance with the following equation (in the range domain):

$$O_{WL}=O_1\frac{f_1}{f_1-f_2}-O_2\frac{f_2}{f_1-f_2} \qquad \text{(C.21)}$$

For carrier phase observations, this combination is designated as L5 [Datch *et al.*, 2007]:

$$\Phi^s_{r,WL}(t_r)=\rho(t_r)+\delta t_r\cdot\left(c-\frac{d\rho(t_r)}{dt}\right)-c\cdot\delta t^s+\delta_{rel}+\delta_{trop}+\delta_{ion,WL}$$
$$\lambda_{WL}\cdot N^s_{r,WL}+\delta\Phi_{mult,WL}+\lambda_{WL}\cdot\delta_{wnd}+\delta a_{r,WL}+\delta a^{s,WL}+b\Phi_{r,WL}+b\Phi^{s,WL}+\varepsilon_{WL} \qquad \text{(C.22)}$$

The standard deviation is 5.7 times bigger when compared with the L1 basic observable.

Looking more carefully at the ambiguity parcel and windup effect:

$$(\lambda \cdot N)_{WL} = \frac{f_1 \lambda_1 N_1}{f_1 - f_2} - \frac{f_2 \lambda_2 N_2}{f_1 - f_2} = \frac{c}{f_1 - f_2}(N_1 - N_2) = \lambda_{WL} \cdot N_{WL} \tag{C.23}$$

Where $\lambda_{WL} = \dfrac{c}{f_1 - f_2}$ is the wide-lane wavelength, 86.2 cm, which is roughly four times larger than the L1 and L2 wavelengths.

For the windup parcel:

$$(\lambda \cdot \delta_{wnd})_{WL} = \frac{f_1 \lambda_1 \delta_{wnd}}{f_1 - f_2} - \frac{f_2 \lambda_2 \delta_{wnd}}{f_1 - f_2} = \frac{c}{f_1 - f_2}\delta_{wnd} = \lambda_{WL} \cdot \delta_{wnd} \tag{C.24}$$

C.3.4.   Narrow-lane linear combination

The narrow-lane is formed by the combination of two observations of the same type in accordance with the following equation (in the range domain):

$$O_{NL} = O_1 \frac{f_1}{f_1 + f_2} + O_2 \frac{f_2}{f_1 + f_2} \tag{C.25}$$

For carrier phase observations:

$$\Phi_{r,NL}^{s}(t_r) = \rho(t_r) + \delta t_r \cdot \left(c - \frac{d\rho(t_r)}{dt}\right) - c \cdot \delta t^s + \delta_{rel} + \delta_{trop} + \delta_{ion,NL} + \\ \lambda_{NL} \cdot N_{r,NL}^{s} + \delta\Phi_{mult,NL} + \lambda_{NL} \cdot \delta_{wnd} + \delta a_{r,NL} + \delta a^{s,NL} + b\Phi_{r,NL} + b\Phi^{s,NL} + \varepsilon_{NL} \tag{C.26}$$

The standard deviation is 0.7 times with reference to the L1 basic observable.

Looking more carefully at the ambiguity parcel and windup effect:

$$(\lambda \cdot N)_{NL} = \frac{f_1 \lambda_1 N_1}{f_1 + f_2} + \frac{f_2 \lambda_2 N_2}{f_1 + f_2} = \frac{c}{f_1 + f_2}(N_1 + N_2) = \lambda_{NL} \cdot N_{NL} \tag{C.27}$$

Where $\lambda_{NL} = \dfrac{c}{f_1 + f_2}$ is the wide-lane wavelength, 10.6 cm, which is roughly half the value of the L1 and L2 wavelengths.

For the windup parcel:

$$\left(\lambda \cdot \delta_{wnd}\right)_{NL} = \frac{f_1 \lambda_1 \delta_{wnd}}{f_1 + f_2} + \frac{f_2 \lambda_2 \delta_{wnd}}{f_1 + f_2} = \frac{2 \cdot c}{f_1 + f_2} \delta_{wnd} = 2 \cdot \lambda_{WL} \cdot \delta_{wnd} \tag{C.28}$$

C.4. Linear combinations of observations of different type

C.4.1. Code-phase average linear combination

The pseudorange and phase observations on the same frequency suffer the same amount of ionospheric effect but with opposite sign, therefore, their sum is ionosphere-free. The code-phase combination [Gao and Shen, 2001] also removes the ionosphere effect and its standard deviation is smaller than the pseudorange IF combination. It is a linear combination of pseudorange and carrier phase observations at the same frequency:

$$C_{CP,f} = \frac{P_f}{2} + \frac{\Phi_f}{2} \tag{C.29}$$

$$C_{CP,f} = \rho(t_r) + \delta t_r \cdot \left(c - \frac{d\rho(t_r)}{dt}\right) - c \cdot \delta t^s + \delta_{rel} + \delta_{trop} +$$

$$+ \frac{\lambda_f \cdot N_f}{2} + \frac{\delta P_{mult,f}}{2} + \frac{\delta \Phi_{mult,f}}{2} + \frac{\lambda_f \cdot \delta_{wnd}}{2} + \delta a_{r,f} + \delta a^{s,f} + \frac{b P_{r,f}}{2} + \frac{b \Phi_{r,f}}{2} + \frac{b P^{s,f}}{2} + \frac{b \Phi^{s,f}}{2} + \varepsilon_{CP}$$

The standard deviation for this combination is the same as for the pseudorange, which is an advantage when compared to the code ionosphere free combination. Also note that the integer ambiguity also remains an integer number.

C.4.2. Melbourne-Wübbena linear combination (MW)

The Melbourne-Wübbena is formed by the combination of two of the two carrier phase and the two pseudorange observations as described by Melbourne (1985) and Wübbena (1985). It is a combination of the WL (phase) minus NL (code). The combination is given by:

$$C_{MW} = \Phi_{WL} - P_{NL} = \Phi_1 \frac{f_1}{f_1 - f_2} - \Phi_2 \frac{f_2}{f_1 - f_2} - P_1 \frac{f_1}{f_1 + f_2} - P_2 \frac{f_2}{f_1 + f_2} \tag{C.30}$$

This combination eliminates the effect of the ionosphere, the geometry, the clocks and the troposphere. With good quality pseudorange observations (rms < 1 m) may be used for the resolution of wide lane ambiguities.

C.4.2.1. Ionospheric-free carrier-phase and pseudorange smoothing

The key idea is choose data combination parameters for dual frequency carrier phase and pseudorange combinations which eliminates the effect of the ionosphere. Given a generic data combination of dual frequency carrier phase and pseudorange measurements:

$$C = \alpha_1 \Phi_1 + \alpha_2 \Phi_2 + \beta_1 P_1 + \beta_2 P_2 \tag{C.31}$$

Where $\alpha_1, \alpha_2, \beta_1, \beta_2$ are the parameters of the data combination, with real number values. In order to fulfil the condition of being an ionospheric free combination, the parameters should be chosen such as:

$$\begin{aligned}
\alpha_1 \delta\Phi_{ION,1} + \alpha_2 \delta\Phi_{ION,2} + \beta_1 \delta P_{ION,1} + \beta_2 \delta P_{ION,2} = \\
= \alpha_1 \delta\Phi_{ION,1} + \alpha_2 \delta\Phi_{ION,2} - \beta_1 \delta\Phi_{ION,1} - \beta_2 \delta\Phi_{ION,2} = 0
\end{aligned} \tag{C.32}$$

Where $\delta\Phi_{ION,1}, \delta\Phi_{ION,2}$ are the carrier phase ionospheric delays for each and frequency, which is symmetric with relation to pseudorange ionospheric delay. Considering that $\frac{\delta\Phi_{ION,1}}{\delta\Phi_{ION,2}} = \frac{f_2^2}{f_1^2}$ we get:

$$\alpha_1 + \frac{f_1^2}{f_2^2}\alpha_2 - \beta_1 - \frac{f_1^2}{f_2^2}\beta_2 = 0 \Leftrightarrow \alpha_1 - \beta_1 + \frac{f_1^2}{f_2^2}(\alpha_2 - \beta_2) = 0$$
$$\Leftrightarrow f_2^2(\alpha_1 - \beta_1) + f_1^2(\alpha_2 - \beta_2) = 0 \tag{C.33}$$

Where f is the carrier frequency.

The coefficients must also allow the combination to maintain the scale equivalent to the line of sight range. This implies that:

$$\begin{cases} \alpha_1 + \alpha_2 = 1 \\ \beta_1 + \beta_2 = 1 \end{cases} \tag{C.34}$$

C.4.2.2. Divergence Free ionospheric combination (DF)

For $\beta_1 = 1 \Rightarrow \beta_2 = 0$ it is equivalent to combine the pseudorange observation, P_1, using a combination of dual frequency carrier phase observations to reduce the impact of the ionosphere. It is designated as Divergence-Free (DF) ionospheric combination. The DF combination corrects the effect of the ionosphere temporal variation in a pseudorange minus carrier phase smoothing process [MacGraw, 2006; Konno, 2007].

The value of the carrier phase parameters are:

$$\alpha_1 = \frac{f_1^2 + f_2^2}{f_1^2 - f_2^2} \quad \alpha_2 = -\frac{2f_2^2}{f_1^2 - f_2^2} \tag{C.35}$$

A similar derivation can be made for $\beta_1 = 0 \Rightarrow \beta_2 = 1$ which corresponds to combine the pseudorange observation, P_2. The complete DF combination for P1 and P2 are:

$$
\begin{aligned}
C_{DF,1} &= P_1 - \frac{f_1^2 + f_2^2}{f_1^2 - f_2^2}\,\Phi_1 + \frac{2f_2^2}{f_1^2 - f_2^2}\,\Phi_2 \\
C_{DF,2} &= P_2 - \frac{2f_2^2}{f_1^2 - f_2^2}\,\Phi_1 + \frac{f_1^2 + f_2^2}{f_1^2 - f_2^2}\,\Phi_2
\end{aligned}
\tag{C.36}
$$

The carrier phase coefficients in units of cycle are (recalling table C.1):

$$
\begin{aligned}
i_1 &= -\frac{f_1^2 + f_2^2}{2f_1 f_2} \\
i_2 &= 1
\end{aligned}
\tag{C.37}
$$

This means that the combined ambiguity is no longer an integer number.

C.4.2.3. Ionospheric Free combination (IF)

The IF combination already explained for the carrier phase observation may also be applied to pseudorange observations on two frequencies. In this case the ionosphere effect is eliminated by combining dual frequency observations on the carrier the carrier phase and pseudorange individually. It is achieved by making the data combination coefficients as:

$$\alpha_1 = \beta_1 = \frac{f_1^2}{f_1^2 - f_2^2} \text{ and } \alpha_2 = \beta_2 = -\frac{f_2^2}{f_1^2 - f_2^2} \tag{C.38}$$

which leads to:

$$C_{IF,\Phi} = \frac{f_1^2}{f_1^2 - f_2^2}\,\Phi_1 - \frac{f_2^2}{f_1^2 - f_2^2}\,\Phi_2 \qquad C_{IF,P} = \frac{f_1^2}{f_1^2 - f_2^2}\,P_1 - \frac{f_2^2}{f_1^2 - f_2^2}\,P_2 \tag{C.39}$$

References

Dach, R., Hugentobler, U., Fridez, P., Meidl and M. (2007) *Bernese GPS software*, version 5.0, Astronomical Institute, University of Bern, January 2007. http://www.bernese.unibe.ch/docs/DOCU50.pdf (accessed 14 May 2012).

Konno, H. (2007) *Design of an aircraft landing system using dual-frequency GNSS*, Ph.D. Dissertation, Department of Aeronautics and Astronautics, Stanford University, USA, December 2007.

MacGraw, G. (2006) "How can dual frequency code and carrier measurements be optimally combined to enhance position solution accuracy?" *InsideGNSS*, July/August 2006.

Melbourne, W.G. (1985) "The Case for Ranging in GPS Based Geodetic Systems" *Proceedings of 1st Int. Symp. on Precise Positioning with the GPS*, ed. Clyde Goad, U.S. Dep. of Commerce, Rockville, Maryland, 15-19 April, 373-386.

Wübbena, G. (1985). "Software Developments for Geodetic Positioning with GPS Using TI 4100 Code and Carrier Measurements". *Proceedings of 1st Int. Symp. on Precise Positioning with the GPS*, ed. Clyde Goad, U.S. Dep. of Commerce, Rockville, Maryland, 15-19 April, 403-412.

Annex D.   Notes about the GPS Toolkit (GPSTk)

D.1. What is the GPSTk?

The GPSTk is an open source project sponsored by the Applied Research Laboratories of the University of Texas (ARL:UT), having several collaborations around the world. It aims to provide a Global Navigation Satellite System (GNSS) computing suite available to the satellite navigation community.

The initial release of the GPSTk was performed in the summer of 2004 and has been presented for the first time at ION-GNSS-2004 [Tolman *et al.*, 2004]. The GPSTk software suite is available to the user under the Lesser GNU Public License (LGPL). The LGPL grants the user a number of rights; notably, the ability to choose whether to modify and redistribute the source code. It does not require that works based on the GPSTk adopt an open source license (http://www.gnu.org/licenses/lgpl.html).

D.2. Why the GPSTk?

GPSTk may be a good option for the student that intends to create its own software for GNSS related applications. GPSTk provides a wide set of already tested routines and source code that can be incorporated directly in to any personal project. In this way, the project developer allows the developer to reduce the effort in computer programming and may devote its expertise to the development of the particularities of its project.

Any GPSTk user may join the wide community of developers and contribute, with its routines, to the software development, by submitting its own code according with given guidelines. Development facilities are provided by the popular Sourceforge (http://sourceforge.net/) open source

The core of the GPSTk is its software library. The design goals are portability, modularity, easy to use, extensibility and maintainability. These goals allow the GPSTk to maximize the number of possible users and lifetime of the library while decreasing the effort and costs with long-term maintenance. These goals were achieved due to strict adherence to the ANSI standard C++ and Object Oriented Programming (OOP).

One of the great advantages of the GPSTk is its flexibility and ease to use. The GPSTk supports a wide range of functions generally necessary for processing GNSS observations. Such functions are commonly described in textbooks.

D.3. GPSTk documentation and information sources

One of the problems when starting with GPSTk is the lack of a dedicated and user friendly manual for the beginner. However very useful information is available and should be read before starting to develop applications. Most of the GPSTk documentation and information sources are available at the project website:

> http://www.gpstk.org/bin/view/Documentation/WebHome

Starting at the GPSTK homepage, you may follow the links to get information concerning with:

- System requirements download and installation: start from the GPSTk home page;
- Publications and presentations devoted to de GPSTk and research publications using the GPSTk in PDF files:

   > http://www.gpstk.org/bin/view/Documentation/GPSTkPublications

- A detailed description of the functionality provided by the GPSTk library can be found in the Aplication Programmer Interface (API) generated by Doxigen. This API is generated daily from the GPSTk Subversion repository:

   > http://www.gpstk.org/doxygen/

- How to ask a support question. Before asking a question is also very useful to read already answered questions:

   > http://www.gpstk.org/bin/view/Documentation/AskedQuestions

- User's guide to GPS applications:

   > http://www.gpstk.org/bin/view/Documentation/UsersGuide

- Some examples of programming with GPSTk were found in the GPSTk main pages and also in the API generated by Doxigen. We found the latter more useful and up to date.

D.4. Download and installation under MSWindows

D.4.1. Download and installation of the MS Visual C++ compiler

A free of charge Visual C++ compiler express product is available for download at Microsoft website. The Microsoft express products do not have all the features as the regular ones, but the C++ express edition includes all the features to work with GPSTk libraries and source files. Although Microsoft® Visual Express products are provided free of charge, it is required to register your product within 30 days of installation for continued use. Download site: http://www.microsoft.com/express/Downloads/#2008-Visual-CPP

For the installation process, just follow the recommended options. After installation you may wish visit Microsoft update to check for latest updates for your computer. After installation you have 30 days to register at Microsoft. It's free of charge.

D.4.2. Download and installation of the latest GPSTk stable version

The latest stable version is available online on Sourceforge (http://sourceforge.net/projects/gpstk/files/) for most desktop platforms. The stable release is intended for general use. Each version is in the form of a tarball containing the platform independent GPSTk project source code and supporting information. Additional files contain compiled binaries for several common platforms. MD5 and SHA1 hashes are provided in the Release Notes for each version. GPSTk uses the GNU "standard" for naming releases, *e.g.* gpstk-1.1.07. The first number is a major release identifier, the second is a revision, and the third is a patchlevel. After the version number will be a descriptor that indicates the contents of the particular file. At present date (December 2012) the latest sable version is gpstk-2.0.

For the installation process, just follow the recommended options. A directory will be created with all already compiled lib, hpp and exe files, ready to be linked with your C++ project.

D.4.3 Download and installation of the latest GPSTk development version

For investigation and software development may be advantageous to download the GPSTk development version. The development version is not completely tested and approved for release as the stable version but may include new classes and modifications of previous ones, considering the latest advances in GNSS technology and methods for data processing. The

instructions to download the latest stable version are provided in: http://www.gpstk.org/bin/view/Documentation/GPSTkDownloads.

The latest development code can be obtained using SourceForge's Subversion repository for the GSPTk. The contents of the repository can be browsed over the web (http://gpstk.svn.sourceforge.net/viewvc/gpstk/), or downloaded using the Subversion utility svn. The following command can be used to obtain a copy of the latest code using the svn utility: "svn checkout https://gpstk.svn.sourceforge.net/svnroot/gpstk"

Subversion is an open source system for code revision. It is available for download online: http://subversion.tigris.org/project_packages.html. The full text of the Subversion manual is also available over the web: http://svnbook.red-bean.com/en/1.1/.

D.5. Build a C++ project using pre-compiled GPSTK files

Follow the main steps by the described order and in accordance with the windows:

1. Start the MS Microsoft Visual C++ compiler.
2. In the menu, select File -> New -> Project.

In the New Project window, select as the figure bellow:
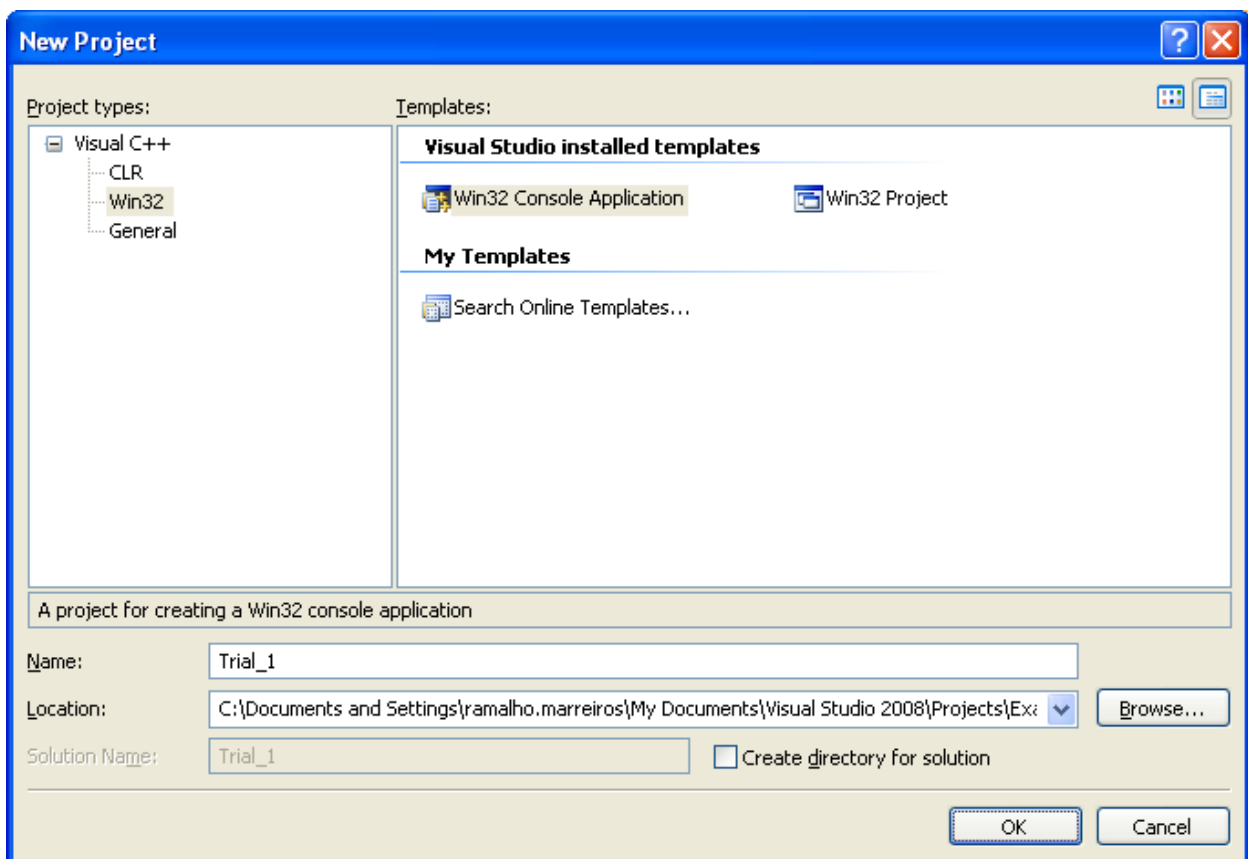
1. Enter the name of your Project, select a location and do not create a directory for solution.

2. In the next window, click "Finish". This will create a console application with a precompiled header.

Now your project is ready to be linked with the pre-compiled GPSTK lib and hpp files, but you must change the project properties, according with the procedure:

1. Select the project properties, by clicking on the project name of the solution explorer window with the right button of the mouse. The project properties will shows up.

2. Change the Active solution configuration to Release (instead of Debug).
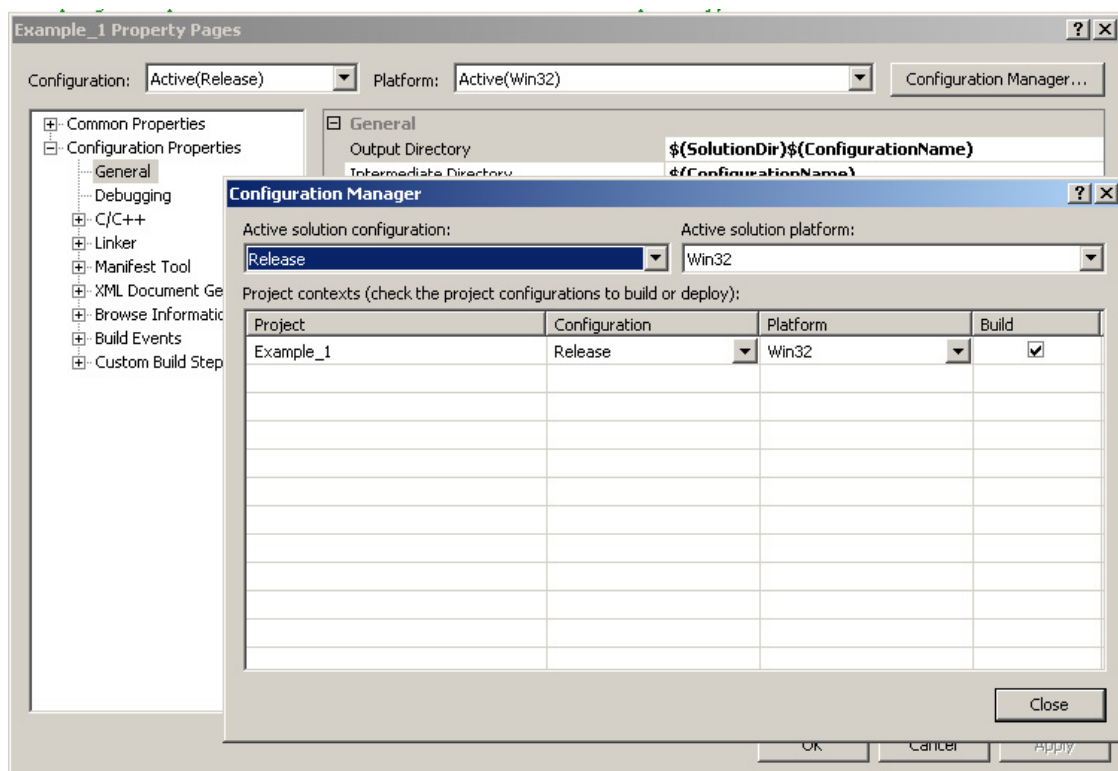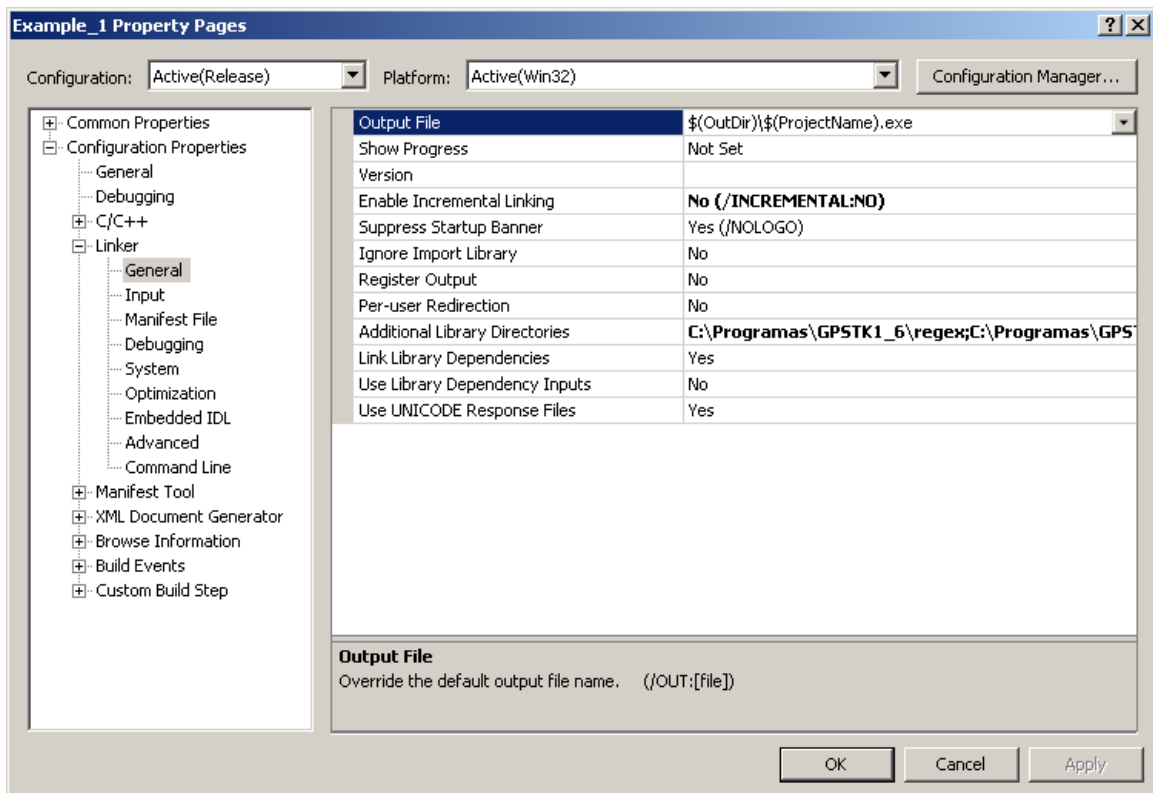
3. Add Include directories. The GPSTK include directory is in `…\GPSTK1_6\include`. You must also add the REGEX (Regular Expression Library) include directory located in `…\GPSTK1_6\regex`.
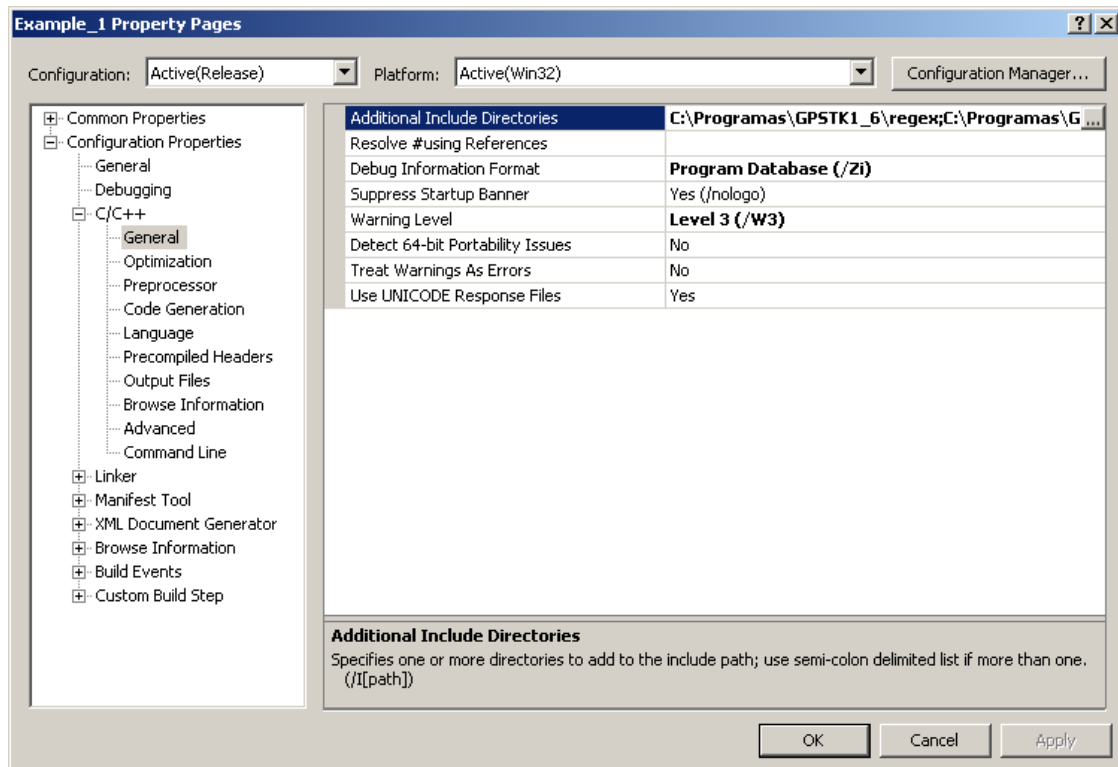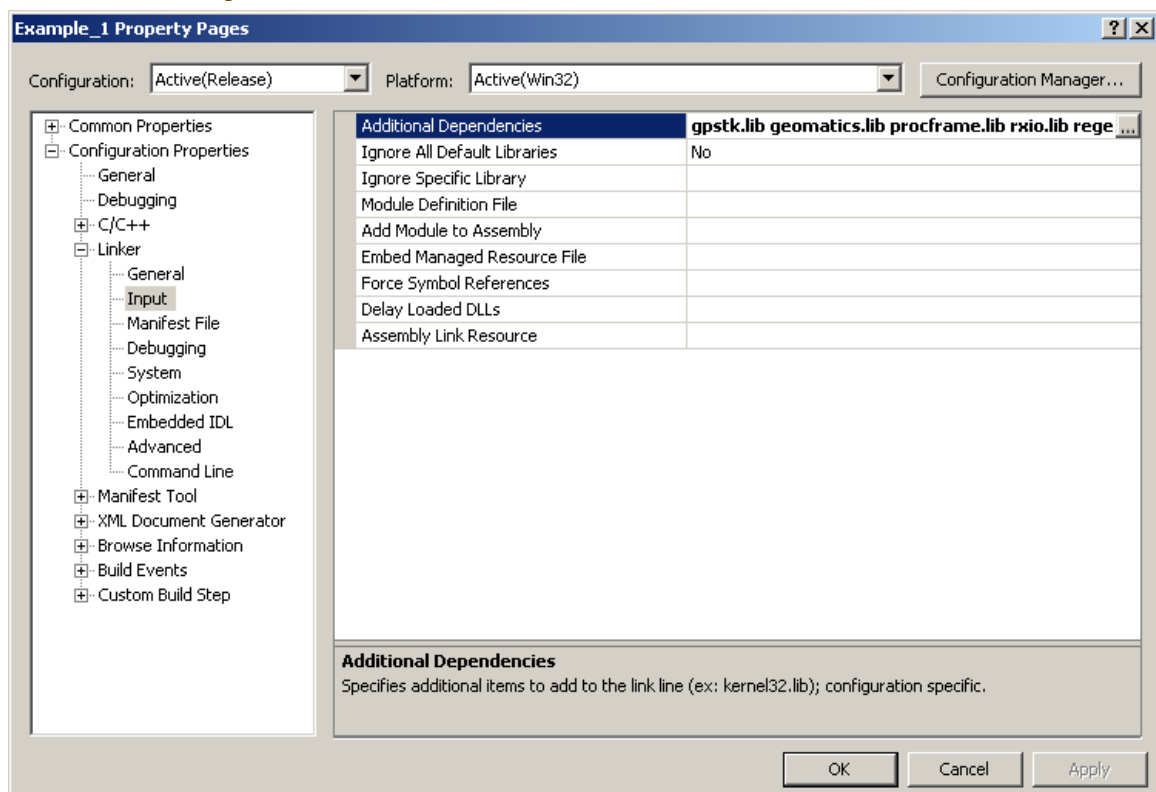

4. Change the Runtime Library to Multi-threaded(/MT).
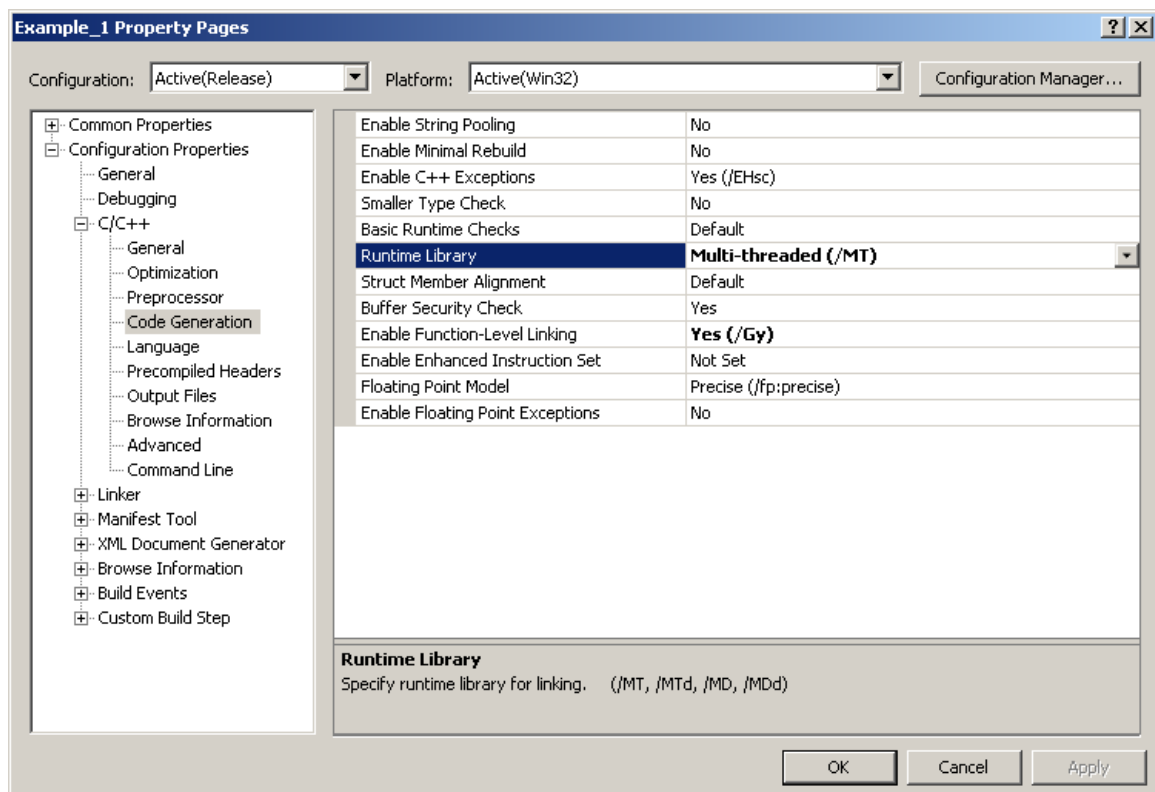
5. Add library directories. The GPSTK include directory is in …\GPSTK1_6\lib. You must also add the REGEX (Regular Expression Library) include directory located in …\GPSTK1_6\regex.

6. Input additional dependencies: gpstk.lib geomatics.lib procframe.lib rxio.lib regex.lib.

D.6. Building GPSTk under MSWindows

Information about this topic is provided at: http://www.gpstk.org/bin/view/Documentation/BuildingGPSTkUnderWindows. The GPSTk is not supported under Microsoft Visual C++ Version 6.0, or earlier, because templates in classes are not supported. Currently there is support for Microsoft Visual Studio C++ .NET 2003 (Version 7) and the Microsoft Visual C++ Express 2005 (Version 8, freely available at MSWindows website). Makefiles for Microsoft Visual C++ are not provided in the toolkit, however note that the Visual C++ IDE is able to import existing code, and so makefiles could be generated via the IDE. The GPSTk supports using "jam" and the command line tools to build. Here are the 5 steps (followed by 6 notes) needed to build under Microsoft Visual C++:

1. Ensure that prerequisites such as "jam" (http://www.perforce.com/jam/jam.html) have been installed.

2. Ensure that there is a system regular expression library installed. See D.7.

3. "jam" must be told where to find the command line tools (compiler and linker). It does this through the environment variable MSVCNT; see step 5. Problems have arisen here when the installation directory has whitespace in it. It has worked correctly with Visual Studio Express 2005 with white space. You could also try quoting the string with whitespace. Another option is to install the MS VC++ tools into a directory with no whitespace; for example C:\MSVC2003. Some have said that jam can be made to work using the "DOS 8.3" version of the path, but this has not been tested.

4. Open a command window in which to build the toolkit. The MS VC++ tools require that appropriate paths be defined before the command line tools will work. MS provides a batch file that sets the PATH and other environment variables; it is called VSVARS32.bat and is found in the directory `C:\MSVC2003\Common7\Tools`. Don't confuse this with VCVARS32.bat. After you have run VSVARS32, you should be able to type "cl" at the command prompt and get the MS compiler.

5. "jam" also relies on environment variables, two of them, in order to run. The jam executable looks at the variable MSVCNT to find the path of the command line tools. Also, the Jamrules file has been set up to look at the variable MSCVER to determine which set of compiler and linker options is to be used. Thus for the 2003 compiler:

```
set MSVCNT=C:\MSVC2003\VC7
set MSCVER=1300
```

or if you are using the 2005 compiler instead:

```
set MSVCNT=C:\MSVC2005\VC
set MSCVER=1400
```

Of course you may have other install directories; this example uses `C:\MSVC2003` for the 2003 tools and `C:\MSVC2005` for the 2005 tools. Note the different subdirectories `\VC7` and `\VC`; this is an MS thing, these are the directories where the \bin, \lib, and \include directories are found. (The values 1300 and 1400 were chosen because all MS compilers define the macro _MSC_VER as a float number of the form 'MMmm.mm' where MM is the major version, and mm.mm is the minor version number; in MS VC++ versions 6, 7 and 8 the major versions are 12, 13, and 14 respectively).

8. At this point, change directory (cd) to your copy of the `\dev` directory (if using Subversion) or the `\gpstk` directory (if using the tarball) of the toolkit, *i.e.* the directory that contains Jamrules, and simply type jam to build the entire toolkit. Jam will tell you which compiler you are using, and then get to work. To install, define the environment variable PREFIX to point to the root of the installation and then type jam install.

Note 1: You could install BOTH MS compilers, in different directories, and then put all this setup into batch files that allow you to run either one independently. For example:

```
REM Batch file go2005.bat  Run from the command line
REM    before using jam and the MS 2005 build tools.
set MSVCNT=C:\MSVC2005\VC
set MSCVER=1400
REM This is a copy of VSVARS32.bat that came with MS VC++ 2005
call VSVARS32_2005
REM Move to my working directory
cd C:\WorkingDirectory
```

and

```
REM Batch file go2003.bat  Run from the command line
REM    before using jam and the MS 2003 build tools.
set MSVCNT=C:\MSVC2003\VC7
set MSCVER=1300
REM This is a copy of VSVARS32.bat that came with MS VC++.NET 2003
call VSVARS32_2003
REM Move to my working directory
cd C:\WorkingDirectory
```

With these batch files the whole process is a simple as:

- Open command window;
- Type go2005 (or go2003);
- Type jam.
- Type 'jam clean' to delete all the object (.obj) and executable (.exe) files.

Note 2: The Jamrules file is where the MSCVER variable is required (unlike the MSVCNT variable, which the jam *executable* requires). If you use only one compiler exclusively, you might edit the Jamrules file and remove this version dependency; then you would not need MSCVER at all.

Note 3: In any case you ought to look at the Jamrules file; look for $(NT), which the Windows executable jam.exe defines, for items relevant to Windows. C++FLAGS contains C++ compiler options, CCFLAGS contains C compiler options (but note that CCFLAGS is changed in `\src\Jamfile` for compiling `regex.c`), LINKFLAGS are linker options, and LINKLIBS are extra libraries included in the link.

Note 4: We have found that optimization is a practical necessity in building with these compilers. The option /O2 (that's capital 'oh' not 'zero') seems to be best for speed. Jamrules now includes /O2 in both versions of the MS compilers. Of course you may change this, or any compiler or linker options, by editing Jamrules.

Note 5: In the past one of the problems in using jam with the MS compilers beyond version 6.0 has been that the libraries advapi32.lib and kernel32.lib seemed to be missing. This, however, comes from the jam *executable*, not from MS. These libraries are required, and provided, in MS VC++ 6.0, and this is the *default for the jam executable*. Jam.exe does this by defining the default LINKLIBS to include these libraries. Since they are not required for later versions, Jamrules now redefines LINKLIBS to be empty. If you want to understand the defaults in jam.exe, go to the jam website and find the Jambase file - it is a 'Jamrules' file that contains all the defaults.

D.7. Building GPSTk from the source code under MSVC++

Apart from the instructions described above, here is another receipt for using GPSTk core libraries in Visual Studio 200X without using "jam":

1. Download the project source files from Sourceforge and extract the tar files to a directory.

2. In MSVC++ create a new Win32 console application project. (In order to avoid using precompiled headers, you must select 'Empty Project' option in the application wizard dialog)

3. Right click on the project name (this is the name that is specified during creation of the project) in the solution explorer and click on *Add -> Existing Item* and add all the files in the 'src' directory (under the extracted files location that is created in step 1) to the project.

4. (Again) Right click on project name in the solution explorer and click on *Add -> Existing Item* and add only 'example1.cpp' which is located under the examples directory.

5. Open the project property page (Right click on the project name in the solution explorer and select properties)

6. In the opened properties dialog expand the *Configuration Properties -> C/C++* tab and select *Command Line*. Copy the following line to the *Additional Options* text box:

    `-D_CRT_SECURE_NO_DEPRECATE -wd4274 -DWIN32 /EHsc /GR -wd4290 -wd4267`

7. Again in the same project properties dialog box expand *Configuration Properties -> C/C++* tab and select *General*. Add the location of 'src' directory to the *Additional Include Directories*. (This is necessary because, unfortunately, some non-system header files in the source files were included using < >) Also, add the location of the regex library that you have installed. This should contain a file regex.h.

8. That is all. Build the program (building takes some time) and run. You will see the output of example1 in the output window.

D.8. Installation of Regex for MSVC++

Starting with GPSTk version 1.6 (and currently in the development version in subversion), the GPSTk will require the system provide regular expression (regex) support. All supported platforms except MSVC++ provide this functionality. There are multiple ways this could be

provided on Visual C++ however the following approach has been and will continue to be tested:

1. Download setup of the Regex package (GNU regular expression library) at http://gnuwin32.sourceforge.net/.

2. Run the installer and install to the location of your choice (*e.g.* `c:\Program Files\GnuWin32`).

3. Choose a "Full installation".

4. Update the PATH, LIB, and INCLUDE variables in your compiler configuration settings for your platform with the paths of the newly install regex library. For example, this file might be:

   `c:\Program Files\Microsoft Visual Studio8\Common7\Tools\vsvars32.bat`

Add `c:\Program Files\GnuWin32\include` (or the appropriate install directory) to the INCLUDE variable, `c:\Program Files\GnuWin32\lib` to the LIB variable, and `c:\Program Files\GnuWin32\bin` to the PATH variable. Here are the detailed steps for the modification on one system, This uses the free version of Microsoft Visual Studio 8:

- The build shell is run with the command:

  %comspec% /k ""`C:\Program Files\Microsoft Visual Studio 8\VC\vcvarsall.bat`"" x86

- Regex is installed into c:\Program Files\GnuWin32\. In the GnuWin32\lib directory are the files libregex.dll, a libregex.la regex-bcc.lib regex.lib regex2.def. In the `GnuWin32\include` directory is the file regex.h.

- For this system, the file updated was:

  `c:\Program Files\Microsoft Visual Studio 8\Common7\Tools\vsvars32.bat.`

It is recommended that you add the Regex library to the system PATH variable in order to prevent having to add it to your path each time you want to run or compile a GPSTk program. This can be done by doing the following:

1. Clicking start, right clicking on My Computer, and clicking properties;

2. Go to the "Advanced" tab;

3. Click "Environment Variables";

4. Edit the PATH variable, if it doesn't exist, create it.

Append the path to the "bin" directory in the location where you installed GNUWin32 Regex into. The default for this is `C:\Program Files\GnuWin32\bin`, usually you put a semicolon before the location to append a directory to the Path variable.

This page was intentionally left blank

Annex E. Source code developed in this study (on a CD)

This annex contains the source code developed in the scope of this study and the GPSTk library version 1.6.

This annex is on a CD with the following directories:

- GPSTk library version 1.6. Some of these classes were modified in order to allow kinematic positioning, the use of new data combination, tropospheric models and initial ambiguity determination;

- GPSTk under development. This directory contains GPSTk that were under development for reading the data records on CLK files;

- Main Module: Contains the main components of the software.

- New classes: The new classes were developed to perform GNSS data processing tasks required to achieve the goal of this study, not included on the GPSTk library:

  o Filter for GNSS observations to remove form the GNSS data structure carrier phase observations with value "0";

  o Work with GMF mapping functions;

  o Work with the GPT model;

  o Read satellite precise clock files in the format CLK.

- Regex support: Contains the routines required to run the Regular Expression Library under Windows.